Analysis of Heterogeneously Catalyzed Ester Hydrolysis Reactions in a Fixed-Bed Chromatographic Reactor

Dissertation

zur Erlangung des akademischen Grades

Doktoringenieur
(Dr.-Ing.)

von M. Eng. **Vu-Dinh, Tien**

geb. am 30.06.1974 in Hanoi, Vietnam

genehmigt durch Fakultät für Verfahrens- und Systemtechnik
der Otto-von-Guericke-Universität Magdeburg

Gutachter: Prof. Dr.-Ing. habil. Andreas Seidel-Morgenstern

                     Prof. Dr.-Ing. habil. Achim Kienle

Promotionskolloquium am 02. Juli 2007

ii

Zusammenfassung

Reaktionschromatographie basiert auf der Kopplung von chemischer Reaktion und chromatographische Trennung in einem Apparat. Im Vergleich zu konventionellen in Reihe geschalteten Reaktoren und Trenneinrichtungen besitzt ihr Einsatz das Potential zur Erhöhung der Produktivität, der Reinheit und der Selektivität mit der Produkte gewonnen werden können. Auf Grund des Mangels, an präzisen Modellen und Daten ist die industrielle Anwendung chromatographischer Reaktoren noch nicht etabliert. Um einen Beitrag zur Entwicklung und Einsatz von dieser viel versprechenden Technik zu leisten, werden in dieser Arbeit mehrere Hydrolysereaktionen von Estern in einem chromatographischen Festbettreaktor theoretisch und experimentell untersucht.

Ein erfolgreicher Einsatz der Reaktionschromatographie hängt entscheidend von den Reaktionsraten, der Stöchiometrie und den Wechselwirkungen der Komponenten mit den eingesetzten stationären Phasen ab. Um die Möglichkeiten dieser Technik zu überprüfen, sind theoretische Werkzeuge notwendig. Für das konzeptionelle Design von chromatographischen Festbettreaktoren wird in dieser Arbeit ein neuer, auf zwei Schritten basierender Modellierungsansatz vorgestellt. Als erstes wird ein Gleichgewichtsmodell zum Überprüfen der prinzipiellen Möglichkeit einer kompletten Umsetzung und Trennung angewendet. Anschliessend wird zur Simulation und Optimierung der Leistung des chromatographischen Reaktors ein detailliertes Gleichgewichts-Dispersionsmodell verwendet.

Zur Verifizierung der theoretischen Studien wurde experimentell die Hydrolyse von Methylformiat, Ethylformiat, Methylacetat und Ethylacetat untersucht. Diese vier Ester weisen unterschiedlichen Reaktionskinetiken auf. Ein Ionenaustauscher wurde als Adsorbent und Katalysator verwendet. Zur Modellierung der Teilprozesse wurden das chemische Gleichgewicht und das Adsorptionsgleichgewicht, die Dispersionskoeffizienten

und weitere wichtige Parameter experimentell bestimmt. Der Einfluss der Temperatur wurde detailliert quantifiziert. Weiterhin wurden die Rektionsraten der vier Reaktionen bestimmt. Dafür wurde eine Anpassung durch einen Vergleich von simulierten und experimentellen Elutionsprofilen durch geführt. Anschliessend wurde das Gleichgewichts-Dispersionsmodell zur Simulation der Leistung des chromatographischen Festbettreaktors eingesetzt.

Die vorgestellten Ergebnisse und Modellierungsansätze können zur Durchführung von Studien für weitere Reaktionssysteme sowie andere Betriebsweisen der Reaktionschromatographie und bzw. für die Analyse ähnlicher integrierter Reaktionstrennprozesse verwendet werden.

Abstract

Reactive chromatography is based on a combination of chemical reactions and chromatographic separations performed in a single apparatus. In comparison with sequentially connected conventional reactors and separators its performance promises the advantage to improve objectives as productivity, purity and selectivity. However, industrial applications of reactive chromatography are still absent due to technical problems and lack of accurate data and models. In an attempt to contribute to the development and application of this promising technique, in this dissertation several ester hydrolysis reactions performed in fixed-bed chromatographic reactors have been studied theoretically and experimentally.

Whether reactive chromatography can be applied successfully for a certain chemical reaction depends on reaction stoichiometries and rates, and on interactions of the species involved with the stationary phases applied. Therefore, theoretical tools are desirable to evaluate feasibility before going into further details. In this work, a new modeling approach consisting out of two steps is proposed for conceptual design of fixed-bed chromatographic reactors. In a first step, an extended equilibrium model is used to study feasibility of joint complete conversion and complete separation. In a second step, a more detailed equilibrium-dispersion model is used to simulate and optimize the performance of fixed-bed chromatographic reactors.

In order to verify theoretical predictions, the hydrolysis reactions of methyl formate, ethyl formate, methyl acetate and ethyl acetate were investigated experimentally in fixed-bed chromatographic reactors. These four ester hydrolysis reactions are characterized by different behavior regarding reaction kinetics. An ion exchange resin was used as adsorbent and catalyst. To model the relevant subprocesses, chemical and adsorption equilibria, dispersion coefficients, and other parameters were determined experimentally. In particular, the influence of the temperature on these parameters was quantified. Furthermore, the reaction rate constants were estimated for the four reactions using curve fitting procedures based on comparing simulated and experimentally determined elution

profiles. Finally, the equilibrium-dispersion model was used to simulate the performance of the fixed-bed chromatographic reactor and a wide parameter range.

The results obtained and the modeling approach presented can be used to study other reaction system, other modes of operation of reactive chromatography and other integrated reaction-separation processes.

Acknowledgements

Contents

C H A P T E R 1

Introduction

1.1. Multifunctional reactors and motivation

Looking back in the history of chemical engineering, some authors distinguished two paradigms regarding "unit operations" and "transport phenomena". According to [Wei96], the former paradigm was initiated by Arthus D. Little in 1920s and it reflects the investigation of single equipments, including their structures and operations. The concept of "*unit operation*" was extended and gradually replaced by attentions paid more to "*transport phenomena*". Naturally, the appearance of the later paradigm was remarked by the famous textbook "*Transport Phenomena*" of Bird, Stewart and Lightfoot [Bird60]. After several decades of successes, these two paradigms did not keep their potentials for creativeness and invention to develop chemical engineering. Since the late 1980s, there have been numerous discussions about "*What will be the core of the new third paradigm?*" The concept of "*process intensification*" given by Stankiewicz and Moulijn in two widely cited articles [Stan00, Stan02] can be a good answer for this question. In the domain of learning, this concept seems to be a new paradigm for discussion and it shows the potential of process engineering to revolutionize industrial chemistry. However, it is not quite new when the concept of multifunctional reactors is considered as a very important sub-class of the process intensification.

In the pharmaceutical and chemical industries, some conventional processes with sequentially structured chain of operational units can be significantly improved by integrated processes using multifunctional reactors. These performances aim to save capital investment, energy and operating cost, reduce equipment size, minimize waste and pollution and, most importantly, improve selectivity and productivity. From 1970s up to now, there have been a large amount of researches focused on chemical engineering domain to develop new concepts of the multifunctional reactors in particular and integrated processes in general.

The multifunctional reactors and their potential advantages for development of chemical engineering were made clear by some authors such as [Agar88], [Agar99], [West92], [Hoff97]. *"Integrated Chemical Processes: Synthesis, Operation, Analysis, and Control"* edited by Sundmacher *et al.* and *"Reactive Separation Process"* edited by Kulprathipanja [Sund05, Kulp02] are considered as the best review books for this area. The multifunctional reactors are also the theme for a series of the International Symposium on Multifunctional Reactors (ISMR) first organized in Amsterdam since 1999 and every two years later. In these references cited here, there are several ways to approach and classify the multifunctional reactors, but it should be better to divide them into three categories:

- Integration of heat transfer and chemical reactions
- Integration of separation processes and chemical reactions
- Integration of mechanical processes and chemical reactions

Because most chemical reactions are reversible with two or more products, separation processes are always required to take desired products out of unconverted reactants and other by-products. Therefore, the integration of chemical reactions and separation processes into a single unit is more attractive and widely applicable than the other integrations. The main advantage of these integrations lies in a possible shift of chemical equilibrium to the product side by simultaneous separation of the reaction products. However, due to the coupling of two or many process steps into one apparatus, the degree of freedom for adjusting the integrated processes can be decreased and the control is often much more complex than non-integrated units. Summary of the advantages and disadvantages of reactive separation processes were made by [Kulp02] as Table 1-1.

The capabilities of incorporation of variety separation processes into the reactor were identified by [Kris02] in Fig. 1-1. However, until now, there are few integrated processes that seem to be well understood and has several attractive industrial applications. For example, large scale applications concerning to reactive distillation [e.g., Agre84, Smit81b], reactive extraction [e.g., Bart01], reactive absorption [e.g., Keni05], reactive crystallization [e.g., Myer02, Tava95, Wibo05], and reactive adsorption [e.g., Agar05] have been reported in the literature. The other developing concepts of multifunctional reactors are not yet commercialized because of technical barriers. In these cases, reactive chromatography (highlighted in Figure 1-1) is paid more attention than the other because of its potentials for efficiency production of high purity products and many impressive industrial applications of preparative chromatographic separations. Although there are several investigations related to the reactive chromatography (see a review in Section 1.2), its theoretical basis and accurate database are still not sufficient for commercialization. Hence, much research is motivated in an effort to provide profound insights into all aspects

of reactive chromatography. The ultimate aim is to possibly scale it up for industrial applications.

Table 1-1: Advantages and disadvantages
of reactive separation process commercialization [Kulp02]

Advantages	Disadvantages
Enhanced reaction rates	Relatively new technology
Increased reaction conversion	Limited applications window
Enhanced reaction selectivity	Extensive experimental development
Reduced reaction severity	Complex modeling requirements
Increased catalyst life	Extensive equipment design effort
Simplified separations	Increased operational complexity
Improved product quality	Significant development costs
Heat integration benefits	Increased scale-up risks
Reduced equipment fouling/coking	
Inherently safer unit	
Reduced operating cost	
Reduced capital investment	
Novel process configurations	
Novel equipment designs	
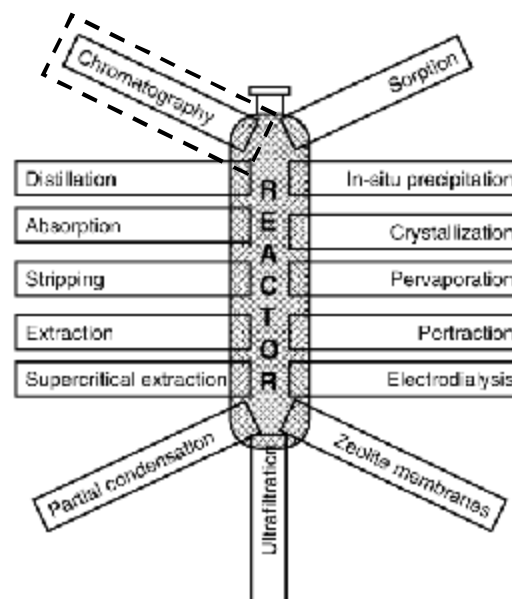
Figure 1-1: Various *in-situ* separation functions integrated in to reactor [Kris02]
(dashed rectangular: the objective of this study)

1.2 Literature review on reactive chromatography

A chromatographic reactor combines a chemical reaction or biochemical reaction with a chromatographic separation. Therefore, the conversion of equilibrium limited reversible reactions can be significantly improved by a possible shift of the chemical equilibrium to product side due to simultaneous separation of the products. Basset and Habgood [Bass60] are the presumed authors of first experimental study on a fixed-bed chromatographic reactor [Sard93]. The descriptions of devices as chromatographic reactors were simultaneously registered patents at the beginning of the 1960s (*e.g.*, US 2 976 132 [Dinw61], CA 631 882 [Mage61], and SU 149 398 [Gazi62]). Because of the lack of industrial applications, there is not any published book specialized only for the reactive chromatography. However, it can be found in some books as the specific chapters (*e.g.*, Ref. [Sard93, Vill81, Fric05b, Borr05]) and a lot published papers in most journals concerning to chemical engineering.

Generally, chromatographic reactors consist of a stationary phase and a mobile phase in constant contact. Depending on principles and operating modes, the reactant or the reactant mixture are dosed continuously or periodically into the reactor. Because the stationary phase acts as adsorbent and catalyst, the reaction and the separation take place simultaneously inside the reactor. Based on the employed phases and the principles, the reactive chromatography identified in the literature can be classified as Figure 1-2.

Depending on gases or liquids used as mobile phase, the reactive chromatography can be distinguished between gas chromatographic reactors or liquid chromatographic reactors as Figure 1-2a. The common stationary phases are solids typically in the form of porous media with large specific surface areas. The solid phases can be individual adsorbent for self-catalytic or homogeneous catalyzed reactions, activated adsorbent by metal ions or function groups, or a mixture of catalyst and adsorbent with suitable ratio. The stationary phase may be a liquid coated on a solid support or a liquid retained by centrifugal force. On other hand, the reactive chromatography can be also classified by operation mode as Figure 1-2b. All principles in Figure 1-2 are reviewed below.

(a)

Reactive chromatography

Mobile phase

| Gas | Liquid |

Stationary phase

- Adsorbent (homo.-catalyst)
- Adsorbent + Catalyst
- Liquid on support
- Adsorbent (homo.-catalyst)
- Adsorbent + Catalyst
- Ion-exchang resin
- Liquid on support
- Liquid held by centrifugal force

(b)

Chromatographic reactors

Operation mode

| Discontinuous | Continuous |

Principle

- Fixed-bed (FBCR)
- Reversed-flow (RFCR)
- Continuous rotating annulus (CRACR)
- True moving-bed (TMBCR)
- Simulated moving-bed (SMBCR)
- "Hashimoto" reactor (SMB with side reactor)
- Centrifugal partition (CPCR)

Figure 1-2: The classifications of reactive chromatography
(A) Phase situations   (B) Operation modes

1.2.1 Principle of chromatographic reactors

As the classification in Figure 1-2, most chromatographic reactors analogize in operating principle with preparative separation chromatography, except the reversed flow reactor, the centrifugal partition chromatographic reactor and the Hashimoto reactor.

Fixed-bed chromatographic reactor (FBCR): A FBCR can be defined by [Lang74] as "*a chromatographic column in which a solute or several solutes are intentionally converted, either partially or totally, to products during their residence in the column. The solute reactant or reactant mixture is injected into the chromatographic reactor as a pulse. Both conversion to product and separation take place in the course of passage through the column; the device is truly both a reactor and a chromatograph*". The principle of a FBCR applied for reversible reactions type of $2A \leftrightarrows B + C$ or $A \leftrightarrows B + C$ are illustrated in Figure 1-3. The reactant A is injected as a rectangular pulse into column and it is converted to B and C by catalytic effects of the stationary phase during its propagation. The different affinities of B and C lead to different propagation velocities and the products are separated from each other. The advantages of the fixed-bed chromatographic reactor compared to the plus flow tubular reactor have been analyzed by [Falk99]. The comparison showed that the conversions of both reactors seem to be similar at the same dilution ratio, but the fixed-bed chromatographic reactor is more attractive for products separation without assistance of a downstream separator.
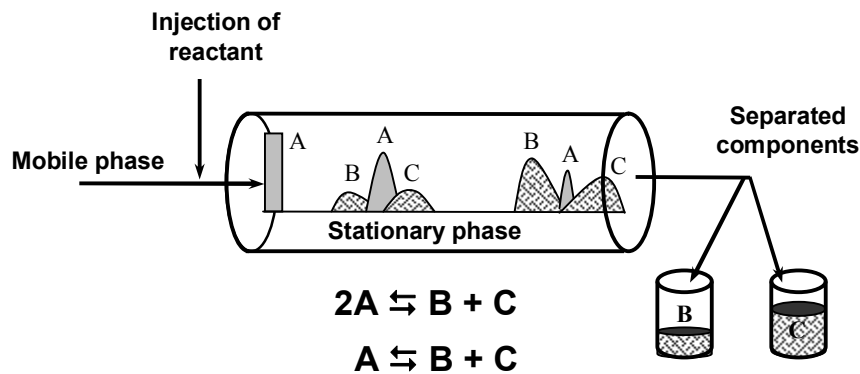
Figure 1-3: The principle of a fixed-bed chromatographic reactor

In order to operate efficiently a FBCR, several conditions are requested as follows [Mats65]:

      1. The equilibrium constant for the reaction must be small (*i.e.*, the reaction must be reversible).

      2. Reaction rates should be high enough so that separation of products rather than rate of reaction limits the extent of reaction.

      3. At least two products must be formed which are chromatographically separated in the reactor.

      4. Reactants must not be separated in the reactor.

Continuous rotating annular chromatographic reactor (CRACR): Based on the principle of an annular chromatograph rotating first introduced by [Mart49], the CRACR was applied for homogeneously catalyzed hydrolysis of methyl formate by [Cho80]. In a CRACR, the stationary phase is packed into the space between two concentric cylinders, rotating continuously about the common axis. While the mobile phase is fed uniformly over whole cross section at the top of the annular, the reactant is fed into a fixed port. The reacting specials are conveyed along the longitudinal axis of the annular due to mobile phase flow, whereas they have a circumferential displacement by adsorption, desorption and rotational movement of annular. Hence, the specials are separated and eluted from the reactor in different angles, comparing to the fixed feed port (see Figure 1-4). This principle is modified by the replacing the rotation of annular with a simulated rotation of feed and collection nozzles using controlled switching valves. The modified principle has more advantages than the conventional one for saving energy, especially in the case of a heavy annular bed.

True moving-bed chromatographic reactor (TMBCR): Figure 1-5 shows the principle of a TMBCR introduced first by [Take76, Take77], also called counter-current moving-bed chromatographic reactor. There are four sections in this reactor system with different functions to archive complete conversion and separation and the solid phase have a true motion in the opposite direction to the liquid flow. The reactant A is fed in the middle, the product B with higher adsorptivity is withdrawn with extract phase and the product C with less adsorptivity comes out with raffinate phase. The movement of solid particles is difficult for avoidance of back-mixing and abrasion between the particles. Therefore, it leads to reduce the reliability in the operation and the efficiency of the process.

Simulated moving-bed chromatographic reactor (SMBCR): In order to overcome the difficulties of TMBCR in conveying solid particles, an invention of Universal Oil Products Company for a simulated moving bed separation was registered for the patent US 2 985 589 [Brou61]. After that, this principle was initially applied for reactive chromatography by [Ray90]. The configuration of a SMBCR with two units for each section is illustrated in Figure 1-6. The true moving of stationary phase in TMBCR is replaced by changing sequentially inlet and outlet positions in SMBCR, using controlled switching valves.
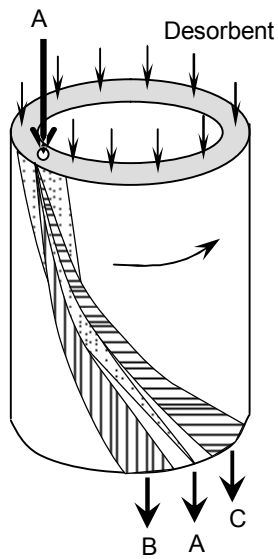
Figure 1-4: The principle of a continuous rotating annular chromatographic reactor (CRACR)
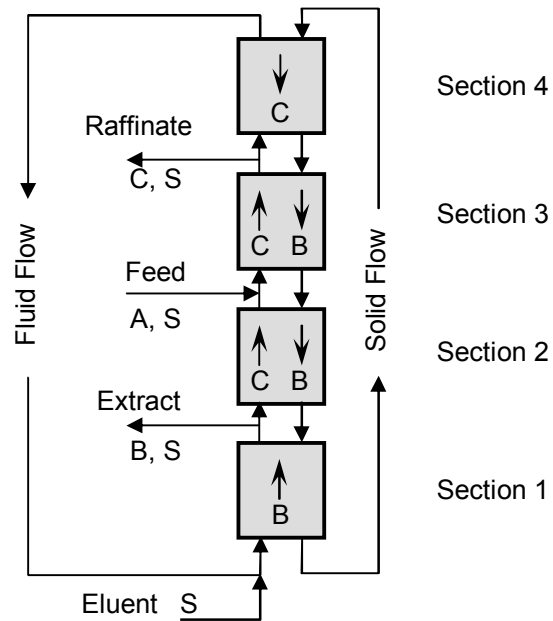
Figure 1-5: The principle of a true moving-bed chromatographic reactor (TMBCR)
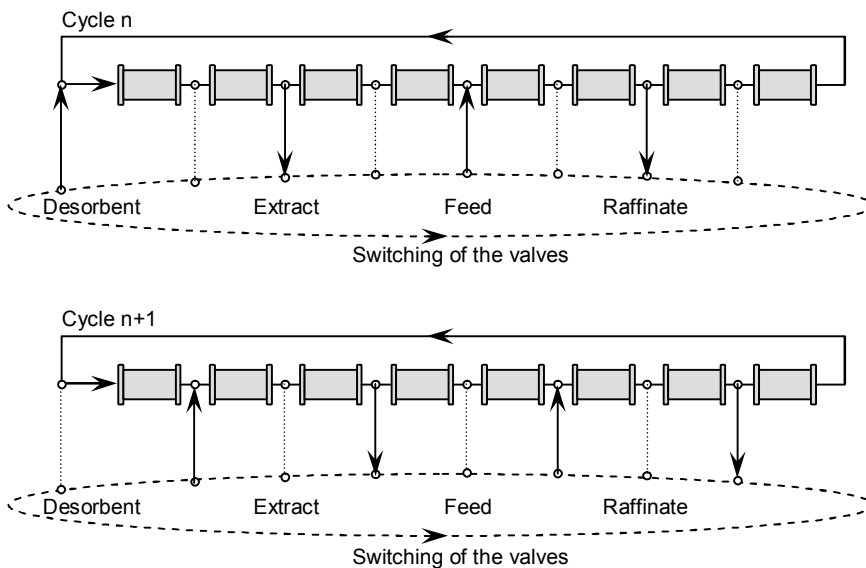
Figure 1-6: The principle of a simulated moving-bed chromatographic reactor [Fric05]

Hashimoto process: SMBCRs mentioned above are not well suited for reactions of the type A ⇆ B. Because of the homogeneous mixture of adsorbent and catalyst, a total conversion is not possible. Hashimoto process is a modified configuration of SMBCR, in

which reactive and separation columns are arranged separately (see Figure 1-7). It is also called the Hashimoto reactor because it was applied first for the isomerization of glucose to fructose by [Hash83]. Although, it is also possible to apply this principle to reactive systems with more than two components, an even more complex design, as well as control of the process has to be taken into consideration.
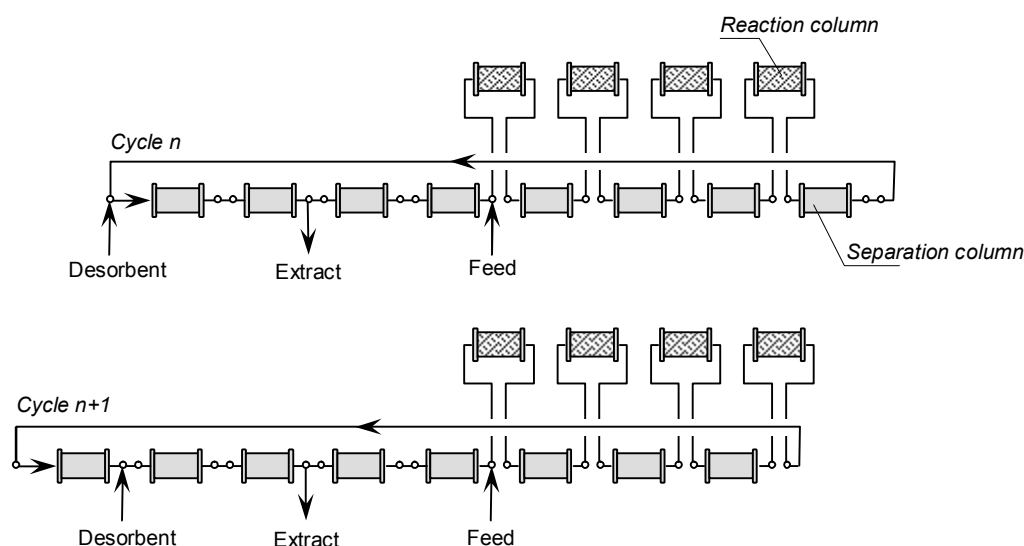
Figure 1-7: Schematic representation of a Hashimoto reactor [Fric05]

Reversed flow chromatographic reactor (RFCR): The concept of a reversed flow reactor is similar to that of an adsorptive reactor used heat accumulation for regeneration, but it is related to mass accumulation. The reaction type of $A + B \leftrightarrows C$ is considered as an example to explain the principle of a RFCR in Figure 1-8. The reactant B is fed in the middle of the column and adsorbed on the stationary phase, where the reactant A and the product C are not adsorbed. Two three way valves are controlled to keep the concentration profile of B propagated in both direction, but not out of the column. It was first applied by [Agar88] for the reduction of nitrogen oxides with ammonia.

Centrifugal partition chromatographic reactor (CPCR): CPCR is an integration of reaction and centrifugal partition chromatographic separation, with counter-current distribution in the absence of a solid support. In this technique, there are two immiscible liquid phases with different density. The stationary phase with higher density is retained in the column by a combination of centrifugal force and geometric channel, while the mobile phase passes through the column as micro-droplets. The separation in CPCR refers to liquid-liquid extraction and the advantage of this technique is a large capacity of stationary

phase compared to the conventional technique with liquid on solid support. However, CPCR is relatively new technique and it was applied for enzymatic reactions [Holl98].
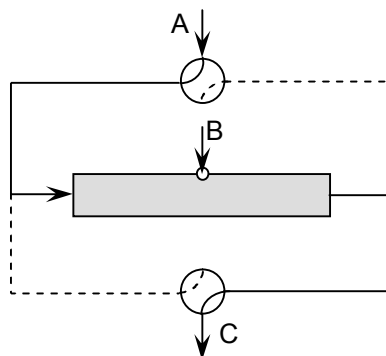
Figure 1-8: The principle of a reversed flow chromatographic reactor.

1.2.2 Theoretical studies

The models for the principles mentioned above have been summarized by [Borr05, Fric05b] generally. Most models are based on conservative mass balance equation and they can be considered as extension of models used for preparative chromatography with reaction kinetics additionally taken into account. Some simple models were solved by analytic solution, whereas the complicated ones were computerized using numerical method with computer aids. In the literature, a brief review is given here. Models for FBCR were surveyed by [Vill81, Sard93, Rhee86a] and will be discussed in very detail in Section 2-1. Different models for CRACR were independently developed by [Carr93, Sarm93]. Overviews for modeling approaches of SMBCR have been given by [Borr05, Fric05a], in which, two modeling approaches can be distinguished. The first approach combines the model of several batch columns with mass balance for inlet and outlet streams of the whole system. The second approach assumes that a SMBCR is equivalent to a TMBR, thus this approach is called the TMBR model. For example, the TMBR have been applied successfully by [Lode02]. A model for CPCR has been introduced by [Holl98].

Conversion can be improved by chromatographic reactors if reversible or consecutive reactions are applied. In the literature, there are several reaction models considered. For reaction (e.g., isomerizations) $A \leftrightarrows B$, although the FBCR is often used to determine the reaction kinetics, it does not offer any advantages to improve conversion in comparisons with a conventional fixed-bed reactor [Vill81, Trap06]. However, the conversion of $A \leftrightarrows B$ can be significantly increased beyond chemical equilibrium if Hashimoto reactor is

employed. There are many experimental and theoretical studies for dealing with reaction A ⇆ B + C and it fully matches the requirements stated by [Mats65] above. For both the FBCR and SMBCR, conversion was found to exceed the limit set by reaction equilibrium. Reaction A + B ⇆ C +D can be simplified to A ⇆ B +C if one of the reactants was used as the mobile phase. Although, due to [Sard93], potential applications of consecutive reactions A +B → R, R +B → S was theoretically demonstrated, there have no experimental studies on this case. Experimental studies on specific reactions are reviewed below.

1.2.3 Experimental studies

Although industrial application of reactive chromatography is still absent, several experimental studies of all principles of chromatographic reactors are reported. Based on the summary in of [Fric05b], an updated survey regarding experiments on gas and liquid chromatographic reactors are given in Tables 1-2 and 1-3. The aim of most of the works performed was essentially to improve the conversion of reversible reactions by equilibrium shifting.

Gas chromatographic reactor: Recently, the gas chromatographic reactors are not continuously developed due to the deficiency of interesting reactions in gas phases comparing to many favorable reactions in liquid phases.

Liquid chromatographic reactor: The liquid chromatographic reactors are more favorable to develop. While most research focused on counter current reactive chromatography to exploit advantages of continuous operation, still fixed-bed reactive chromatography is used as a tool to quantify the reaction rates and to characterize stationary phases. Ion-exchange resins become interesting stationary phases for the most studies due to their advantages of no corrosiveness, high selectivity and resistant strengths. In some recent work (e.g., Ref. [Lode02, Gelo03, Falk03, Sain05, Schl06, Strö06], several esterification reactions were chosen as a typical heterogeneous catalyzed reaction to study reactive chromatography. Beside dynamic and kinetic studies, the behaviors of ion-exchange resin and phase equilibrium were investigated by [Lode02] and [Sanio05]. The methyl formate hydrolysis reaction (i.e., the backward reaction of esterification) was explored partially by [Falk03] and [Schl06], using fixed-bed chromatographic reactors.

Table 1-2: Updated survey based on [Fric05b] for experimental applications
of gas chromatographic reactors

Reaction and references	Catalyst	Adsorbent	Carrier	Reactor
Isomerization cyclopropane to propylene [Bass60]	Moleccular sieve 13X (modified by Ni)	Moleccular sieve 13X (modified by Ni)	He	FBCR
Dehydrogenation of cyclohexane [Mats65, Schw78, Vill81, Schw80, Schw82a, Schw82b]	platinum-alumina supported catalyst	alumina	He	FBCR
Dehydroisomerization of n-butane to isobutene [Sad96]	Zeolites (modified with Cd, Pt)	zeolites	N_2	FBCR
Ammonia synthesis [Unge76]	promoted iron oxide	molecular sieves, alumina	N_2	FBCR
Cracking of cumene [Mura68]	silica-alumina	silica-alumina	H_2	FBCR
Dehydrogenation of cyclohexane [Carr93]	Platinum-alumina supported catalyst	alumina	He	CRACR
Hydrogenation of 1,3,5-trimethyl-benzene [Fish86, Fish89, Petr85]	$Pt-Al_2O_3$	Al_2O_3	N_2, H_2	TMBCR
Oxidation of carbon monoxide [Take77]	activated alumina	activated alumina	N_2	TMBCR
Oxidative coupling of methane [Tonk94, Krug96]	Sm_2O_3, $Y_1Ba_2Zr_3O_{9.5}$, $Y_1Ba_2Ge_3O_{3.5}/Al_2O_3$	molecular sieves, activated charcoal, zeolite with high silica/alumina ratio	N_2	SMBCR
Hydrogenation of 1,3,5-trimethyl-benzene [Bjor95, Ray95]	activated platinum on alumina	Chromosorb 106 (porous polymer adsorbent, cross-linked polystyrenne)	N_2, H_2	SMBCR
Reduction of nitrogen oxide [Agar88, Fiss06]	monoliths	monoliths	N_2, O_2	RFCR
Direct partial oxidation of methane to methanol [Bjor02]	activated charcoal	activated charcoal	He	SMBCR

Table 1-3: Updated survey for experimental applications of liquid chromatographic reactors based on [Fric05b]

Reaction and references	Catalyst	Adsorbent	Reactor
Racemic resolution of amino acid esters [Kalb89]	immobilized α-chymotrypsin and trypsin	Various	FBCR
Acid-catalyzed sucorose inversion [Laue80]	cation-exchange resin	cation-exchange resin	FBCR
Production of dextran [Bark87a, Bark87b, Zafa88]	dextransucrase	cation-exchange resin	FBCR
Esterification of acetic acid by ethanol [Sard93, Sard79]	Amberlyst 15	ion-exchange resin	FBCR
Transesterification of methyl acetate [Sard93]	acedic cation-exchange resin	acedic cation-exchange resin	FBCR
Hydrolysis of glycol diacetate [Sard93]	OH⁻	activated carbon	FBCR
Saccarification of starch to maltose [Sarm93]	maltogenase	ion-exchange resin	FBCR, CRACR
Hydrolysis of methyl formate [Cho80, Carr93]	H⁺	activated carbon	CRACR
Production of Bisphenol A [Kawa99]	Amberlyst 31	Amberlyst 31	SMBCR
Esterification of acetic acid by β-phenethyl alcohol [Kawa96]	Amberlyst 15	Amberlyst 15	SMBCR
Esterification of acetic acid by ethanol [Morb96]	Amberlyst 15	Amberlyst 15	SMBCR
Enzyme catalyzed sucrose inversion [Gane93b]	invertase	cation-exchange resin	SMBCR
Production of dextran [Bark89, Gane90, Bark92, Gane93]	dextrasucrase	cation-exchange resin	SMBCR
Isomerization of glucose [Hash93, Adac94]	Immobilized glucose isomerase	Ca^{2+} form of Y zeolite	CRHFS
Esterification of acetic acid and methanol [Lode02]	Amberlyst 15	Amberlyst 15	SMBR
Esterification of acetic acid and glycerol [Gelo03]	Amberlyst 15	Amberlyst 15	FBCR
Hydrolysis of methyl formate [Falk03, Schl06]	Dowex 50W-X8	Dowex 50W-X8	FBCR
Esterification of acetic acid by ethanol [Sain05]	Ion-exchange resins	Ion-exchange resins	FBCR
Esterification of acrylic acid and methanol [Strö05]	Amberlyst 15	Amberlyst 15	FBCR

In brief, reactive chromatography is still developing and there is deficit in accurate data to achieve reliable predictions of chromatographic reactors. More systematic studies are needed. In parallel with the studies on the esterfications carried out e.g. by Mazzoti et al. [e.g. Lode02, Gelo03, Strö06], further investigation on kinetics of ester hydrolysis reactions and also temperature optimization for performance of fixed-bed chromatographic reactors is necessary.

1.3 Research objectives and outline

To build up a database for the evaluation of the potential of chromatographic reactors systematic theoretical and experimental studies are performed regarding heterogeneously catalyzed hydrolysis reactions of the four esters methyl formate, ethyl formate, methyl acetate, and ethyl acetate. Studying these different reactions allows characterizing the different behaviour of fast and slow reactions. Strongly acidic cation-exchange resins are used simultaneously as catalyst and adsorbent. Experiments are carried out systematically using fixed-bed chromatographic reactors discontinuously operated at various temperatures, feed concentrations and flow rates. In particular, temperature effects on adsorption, desorption, reaction and separation are considered and quantified. Based on the parameters determined an extended equilibrium theory and a more detailed equilibrium-dispersion model will be used to estimate the feasibility of the chromatographic reactor operation and to compare theoretical predictions with experiments.

Chapter 2 summarized basics of a theoretical description of fixed-bed chromatographic reactors. Based on analyses of physicochemical phenomena and typical models of reactive chromatography, a two step modeling approach is proposed for feasibility studies and optimizations. In particular, the general feasibility of several types of reaction in a chromatographic reactor is studied and discussed in this chapter.

The four model reactions investigated the catalytic mechanisms and the characteristics of the stationary phases and catalysts applied are introduced in more detail in Chapter 3. Physical and thermodynamic properties of reactants and products are also provided.

In Chapter 4 are described the experimental set ups and the procedures applied for determination of model parameters.

Based on the experiments performed, important parameters of the presented models are estimated and given in Chapter 5. The dependence of the determined parameters on relevant operating conditions is discussed as well in this chapter.

Based on the determined parameters, the general feasibility of performing the hydrolysis reactions in a chromatographic reactor is predicted by the extended equilibrium model in Chapter 6. Selected experiments of the hydrolysis reactions are discussed qualitatively and compared with there predictions.

Chapter 7 contains an important result of this dissertation. This is the quantification of the rates of the hydrolysis reactions. This information is obtained from curve fittings between simulations using the equilibrium-dispersion model and experimental elution profiles. The results are validated at different conditions to ensure that the model is reliable and the model parameters are determined precisely.

Based on the validated model and the parameters obtained, the productivity and other objective functions of the hydrolysis reactions are evaluated theoretically in a broader parameter space in Chapter 8. In order to analysis the productivity, the impact of flow rate, temperature and injection volume is evaluated in parametric calculation.

In Chapter 9, final conclusions are made and an outlook regarding the applicability and potential of chromatographic reactors is given based on the theoretical and experimental results of this work.

Theoretical Description of Fixed-Bed Chromatographic Reactors (FBCRs)

A FBCR is a tubular reactor packed with a catalytic stationary phase. Through this packing, a mobile fluid phase is transported continuously. However, unlike to classical operation mode in plus flow tubular reactor with continuous feeding, reactants are periodically dosed into the FBCR as rectangular pulses. Due to coupling of reaction and chromatographic separation, the processes that take place simultaneously inside a FBCR are very complicated and their description has to be based on a comprehensive understanding about characteristics of solid particles, fixed-bed structure, convection, diffusion, adsorption, and reaction kinetics. The theoretical description of FBCRs introduced in this chapter is the basis for the experimental and simulation studies presented in Chapters 4, 5, 6 and 7.

2.1 Mathematical modeling of FBCRs

2.1.1 Overview

Modeling is an important step to design processes in chemical engineering. From limited preliminary experiments studied for parameters determination and model validation, validated models allow virtual predicting conditions not studied experimentally, optimize and scale-up the process. Modeling studies become more and more important for designing complicated and expensive processes like chromatographic separation techniques. To quantify chromatographic separations, the first mathematical models were presented in the 1930s and early 1940s (e.g., [Wils40, Vaul43]). Recent developments have been summarized by [Bell 91, Gane93a, Seid95, Gu95, Guio03, Mich05 and Guio06].

In general, models used to describe chromatographic reactors can be considered as extended models of chromatographic separation columns taking into account reactions.

They are also developed based on general theories of fixed-bed reactors that have been reviewed e.g. by [Eigen05]. Summaries of models developed for FBCRs were given by [Vill81, Sard93, Fick05, and Borr05]. Depending on different initial assumptions, the complexity of the models depends on how many physicochemical phenomena are accounted for and in which detail. A simple classification of developed FBCR models is given in Figure 2-1.
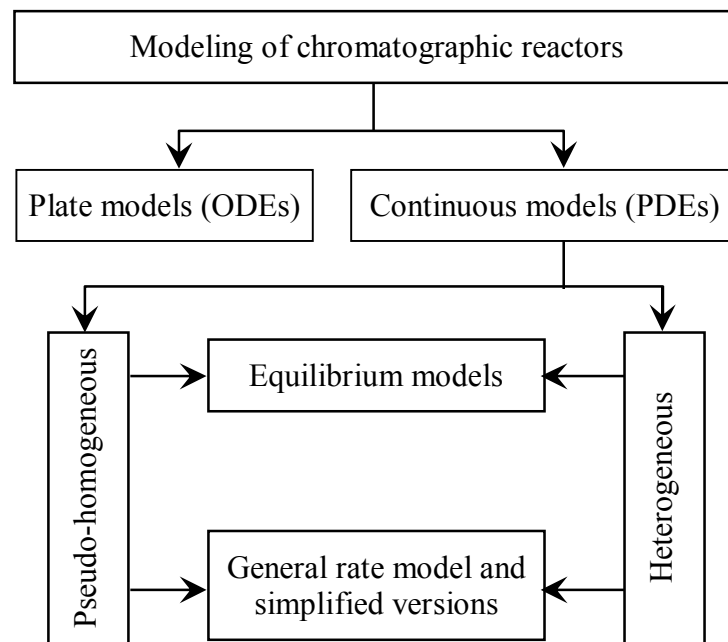
Figure 2-1: Classification of models used for FBCRs

In Figure 2-1, two classes of models can be distinguished. The plate models result in systems of ordinary differential equations (ODEs) describing the mass and energy balances of a discrete number of plates, whereas the continuous models are given in the form of partial differential equations (PDEs). Although most models consider propagation of components essentially in axial direction (1D), a few researchers have attempted the mathematical description of both axial and radial profiles in a column (e.g., [Gu95]). Due to the homogeneous packings achieved in chromatographic columns filled with relative small particles, radial profiles of concentration and temperature are often negligible.

Plate models:

The chromatographic column is considered as a series of interconnected theoretical plates. In each plate, the mobile phase and the stationary phase are considered to be in equilibrium. Axial dispersion is indirectly represented in these models through the number

of plates. All effects of mass transfer resistances are typically neglected. There are two different plate models applied to describe chromatographic separations. The Martin and Synge model is a continuous plate model [Mart41], whereas the Craig model is a discontinuous plate model [Crai44]. For pulse injections typical in linear chromatography, the responses given by Martin and Synge model follow a Poisson distribution, while the Craig model gives binomial distributions [Guio06]. Both models are equivalent at high number of theoretical plates, because for small injections the predicted elution profiles have then a tendency to reach the Gaussian distribution. The Martin and Synge model was applied e.g. by [Schw78] for modeling of chromatographic reactors.

[Seid95] applied a mathematical description based on the simple mixed cells in series model given by [West84]. This model has been successfully applied for modeling reactive chromatography by [Falk03].

Although plate models offer a simple way to describe chromatographic processes, they have some drawbacks. These models can not be used easily to describe separately different physical kinetic phenomena causing band broadening. In principle the number of theoretical plates depends on specific interactions between each components and the stationary phase. Therefore, using an average number of theoretical plates for all components leads to reduced accuracy of calculations.

Continuous models:

Equilibrium models: The equilibrium theory was used in the first mathematical models to describe single component chromatography (e.g., [Wilson40, Vaul43, etc.]). This theory is based on the assumptions that equilibrium between solution and adsorbent is instantaneously established and the effects of diffusion can be neglected. Using the same assumptions, many models for multicomponents chromatography were developed to explain interactions of components during percolation. The models are usually represented by systems of PDEs. [Helf67] presented the concept of "coherence of boundaries". Trajectories of components were calculated analytically by "h-transformation". This approach was reviewed by a series of articles by [Helf93], [Helf96], and [Helf97]. Equivalent results were obtained by the so-called method of characteristics given by [Rhee70]. Applications of this theory to nonreactive chromatography were presented in [Rhee86a] and [Rhee86b].

The equilibrium theory has been extended to reactive chromatography by Kienle and co-workers [Grün04, Grün06, and Vu05]. It will be shown later in this dissertation that the extended equilibrium theory can be used as a strong tool to evaluate feasibility, i.e., to

clarify whether total conversion of reactants and total separation of products are possible in a chromatographic reactor.

General rate model and simplified versions: The general rate model [Guio06] allows considering simultaneously all possible contributions to mass transfer kinetics. These contributions are usually expressed as a system of PDEs which states mass conservation and transportation. Although the model is complex with many input parameters, it has the potential to achieve an accurate description of non-ideal reactive chromatographic processes. Depending on the initial assumptions, the general rate model can be simplified into simpler models. In addition to compulsory terms of convection, adsorption and reaction, other terms (e.g., dispersion, limited mass transfer rate) can be considered. Otherwise, two or more effects of dispersion, adsorption kinetic and mass transfer resistances can be lumped into a single effective kinetic parameter. Below, a simplified rate model (equilibrium - dispersion model) with coefficients lumping axial dispersion and mass transfer is represented in Section 2.1.2.2.

Due to the nonlinearity in the mass balance equations, numerical methods are needed to solve these models. However, special cases with linear adsorption isotherm and first order reaction rate expression can be solved analytically (e.g., using Laplace transforms techniques [Vill81]).

Summary, the continuous models have certain advantages in predictions and simulations of FBCRs compared to the plate models. Therefore, only the continuous models are applied below.

2.1.2 Continuous models

2.1.2.1 *Phase distribution*

In chromatographic techniques, distribution of phases is very important for detailed modeling and simulation. That is reason for representing definitions of porosities and phase ratios in the beginning of this section.

With a chromatographic column packed with porous particles and a pore network fully filled with liquid, the volume of a column V_{col} can be divided into a volume of liquid phase V^L and solid material fraction that forms particles in a volume V_{solid}. The volume of the liquid phase includes sub-volumes of interstitial liquid fraction V_{int} and intraparticle liquid fraction V_{pore}.

$$V_{col} = \frac{\pi \, d_{col}^2}{4} L = V^L + V_{solid} = V_{int} + V_{pore} + V_{solid} \qquad (2\text{-}1)$$

The volume of stationary phase V^S consists of the intraparticle liquid fraction and the volume of solid material:

$$V^S = V_{pore} + V_{solid} \qquad (2\text{-}2)$$

If the column is homogeneously and well packed, the total porosity ε_t of a fixed-bed is:

$$\varepsilon_t = \frac{V^L}{V_{col}} \qquad or \qquad (1-\varepsilon_t) = \frac{V_{solid}}{V_{col}} \qquad (2\text{-}3)$$

From these volume definitions, external and internal porosities can be formulated to give:

External porosity: $\qquad \varepsilon = \dfrac{V_{int}}{V_{col}}$ $\qquad\qquad\qquad (2\text{-}4)$

Internal porosity: $\qquad \varepsilon_p = \dfrac{V_{pore}}{V^S}$ $\qquad\qquad\qquad (2\text{-}5)$

The internal porosity is independent on particle size and shape, whereas the external porosity is a function of particle size and shape. Contribution of the external porosity and the internal porosity add up to the total porosity:

$$\varepsilon_t = \frac{V_{int} + V_{pore}}{V_{col}} = \varepsilon + (1-\varepsilon)\varepsilon_p \qquad (2\text{-}6)$$

The phase ratio F is an important characteristic constant of a chromatographic column. It is defined as the ratio between solid phase volume fraction and total volume of the liquid fractions. It is related to the total porosity by equation [Guio06]:

$$F = \frac{V_{solid}}{V_{int} + V_{pore}} = \frac{1 - \varepsilon_t}{\varepsilon_t} \qquad (2\text{-}7)$$

2.1.2.2 Differential mass balance equations and equilibrium-dispersion model

Mathematical models for FBCR are typically derived using the following general assumptions:

(i) The column is homogeneously packed.
(ii) No radial concentration and temperature gradients occur in the column.
(iii) The volumetric flow rate is constant.
(iv) Intraparticle transport can be quantified in a simplified manner using linear driving force expressions.

Let us consider a differential volume element of a column dV_{col}, with a differential length dx, a diameter d_{col}, and the cross-section area of the column A_{col} (Figure 2-2):

$$dV_{col} = \frac{\pi \, d_{col}^2}{4} dx = A_{col} \, dx \qquad\qquad (2\text{-}8)$$
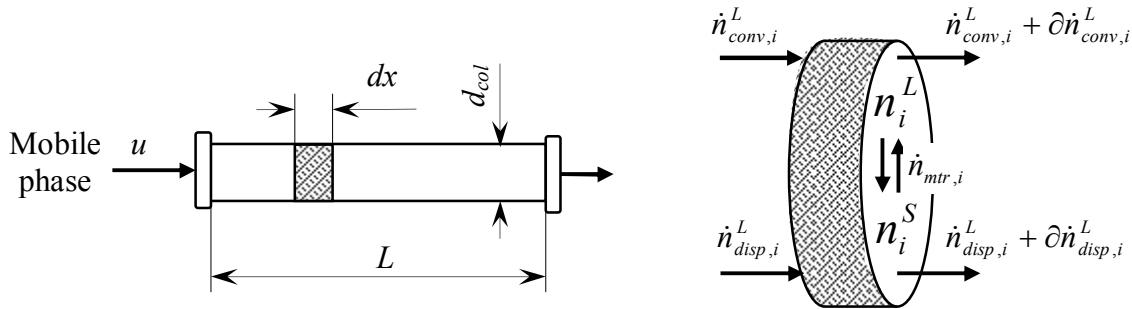
Figure 2-2: Introduction of notation used

The mass balances for one component i of a mixture of N_C components in the differential volume element of the column are:

For the liquid phase (ε_t):

$$\frac{\partial n_i^L}{\partial t} = -\partial \dot{n}_{conv,i}^L - \partial \dot{n}_{disp,i}^L + \partial \dot{n}_{mtr,i} + \left.\frac{\partial n_i^L}{\partial t}\right|_{R,\text{hom}} \qquad for \quad i = 1, N_C \qquad (2\text{-}9a)$$

For the solid phase (1-ε_t):

$$\frac{\partial n_i^S}{\partial t} = -\partial \dot{n}_{mtr,i} + \frac{\partial n_i^S}{\partial t}\bigg|_{R,het} \qquad\qquad for \quad i = 1, N_C \qquad\qquad (2\text{-}9b)$$

The terms in above equations can be characterized as follows:

Accumulation in liquid phase:

$$\frac{\partial n_i^L}{\partial t} = dV^L \frac{\partial c_i}{\partial t} = dV_{col}\varepsilon_t \frac{\partial c_i}{\partial t} \qquad\qquad (2\text{-}10)$$

Accumulation in solid phase:

$$\frac{\partial n_i^S}{\partial t} = dV^S \frac{\partial q_{av,i}}{\partial t} = dV_{col}\left(1 - \varepsilon_t\right)\frac{\partial q_{av,i}}{\partial t} \qquad\qquad (2\text{-}11)$$

Convection:

$$\partial \dot{n}_{conv,i}^L = \dot{V}\,\partial c_i = u\varepsilon_t A_{col}\partial c_i \qquad\qquad (2\text{-}12)$$

Axial dispersion:

$$\partial \dot{n}_{disp,i}^L = \partial\left[-D_{ax,i}\varepsilon_t A_{col}\frac{\partial c_i}{\partial x}\right] = -D_{ax,i}\varepsilon_t A_{col}\,\partial\left(\frac{\partial c_i}{\partial x}\right) \qquad\qquad (2\text{-}13)$$

Mass transfer between phases:

$$\partial \dot{n}_{mtr,i} = \left(1 - \varepsilon_t\right)\beta_i\left[q_{av,i} - q_i^*\left(\overline{c}_i\right)\right] \qquad\qquad (2\text{-}14)$$

Homogeneous reactions:

$$\frac{\partial n_i^L}{\partial t}\bigg|_{R,\text{hom}} = dV^L \frac{\partial c_i}{\partial t}\bigg|_{R,\text{hom}} = dV_{col}\varepsilon_t \sum_{i=1}^{N_R} v_{i,j} r_j^{\text{hom}} \qquad\qquad (2\text{-}15)$$

Heterogeneous reactions:

$$\frac{\partial n_i^S}{\partial t}\bigg|_{R,het} = dV^S \frac{\partial q_{av,i}}{\partial t}\bigg|_{R,het} = dV_{col}\left(1 - \varepsilon_t\right)\sum_{i=1}^{N_R} v_{i,j} r_j^{het} \qquad (2\text{-}16)$$

in which, n_i^L and n_i^S are the amounts of component i in the liquid and solid phases, respectively; c_i and $q_{av,i}$ are the liquid-phase concentrations and the average loadings of component i, respectively; $D_{ax,i}$ in Eq. 2-13 is the axial dispersion coefficient for component i. For the mass transfer term, a linear driving force was applied and β_i is the internal mass transfer coefficient for component i; $q_i^*(\overline{c})$ is the loading of component i in the solid phase in equilibrium with all liquid-phase concentrations; the N_R are the number of reactions involved; $v_{i,j}$ are stoichiometric coefficients of component i in reaction j; r_j^{hom} and r_j^{het} are reaction rates in liquid (homogeneous) and solid (heterogeneous) phases.

If the volumetric flow rate $\dot{V}$ and the total porosity ε_t are constants, the linear velocity u is also a constant:

$$u = \frac{\dot{V}}{\varepsilon_t \frac{\pi\, d_{col}^2}{4}} \tag{2-17}$$

Therefore, Eqs. 2-9a and 2-9b can be rewritten for whole the column to give:

For the liquid phase:

$$\varepsilon_t \frac{\partial c_i}{\partial t} + \varepsilon_t u \frac{\partial c_i}{\partial x} = \varepsilon_t \sum_{i=1}^{N_R} v_{i,j} r_j^{\mathrm{hom}} + \varepsilon_t D_{ax,i} \frac{\partial^2 c_i}{\partial x^2} + \left(1-\varepsilon_t\right)\beta_i \left[q_{av,i} - q_i^* \left(\overline{c}\right) \right] \tag{2-18a}$$

For the solid phase:

$$\left(1-\varepsilon_t\right)\frac{\partial q_{av,i}}{\partial t} = \left(1-\varepsilon_t\right)\sum_{i=1}^{N_R} v_{i,j} r_j^{het} - \left(1-\varepsilon_t\right)\beta_i \left[q_{av,i} - q_i^* \left(\overline{c}\right) \right] \tag{2-18b}$$

The two conservation equations 2-18a and 2-18b represent a typical 1D heterogeneous two-phase model.

If effects of mass transfer resistance can be neglected (i.e., $\beta_i = \infty$ and $q_{av,i} = q_i^* \left(\overline{c}\right)$), these two equations can be lumped together to give:

$$\frac{\partial}{\partial t}\left(c_i + \frac{1-\varepsilon_t}{\varepsilon_t} q_{av,i}(\overline{c}) \right) + u \frac{\partial c_i}{\partial x} = \varepsilon_t \sum_{i=1}^{N_R} v_{i,j} r_j^{\mathrm{hom}} + \frac{1-\varepsilon_t}{\varepsilon_t} v_{i,j} r_j^{het} + D_{ax,i} \frac{\partial^2 c_i}{\partial x^2} \tag{2-19}$$
$$\textit{for } i = 1, N_C \textit{ and } j = 1, N_R$$

Often contribution of homogeneous reactions can be neglected. If instead of $D_{ax,i}$ and β_i, an apparent (lumped) dispersion coefficient $D_{ap,i}$ is used ($D_{ap,i}(D_{ax,i}, \beta_i) > D_{ax,i}$), the following equilibrium-dispersion model can be formulated:

$$\frac{\partial}{\partial t}\left(c_i + \frac{1-\varepsilon_t}{\varepsilon_t} q_{av,i}(\overline{c}) \right) + u \frac{\partial c_i}{\partial x} = \frac{1-\varepsilon_t}{\varepsilon_t} v_{i,j} r_j^{het} + D_{ap,i} \frac{\partial^2 c_i}{\partial x^2} \tag{2-20}$$
$$\textit{for } i = 1, N_C \textit{ and } j = 1, N_R$$

To solve the mass balance equation 2-20, appropriate initial and boundary conditions have to be specified. As the initial condition for the liquid phase concentrations typically a constant is assumed:

$$c_i(x, t=0) = c_i^{init} \qquad for \ i = 1, N_C \qquad (2\text{-}21)$$

The standard Danckwerts boundary conditions for a rectangular injection profile at the column inlet are [Danc53]:

$$c_i(x=0,t) = \begin{cases} c_i^{inj} + \dfrac{D_{ap,i}}{u} \dfrac{\partial c_i}{\partial x}\bigg|_{x=0,t} & for \ 0 \le t \le t^{inj} \\[4mm] \dfrac{D_{ap,i}}{u} \dfrac{\partial c_i}{\partial x}\bigg|_{x=0,t} & for \ t \ge t^{inj} \end{cases} \qquad with \ t^{inj} = \dfrac{V^{inj}}{u \dfrac{\pi}{4} d_{col}^2 \varepsilon_t} \qquad (2\text{-}22)$$

where c_i^{init} are the initial concentrations; c_i^{inj} are the injection concentrations; t^{inj} is the injection time; V^{inj} is the injection volume; L is the column length.

At the outlet holds:

$$\frac{\partial c_i}{\partial x}\bigg|_{x=L,t} = 0 \qquad for \ i = 1, N_C \qquad (2\text{-}23)$$

If the concentrations of all components in the liquid and the solid phases are permanently in equilibrium throughout the entire column and the corresponding adsorption equilibria are linear, Eq. 2-20 can be furthermore simplified through the introduction of the equilibrium constants K_i (i.e., $q_i^* = K_i c_i$):

$$\frac{\partial c_i}{\partial t} = \left(1 + \frac{1-\varepsilon_t}{\varepsilon_t} K_i\right)^{-1} \left[-u \frac{\partial c_i}{\partial x} + D_{ap,i} \frac{\partial^2 c_i}{\partial x^2} + \frac{1-\varepsilon_t}{\varepsilon_t} v_{i,j} r_j^{het}(\overline{c})\right] \qquad (2\text{-}24)$$
$$for \ i = 1, N_C$$

In this work, the equilibrium-dispersion model in Eq. 2-24 will be used for FBCR simulations and kinetics study in Chapters 7 and 8.

To solve Eqs 2-24, the software Presto was employed. This software was developed using the complier Borland C^{++} and commercialized by CIT GmbH[*]. It provides efficient ODE

---

[*] *http://www.cit-wulkow.de/*

and PDE solvers based on Galerkin h-p-algorithm in combination with robust tools for parameter estimation [CIT00]. It further allows for the flexible incorporation of different kinetic models and the convenient input and analysis of various types of primary experimental data.

2.1.2.3 *Extended equilibrium model*

Instead the assumption (iv) given in Section 2.1.2.1, the following assumption used in the equilibrium models is:

(iv) Effects of axial dispersion and mass transfer resistance can be neglected. ($D_{ax,i} = 0$, $\beta_i \rightarrow \infty$, i.e., $D_{ap,i} = 0$).

Thus, the classical equilibrium model can be considered as a simplified model of Eq. 2-20. For non-reactive chromatography ($r_j^{hom} = r_j^{het} = 0$) holds:

$$\frac{\partial}{\partial t}\left(c_i + \frac{1-\varepsilon_t}{\varepsilon_t} q_{av,i}\left(\overline{c}\right) \right) + u \frac{\partial c_i}{\partial x} = 0 \qquad \text{for } i = \overline{1, N_C}$$

$$q_{av,i} = q_{av,i}\left(c_1, c_2, \ldots c_{N_C} \right) \tag{2-25}$$

This model is extensively studied in particular by [Rhee86a, Rhee86b].

The equilibrium model has been extended to reactive chromatography by Kienle and co-worker (e.g., Ref. [Grün04, Grün06, and Vu05]). The right side of Eq. 2-25 then contains a term for heterogeneous reactions:

$$\frac{\partial}{\partial t}\left(c_i + \frac{1-\varepsilon_t}{\varepsilon_t} q_{av,i} \right) + u \frac{\partial c_i}{\partial x} = \sum_{j=1}^{N_R} v_{i,j} r_j^{het} \qquad \text{for } i = 1, N_C$$

$$q_{av,i} = q_{av,i}\left(c_1, c_2, \ldots c_{N_C} \right) \qquad \text{for } j = 1, N_R \tag{2-26}$$

in which, $v_{i,j}$ is again a N_R x N_C matrix of stoichiometric coefficients. Eq. 2-26 is a set of N_C equations constrained by N_R algebraic expressions of reaction rates. In this equation set the indeterminable reaction rates can be eliminated. This model also uses the initial and boundary conditions given in Eqs. 2-21, 2-22 and 2-23. However, if the injection time in Eq. 2-22 is large enough the whole fixed bed reaches an as completely equilibrium state corresponding to the inlet concentration. For a simplified representation, Eq. 2-26 can be rewritten in vector notation:

$$\frac{\partial}{\partial t}\left(c + \frac{1-\varepsilon_t}{\varepsilon_t} q(c)\right) + u\frac{\partial c}{\partial x} = vr \tag{2-27}$$

$$q, c \in R^{N_C} \qquad r \in R^{N_R}$$

For sufficiently fast reversible chemical reactions with linear expression in the term of reaction rates, the ideas of transformed variables given by [Ung95] can be applied. This is achieved by choosing N_R reference components and splitting the concentration vectors into two parts:

$$c = \left[c^I, c^{II}\right], \quad q = \left[q^I, q^{II}\right] \quad \text{with } c^I, q^I \in R^{N_R} \text{ and } c^{II}, q^{II} \in R^{N_C - N_R} \tag{2-28}$$

Accordingly, the matrix of stoichiometric coefficients can be split into two parts v^I and v^{II}. Where v^I has a dimension of N_R x N_R and v^{II} has a dimension of $(N_C - N_R)$ x N_R

$$v = \left[v^I, v^{II}\right] \tag{2-29}$$

Solving a set of N_C equations formulated by Eq. 2-26 is replaced by solving $(N_C - N_R)$ following vector equations:

$$\frac{\partial}{\partial t}\left(C + \frac{1-\varepsilon_t}{\varepsilon_t} Q(C)\right) + u\frac{\partial C}{\partial x} = 0 \tag{2-30}$$

with transformed concentration variables according to:

$$C = c^{II} - v^{II}\left(v^I\right)^{-1} c^I \quad \text{and} \quad Q = q^{II} - v^{II}\left(v^I\right)^{-1} q^I$$

$$C, Q, c^{II}, q^{II} \in R^{N_C - N_R} \qquad\qquad c^I, q^I \in R^{N_R} \tag{2-31}$$

Eq. 2-30 is analogue completely to the non reactive model in given Eq. 2-25.

In order to predict pulse and wave patterns of reactive or nonreactive process, the equilibrium models are usually presented in the hodograph space. The construction of wave solutions for chromatographic reactors is based on the pathgrid of eigenvectors of Jacobians $\partial Q(C)/\partial C$ of transformed equilibrium $Q(C)$ defined by Eq. 2-31. The computation of this Jacobian is not directly possible since the transformed equilibrium functions are not explicitly known. However, this Jacobian can be indirectly calculated using a procedure given by [Grün06]:

$$\frac{\partial \boldsymbol{Q}}{\partial \boldsymbol{C}} = \frac{\partial \boldsymbol{Q}}{\partial \boldsymbol{c}} \frac{\partial \boldsymbol{c}}{\partial \boldsymbol{C}} \qquad (2\text{-}32)$$

In this equation, the former derivative $\partial \boldsymbol{Q} / \partial \boldsymbol{c}$ involves adsorption equilibrium isotherms according to:

$$\frac{\partial \boldsymbol{Q}}{\partial \boldsymbol{c}} = \frac{\partial}{\partial \boldsymbol{c}} \left[\boldsymbol{q}^{II} - \boldsymbol{v}^{II} \left(\boldsymbol{v}^{I} \right)^{-1} \boldsymbol{q}^{I} \right] \qquad (2\text{-}33)$$

The latter derivative $\partial \boldsymbol{c} / \partial \boldsymbol{C}$ can be expressed by the following formula:

$$\frac{\partial \boldsymbol{c}}{\partial \boldsymbol{C}} = -\left(\frac{\partial \boldsymbol{F}}{\partial \boldsymbol{c}} \right)^{-1} \frac{\partial \boldsymbol{F}}{\partial \boldsymbol{C}} \qquad (2\text{-}34)$$

where $\boldsymbol{F}$ involves the concentration vector $\boldsymbol{c}$, transformed concentration $\boldsymbol{C}$ and N_R algebraic constrains for chemical equilibrium of all chemical reactions:

$$0 = \boldsymbol{F}(\boldsymbol{c}, \boldsymbol{C}) = \begin{bmatrix} \boldsymbol{C} - \boldsymbol{c}^{II} + \boldsymbol{v}^{II} \left(\boldsymbol{v}^{I} \right)^{-1} \boldsymbol{c}^{I} \\ f\left(\boldsymbol{K}_{eq}, \boldsymbol{c} \right) \end{bmatrix} \qquad \boldsymbol{K}_{eq} \in N_R \qquad (2\text{-}35)$$

The pathgrid can be computed by integrating along the eigenvectors $r_j(\boldsymbol{C})$ of Jacobian Eqs 2-32, 2-33 and 2-34 for suitable initial conditions according to:

$$\frac{d\boldsymbol{C}}{d\xi} = r_j(\boldsymbol{C}) \qquad \boldsymbol{C}(\xi = 0) = \boldsymbol{C}^{init} \qquad (2\text{-}36)$$

The independent variable ξ in this equation represents some suitable parameterizations of the curve in hodograph space. Since the derivatives in Eqs 2-32, 2-33 and 2-34 depend on the concentration vector $\boldsymbol{c}$, the vector $\boldsymbol{c}$ has to be determined simultaneously for each value of $\boldsymbol{C}$ along the curve from implicit algebraic equations Eq. 2-35. This can be done with a DAE (differential algebraic equation) solver like DASSL introduced by [Bren89].

2.1.3 Performance criteria

Typically, goals of a reactive chromatographic process are higher conversion, purity, productivity and yield. In order to optimize such a process, the relation between these process variables and the operating parameters should be well understood.

2.1.3.1 Cycle time and productivity

The typical periodic dosing performance of a FBCR is illustrated in Figure 2-3. The cycle time t^{cyc} is the time which separates two successive injections.

$$t^{cyc} = t^{end} - t^{begin} \qquad (2\text{-}37)$$

The addition time between the end of one injection and the beginning of the next injection can be called the regeneration time. The cycle time can be defined in the elution profile by the two times t^{begin} and t^{end}. It depends on the injection time and the spreading of the elution profile under operating conditions. The two characteristic times can be specified using a certain threshold concentration marking the beginning and the end of the elution profile at the end of the column. Due to [Guio06], the threshold concentration can be set often at 1 x 10^{-9} mol/L. It might be also formulated as a relative fraction of the injection concentration. The time between two injections is required to avoid band overlapping and to allow for complete column regeneration.

In order to compare different reactor concepts, a dilution ratio can be introduced as follows [Falk03]:

$$\varphi = \left(1 - \frac{t^{inj}}{t^{cyc}} \right) \qquad (2\text{-}38)$$
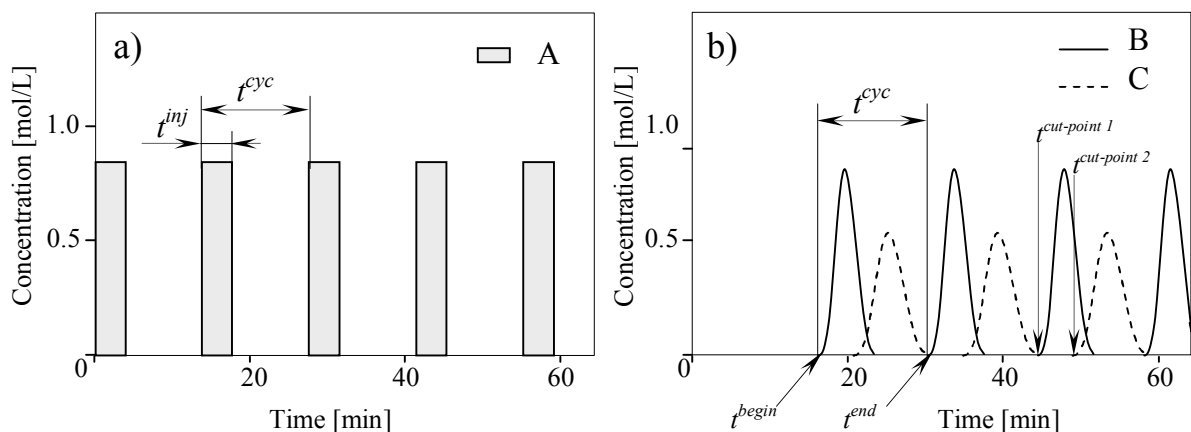
Figure 2-3: Typical pulsed dosing performance for a FBCR (reaction $A \rightarrow B + C$)
a) Periodic pulse dosing of reactant A at reactor inlet
b) Outlet concentrations of B and C

Productivity or production rate is the amount of product per cycle time at the required degree of purity.

$$PR_i = \dot{n}_i^{out} = \frac{\int_{t^{cut-point\,2}}^{t^{cut-point\,1}} c_i(t)\dot{V}dt}{t^{cyc}} \tag{2-39}$$

For scale-up considerations, volume and mass related productivities are used. These parameters are ratios between the productivity and the volume or the cross section area of the column.

$$PR_i^V = \frac{PR_i}{V_{col}} \tag{2-40}$$

or

$$PR_i^A = \frac{PR_i}{A_{col}} \tag{2-41}$$

2.1.3.2 *Conversion*

In order to evaluate the success of the reaction process, conversion is a useful quantity. For a cycle chromatographic reactors, the conversion of a feed component A can be expressed by the following equation:

$$X_A = \frac{\dot{n}_A^{in} - \dot{n}_A^{out}}{\dot{n}_A^{in}} = \frac{c_A^{Feed} t^{inj} - \int_{t^{begin}}^{t^{end}} c_A(t)dt}{c_A^{Feed} t^{inj}} \tag{2-42}$$

For reversible reactions, most reactors can not convert completely reactants. Based on mass conservation, the conversion can be calculated by in coming and out going mass flows of the whole process. The integration of the elution profile of the reactant A corresponds to the unconverted amount.

2.1.3.3 *Yield*

The recovery yield of a desired product is the ratio between its amount collected with the required purity in the purified fraction and its ideal amount which can be collected in case of complete conversion of reactant A.

$$Y_i = \frac{v_A}{v_i} \frac{\int_{t^{cut\,point\,2}}^{t^{cut\,point\,1}} c_i(t)\dot{V}dt}{c_A^{Feed} V^{inj}} \tag{2-43}$$

2.1.3.4 Purity

The purity of a component i is defined as a ratio between amount of this component and total amount of all components in the collected fraction (solvent excluded).

$$Pu_i = \frac{n_i}{\sum_{i=1}^{N_C} n_j} \tag{2-44}$$

where N_C is the number of components in the collected fraction. The purity is a constraint for the separation. As a typical a value of 99% is considered below. The purity requirements determine the cut-points when fraction collection begins and ends. Therefore they determine yield, productivity and thus the economics of the process.

2.2 Model parameters

The models introduced in Section 2.1 contain model parameters. Theories and correlations related to these parameters are shortly summarized here. Experimental procedures to determine some of them are given in Chapter 4.

2.2.1 Adsorption equilibrium isotherms

2.2.1.1 Thermodynamics of adsorption

For dilute concentration, the standard thermodynamic functions for adsorption processes are related to the adsorption equilibrium constant [Ruth84]. The molar Gibbs free energy of adsorption (ΔG_i) is related to the Henrry constant K_i by

$$\Delta G_i = -RT \ln K_i \tag{2-45}$$

Normally, adsorption is an exothermic process because energy is liberated, so the enthalpy of adsorption is negative. Because K_i is an equilibrium constant, the molar enthalpy of adsorption (ΔH_i) can be determined by van't Hoff's formula:

$$\frac{\partial(\ln K_i)}{\partial(1/T)} = -\frac{\Delta H_i}{R} \tag{2-46}$$

The molar entropy of adsorption (ΔS_i) can be calculated from ΔG_i and ΔH_i by

$$\Delta S_i = -\frac{\Delta G_i - \Delta H_i}{T} \tag{2-47}$$

2.2.1.2 *Single component isotherm*

In liquid chromatography, the adsorption equilibria is usually expressed at isothermal conditions by the relationships between the loading of solute in the stationary phase (q_i) and the concentrations in the mobile phase (c_i). These relationships are very important for predictions of elution times and peak shapes. For illustration, Figure 2-4 shows three typical single solute isotherm models and their influences on peak shapes of discontinuous chromatography.

In Figure 2-4a is shown a case for a linear isotherm with a slope K_i (Henrry constant, Eq. 2-48). Ideally, for a rectangular injection, the elution profile of single component is again a rectangular pulse (Equilibrium model). However, due to some band broadening effects, the elution profile for real linear chromatography is a symmetrical peak which is a Gaussian distribution type. The retention time for the maximum of the peak can be calculated by Eq. 2-49.

$$K_i = \frac{q_i}{c_i} \tag{2-48}$$

$$t_{R,i(\max)} = t_0 \left(1 + \frac{1-\varepsilon_t}{\varepsilon_t} K_i \right) \tag{2-49}$$

in which, t_o is hold-up time of a non-retained component through a column length L. It can be determined by:

$$t_o = \frac{L}{u} \tag{2-50}$$

When the maximum concentration of the elution band is out of the linear range of the adsorption isotherm, their slopes can be convex or concave, depending on the interactions of the solute component with the stationary and mobile phases. For convex isotherms (illustrated in Figure 2-4b), the slope decreases by increasing the concentration. Consequently, higher concentration regions move faster than lower concentration regions. Thus, the elution profile is sharpened at the front and spread at the rear. The retention time of the compressed (sharp, shock) front is related to the isotherm chord and can be

calculated by Eq. 2-51, whereas that of the dispersed rear can be calculated by Eq. 2-52 [Guio06, Seid04]:

$$t_{R,i} = t_0 \left(1 + \frac{1-\varepsilon_t}{\varepsilon_t} \frac{\Delta q_i}{\Delta c_i} \right) \tag{2-51}$$

$$t_{R,i}\left(c_i^*\right) = t_0 \left(1 + \frac{1-\varepsilon_t}{\varepsilon_t} \left.\frac{dq_i}{dc_i}\right|_{C_i^*} \right) \tag{2-52}$$

For a concave isotherm shown in Figure 2-4c, opposite behavior is observed and the elution profile is dispersed at the front and compressed at the rear. The retention time of a dispersed front is related to the corresponding local slope of the isotherm and can be calculated by Eq. 2-52, whereas that of a compressed rear can be calculated by Eq. 2-51 [Guio06, Seid04].
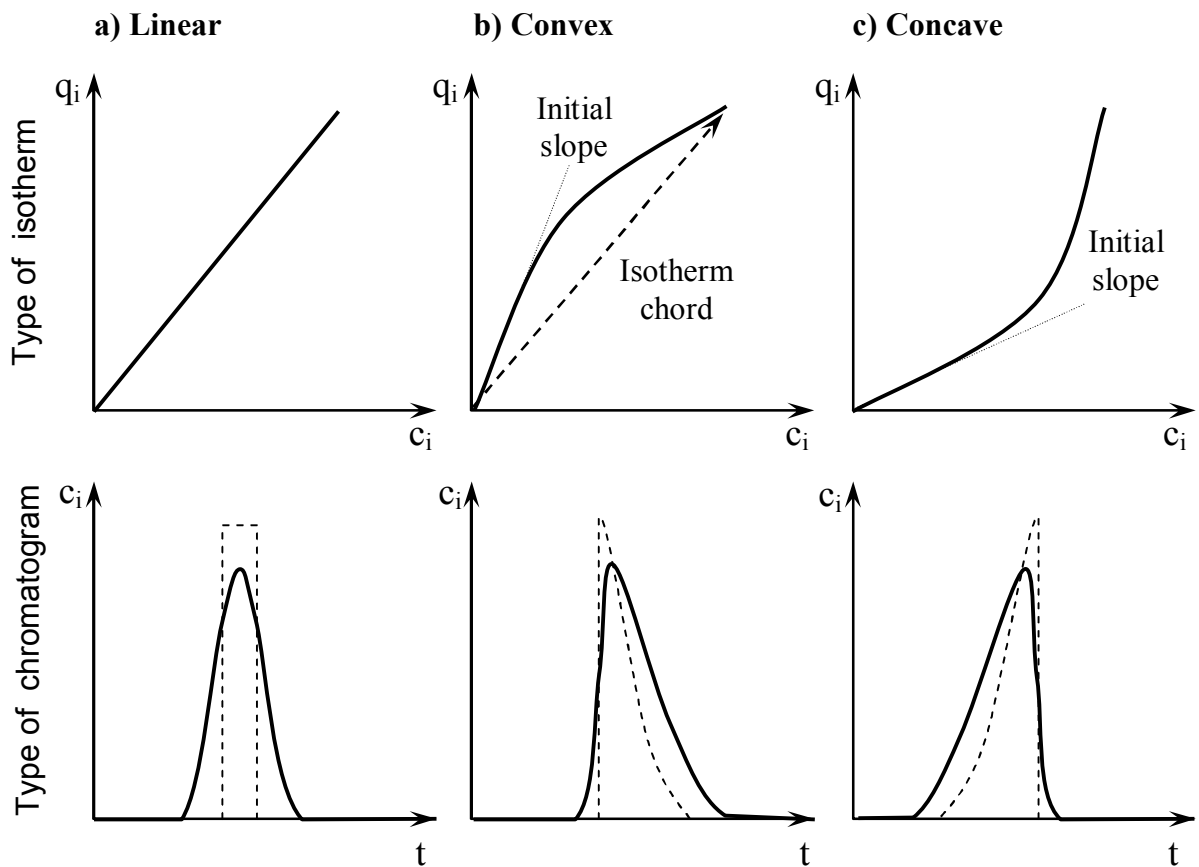
Figure 2-4: The influence of isotherm models on peak shapes
Ideal chromatogram ($D_{ax,i} = 0$, dashed lines);   Real chromatograms (solid lines)

There are many models available describing non-linear isotherms, e.g. Langmuir, Bilangmuir, Freudlich, Flowler models. A summary of these models was given by [Guio06]. However, the simplest and often realistic model is the Langmuir isotherm:

$$q_i = \frac{K_i c_i}{1 + b_i c_i} \tag{2-53}$$

in which K_i is again the initial slope and b_i is a constant quantifying the adsorption energy. The isotherm is convex if $b_i > 0$ or concave if $b_i < 0$. The concave isotherm is also called the anti-Langmuir isotherm [Guio06].

2.2.1.3 Retention factor

The retention time of a component depends on the column geometry and mobile phase flow rate. Therefore the retention behavior is usually characterized by the retention factor ($k_i^{'}$), which is also called the capacity factor.

$$k_i^{'} = \frac{t_{R,i} - t_0}{t_0} \tag{2-54}$$

The retention factor can be calculated from the adsorption equilibrium constant by:

$$k_i^{'} = \left(\frac{1 - \varepsilon_t}{\varepsilon_t} \right) K_i \tag{2-55}$$

2.2.1.4 Separation factor

In order to estimate separation ability of two components *i* and *j*, a separation factor ($\alpha_{i,j}$) is defined by the ratio between their Henrry constants or capacity factors.

$$\alpha_{i,j} = \frac{K_j}{K_i} = \frac{k_j^{'}}{k_i^{'}} \; with \; K_j > K_i \tag{2-56}$$

For this ratio per definition always holds that $\alpha_{i,j} > 1$.

2.2.1.5 Resolution

In linear chromatography, the resolution R_S is defined as the ratio of the differences between the retention times of the maxima of two successive bands and their average width. The definition is also valid in nonlinear chromatography but there it has limited applicability [Guio06].

$$R_S = \frac{2\left(t_{R,j} - t_{R,i}\right)}{w_i + w_j} \qquad with \; t_{R,j} > t_{R,i} \qquad (2\text{-}57)$$

In Eq. 2-57 $t_{R,i}$ and $t_{R,j}$ are the retention times of components i and j; w_i and w_j are their peak widths at a desired baseline. For a baseline separation, the resolution must be greater than 1.5.

The assumption of similarity of dispersed peaks (i.e., the peak widths are approximate equal for two components), leads to the following equation [Schu05]:

$$R_S = \left(\frac{\alpha_{i,j} - 1}{\alpha_{i,j}}\right)\left(\frac{k_j^{'}}{k_j^{'} + 1}\right)\frac{\sqrt{N_j}}{4} \qquad (2\text{-}58)$$

The Eq. 2-58 notes for component *j*, which has the longer retention time.

The minimum number of theoretical plates necessary for a given resolution of two components can be calculated by:

$$N_{i,j}^{min} = \left[4R_S\left(\frac{\alpha}{\alpha - 1}\right)\left(\frac{k_j^{'} + 1}{k_j^{'}}\right)\right]^2 = \left[4R_S\left(\frac{\alpha}{\alpha - 1}\right)\left(\frac{FK_j + 1}{FK_j}\right)\right]^2 \qquad (2\text{-}59)$$

2.2.1.6 Multi-component isotherms

In the case of multi-component mixtures with non-linear isotherms, adsorption of different components is competitive with respect to interactions with the stationary phase. Thus, the loading of a solute on the stationary phase does not only depend on the concentration of its own solute in the mobile phase but also on the concentrations of all the other solutes that are present in the mobile phase. The Langmuir theory can be extended for *n* components system leading to following equation:

$$q_i = \frac{K_i c_i}{1 + \sum_{j=1}^{n} b_j c_j}$$

(2-60)

2.2.2 Apparent dispersion coefficients

The goal of reactive chromatography is to collect target components with concentrations as high as possible. However, concentration profiles always have a tendency to spread during propagation. All causes of band broadening are summarized in the term of apparent dispersion. Under linear conditions, the apparent dispersion coefficient is characterized by the height equivalent to a theoretical plate ($HETP_i$) according to the follow relationship:

$$HETP_i = \frac{L}{N_i} = \frac{2 D_{ap,i}}{u}$$

(2-61)

where L is the length of column; N_i is number of theoretical plates of component *i*. The *HETP* is a function of the linear velocity *u* and is calculated by Van Deemter equation [Deem56] which can be expressed in simplified form:

$$HETP_i = A_i + \frac{B_i}{u} + C_i u$$

(2-62)

In this equation, there are three contributions to the *HETP$_i$*, where *A* is the eddy diffusion term, *B* is the axial diffusion term and *C* is the mass transfer resistance term. With the column packed by porous particles, the contribution of mass transfer between two phases to band broadening is considerable. A typical Van Deemter curve is shown in Figure 2-5. The minimum of this curve corresponds to the optimum linear velocity for analysis separation, where the column has the highest efficiency.

In the case of linear isotherms, Eq. 2-62 can be established as a function of K_i [Deem56]:

$$HETP_i = 2\gamma_2 d_p + \frac{2\gamma_1 D_{ax,i}}{u} + 2u \frac{\varepsilon_t}{(1-\varepsilon_t)} \frac{1}{\beta_i K_i} \left(1 + \frac{\varepsilon_t}{(1-\varepsilon_t) K_i}\right)^{-2}$$

(2-63)

in which, γ_1 and γ_2 are geometrical constants, usually around 0.7 and 0.5, respectively; β_i is mass transfer coefficient; ε_t is total porosity defined by Eq. 2-3; K_i is the Henrry constant given in Eq. 2-48.
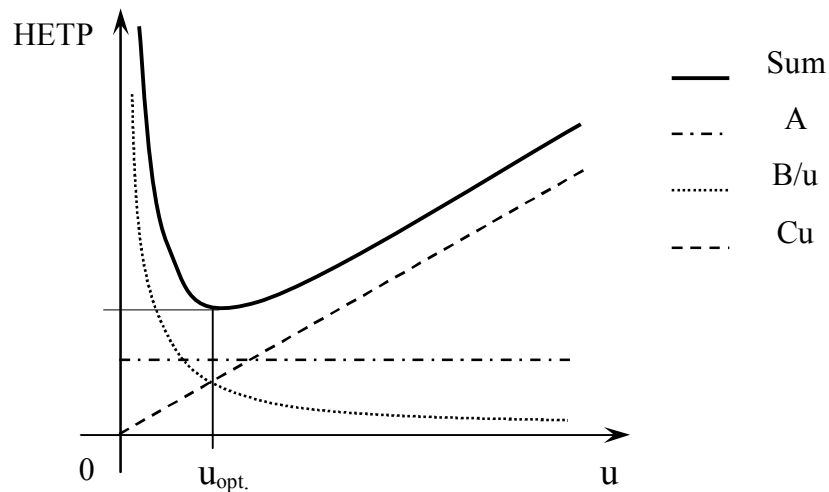
Figure 2-5: A typical Van Deemter curve and the optimum velocity

HETP or the corresponding number of theoretical plates $N_i = L/HETP_i$ can be calculated by statistical moment method from measured elution profiles $c_i(t)$ [e.g., Seid95]

$$\mu_{t,i} = \frac{\int_0^\infty t c_i(t) dt}{\int_0^\infty c_i(t) dt} \tag{2-64}$$

$$\sigma_{t,i}^2 = \frac{\int_0^\infty (t - \mu_{t,i})^2 c_i(t) dt}{\int_0^\infty c_i(t) dt} \tag{2-65}$$

$$N_i = \frac{L}{HETP_i} = \frac{\mu_{t,i}^2}{\sigma_{t,i}^2} \tag{2-66}$$

where $\mu_{t,i}$ is the first normalized moment and $\sigma_{t,i}$ is the second central moment. For symmetrical (Gaussian) peaks, $\mu_{t,i}$ correlates to the retention time of the peak maximum $t_{R,max}$, while $\sigma_{t,i}$ correlates to the standard deviation. For "perfect" Gaussian peaks, N_i can be determined simply from $t_{R,max}$ and the peak width at half height ($w_{0.5,i}$):

$$N_i = 5.54 \frac{t_{R,max,i}^2}{w_{0.5,i}^2} \tag{2-67}$$

Longitudinal dispersion time t_i^{disp} through a column length L can be calculated from apparent dispersion coefficient:

$$t_i^{disp} = \frac{L^2}{D_{ax,i}}$$

(2-68)

A dimensionless number used frequently by many authors is the Peclet number Pe_i. The Peclet number equals to the double value of the number of theoretical plates. It is the ratio between the longitudinal dispersion time (Eq. 2-68) and the convection time t_0 (Eq. 2-50).

$$Pe_i = \frac{t_i^{disp}}{t_0} = \frac{uL}{D_{ax,i}} = 2N_i$$

(2-69)

2.2.3 Chemical equilibria

At equilibrium, the rates of forward and backward reactions are equal to each other and the concentrations of reactants and products do not change anymore. The equilibrium condition for a chemical reaction is stated by the following equation [Silb01, p.135]:

$$\sum_{i=1}^{N_C} v_i \mu_{i,eq} = 0$$

(2-70)

where the v_i are the stoichiometric coefficients of components i; $\mu_{i,eq}$ is the chemical potential of components i at equilibrium. The latter are related to the standard chemical potential μ_i^o and the activities at equilibrium $a_{i,eq}$ by:

$$\mu_{i,eq} = \mu_i^o + RT \ln a_{i,eq}$$

(2-71)

Substituting Eq. 2-71 into Eq. 2-70 yields

$$\sum_{i=1}^{N_C} v_i \mu_i^o = -RT \sum_{i=1}^{N_C} v_i \ln a_{i,eq}$$

(2-72a)

or:

$$\sum_{i=1}^{N_C} v_i \mu_i^o = -RT \ln \prod_{i=1}^{N_C} a_{i,eq}^{v_i}$$

(2-72b)

The standard chemical potentials are related to the standard Gibbs free energies of formation of components $\Delta G_{f,i}^o$ and the standard reaction Gibbs energy ΔG_r^o:

$$\sum_{i=1}^{N_C} v_i \mu_i^o = \sum_{i=1}^{N_C} v_i \Delta G_{f,i}^o = \Delta G_r^o \qquad (2\text{-}73)$$

Thus, it holds:

$$\Delta G_r^o + RT \ln \prod_{i=1}^{N_C} a_{i,eq}^{v_i} = 0 \qquad (2\text{-}74)$$

The product of activities at equilibrium in Eq. 2-74 is also defined as an equilibrium constant of reaction ($K_{eq,a}$).

$$K_{eq,a} = \prod_{i=1}^{N_C} a_{i,eq}^{v_i} \qquad (2\text{-}75)$$

For a real solution holds, $a_i = \gamma_i c_i$, where the γ_i are the activity coefficients and c_i are the molar concentrations of components i. Dilute solutions can be considered as ideal solutions. Thus, the activities can be indirectly replaced by the concentrations and an equilibrium constant K_{eq} can be defined:

$$K_{eq} = \prod_{i=1}^{N_C} c_{i,eq}^{v_i} \qquad (2\text{-}76)$$

Therefore, Eq. 2-74 can be rewritten to give:

$$\Delta G_r^o = -RT \ln K_{eq} \qquad (2\text{-}77)$$

The Gibbs-Helmholtz equation further states for the Gibbs energy of chemical reaction [Silb01, p.114]:

$$\Delta G_r^o = \Delta H_r^o - T\Delta S_r^o \qquad (2\text{-}78)$$

where, ΔH_r^o is the standard reaction enthalpy and ΔS_r^o is the standard reaction entropy. The standard reaction enthalpy can be calculated from the standard enthalpies of formation of the components involved in the reaction according to:

$$\Delta H_r^o = \sum_{i=1}^{N_C} v_i \Delta H_{f,i}^o \qquad\qquad (2\text{-}79)$$

If the reaction enthalpy is supposed to be a constant over the temperature range of interest, the temperature dependence of the equilibrium constants follows van's Hoff equation:

$$\ln \frac{K_{eq}^{T_2}}{K_{eq}^{T_1}} = \frac{\Delta H_r^o}{R}\left[\frac{1}{T_1} - \frac{1}{T_2}\right] \qquad\qquad (2\text{-}80)$$

For many species, the standard free Gibbs energy of formation and the standard enthalpy of formation at 298K are available in thermodynamic handbooks (e.g., [Stull69], [Perr84] [CRC04]) and data banks. Selected thermodynamic data related to ester hydrolysis reactions are given below in Section 3.1.

2.2.5 Reaction kinetics

The most important information needed to characterize chemical reactions are the kinetics. Typically, the rate of a single reaction is defined by Eq. 2-81a as the change in moles of a reactant or product per time unit and volume of the reactor.

$$r = \frac{1}{V_R}\frac{1}{v_i}\frac{dn_i}{dt} \qquad\qquad (2\text{-}81a)$$

where the n_i are the mole numbers of components i and V_R is reactor volume. If the volume of the reactor is constant, the rate of a homogeneous reaction can be defined by:

$$r = \frac{1}{v_i}\frac{dc_i}{dt} \qquad\qquad (2\text{-}81b)$$

Assuming simple formal kinetics based on collision theory [Atki02, p. 945], the dependence of the rate of chemical reaction on the concentrations of reactants can be expressed as:

$$r = k(T)\prod_{k=1}^{Reactants} c_k^{v_k} \qquad\qquad for\ k = 1, N_K \qquad\qquad (2\text{-}82)$$

where, N_K is the number of reactants; $k(T)$ is the reaction rate constant. Its temperature dependence is usually represented by the Arrhenius equation [Silb01, p.672]:

$$k(T) = k_0 e^{-E_A/RT} \tag{2-83}$$

In the Arrhenius equation, k_0 is called the frequency factor and has the same units as $k(T)$ and E_A is the activation energy. The activated energy is considered as a potential energy barrier over which the reactants muss pass if the reaction should take place.

For multi-reaction system with N_C components and N_R reactions, a rate of production of component i (R_i) may be calculated from the rate of all reactions talking place.

$$R_i = \sum_{j=1}^{N_R} v_{i,j} r_j \qquad for\ i = 1, N_C \tag{2-84}$$

in which, $v_{i,j}$ are now the stoichiometric coefficients of a component i in the reaction j.

Related to the reaction processes there is an important dimensionless number, the Damköhler number Da. It is defined as a ratio of the convection time (Eq. 2-50) to a characteristic reaction time. If only one reaction occurs, a single reactant A is enough to describe the development of the concentrations of all other components. The characteristic reaction time can be calculated by:

$$t^{react} = \frac{c_A^{ini}}{r_0\left(c_i^{ini}\right)} \tag{2-85}$$

where c_A^{ini} is the initial or feed concentration of A.

For a reaction of the type $v_A A + v_B B \rightarrow v_C C + v_D D$, the initial reaction rate is $r_0 = k\,c_A^{ini} c_B^{ini}$ and $v_A = v_B = -1$. According to the definition, the Damköhler number for this case can be expressed as:

$$Da = \frac{t_o}{t^{react}} = \frac{L}{u} k c_B^{init} \tag{2-86}$$

In the cases of catalyzed reactions, the action of catalysts reduces the potential energy barrier over which the reactants must pass to form products. Thus the rates of reactions are accelerated. The expression of the reaction rate law for homogeneously catalyzed reactions is similar to that of non-catalyzed reaction. Let us consider a reversible reaction occuring in the homogeneous phase:

$$\nu_A A + \nu_B B \underset{k_{backw}}{\overset{k_{forw}}{\rightleftharpoons}} \nu_C C + \nu_D D \tag{2-87}$$

Based on conventional laws the rate r^{hom} can be written by the following equation:

$$r^{hom} = k_{forw}^{hom} \left(c_A c_B - \frac{c_C c_D}{K_{eq}^{hom}} \right) \tag{2-88}$$

$$K_{eq}^{hom} = \frac{k_{forw}^{hom}}{k_{backw}^{hom}} \tag{2-89}$$

in which, k_{forw}^{hom}, k_{backw}^{hom} are the reaction rate constants for the forward and backward reactions, respectively; K_{eq}^{hom} is the homogeneous equilibrium constant and the c_i are concentrations at equilibrium state.

For heterogeneously catalyzed reactions, the following three steps of reactants adsorption, chemical reactions, and products desorption are often considered under the term of surface reaction. Depending on different assumptions, surface reaction kinetics can be described by some classical mechanisms like Langmuir-Hinshelwood, Eley-Rideal or Hougen-Watson [Thom97, p. 120]. For the example of a simple esterification catalyzed by a solid catalyst, a large amount of specific models for surface reaction kinetics was derived [Bart96].

In the Langmuir-Hinshelwood (LH) mechanism, the reaction takes plate exclusively by encounters between molecules adsorbed on the catalyst surface. The rate of the reversible reaction in Eq. 2-87 catalyzed by a heterogeneous catalyst r^{het} can be expressed by:

$$r^{het,LH} = k_{forw}^{het,LH} \left(q_A q_B - \frac{q_C q_D}{K_{eq}^{het,LH}} \right) \tag{2-90}$$

$$K_{eq}^{het,LH} = \frac{k_{forw}^{het,LH}}{k_{backw}^{het,LH}} \tag{2-91}$$

where, $k_{forw}^{het,LH}$, $k_{backw}^{het,LH}$ are the reaction rate constants for the heterogeneously catalyzed forward and backward reactions, respectively; $K_{eq}^{het,LH}$ is the heterogeneous equilibrium constant and the q_i are the solid phase concentrations at equilibrium state.

In contrast, in the Eley-Redial (EL) mechanism, the reaction is assumed to take plate by encounters between unadsorbed molecules of a reactant (e.g., reactant B) with adsorbed molecules of another reactant (e.g., reactant A). In this case, the reaction rate can be expressed by:

$$r^{het,EL} = k_{forw}^{het,EL} \left(q_A c_B - \frac{q_C q_D}{K_{eq}^{het,EL}} \right) \tag{2-92}$$

with

$$K_{eq}^{het,EL} = \frac{k_{forw}^{het,EL}}{k_{backw}^{het,EL}} \tag{2-93}$$

If reactions take place in both phases, a total rate of reaction can be written by a linear expression adding into account the homogeneous and the heterogeneous contributions according to the volume fractions of the two phases.

$$r^{tot} = \varepsilon_t r^{hom} + (1 - \varepsilon_t) r^{het} \tag{2-94}$$

2.3 New concept to analyze FBCRs

In previous sections of this chapter, continuous models of FBCRs and theoretical backgrounds related to the included parameters have been reviewed. The number of free model parameters is large and a strategy to evaluate the potential and to optimize FBCRs is desirable. In this section, a new and generally applicable conceptual approach to achieve this goal is suggested.

2.3.1 Strategy

Essential goals of reactive chromatographic processes are complete conversion of the reactants and complete separation of the products. However, "*the cabability of a reactive chromatographic process strongly depends on reaction stoichiometries and chromatographic properties of the constituents*" [Sard93, p. 487]. Therefore, a theoretical tool is useful in helping to identify which reaction processes are suitable to apply for chromatographic reactors. Above there were two continuous models of different degree of precision introduced (Section 2.1.2). Below the extended equilibrium theory is initially used for feasibility analysis. The equilibrium-dispersion model which offers more details is used subsequentially for more extensive simulations. Is should be better if the two models

are used in combination. The strategy followed in this dissertation to analyze FBCRs includes two steps:

Step 1 - Using the extended equilibrium theory to study if both complete conversion and complete separation are possible.

Step 2 - If step 1 is successful, the equilibrium-dispersion model can be used for more specific kinetic studies and for design and optimization.

Following this idea, feasibility studies for some typical reactions with arbitrary parameters are given below using the extended equilibrium model (Step 1). The results shown are based on a publication by Vu et al. [Vu05], where more details can be found. The Step 1 is repeated in Chapter 6 for concrete ester hydrolysis reactions studied in this work with parameters determined experimentally. Subsequently, the Step 2 will be represented for the same ester hydrolysis reactions in Chapter 7 and Chapter 8.

2.3.2 Conventional space and hodograph space

For predictions of elution profiles the outlet concentration profiles can be conveniently represented in the so-called hodograph space. In this plot the concentrations as dependent variables are plotted against each other. The hodograph is very useful for illustrating problems of FBCR dynamics. To get acquainted with hodograph representation, two illustrated cases with linear adsorption isotherms will be shown below both in conventional and hodograph spaces. The first case is the separation of a non-reactive binary mixture of two components *B* and *C*. The second case is concerned with a reaction of type $A \rightleftharpoons B + C$.

In the first case, a large plus of the non-reactive mixture of *B* and *C* is injected into the column. To illustrate characteristic features a parameter set was chosen corresponding to typical geometry, how rates and feed concentration applicable in the experimental studies discussed late ($L = 0.25$ m; $u = 1$ m/min; $N = 10^4$; $c_i^{inj} = 0.5$ mol/L; $t^{inj} = 10$ min). For this typical parameter set, the eluted concentration profiles are shown in Figure 2-6a. The adsorptivity of component *B* is higher than that of component *C*. To eliminate the time coordinate, the variable c_C can be expressed as a function of the variable c_B in Figure 2-6b. In this case, the so-called hodograph plot is a rectangular with characteristic points corresponding to initial concentration and plateaus of the elution profiles. P_0 is represented here for an initially unloaded bed and P_2 is represented the feed concentration of *B* and *C*. The two straight lines P_0-P_1 and P_0-P_3 located exclusively on the pure component axes (fat lines) prove the capability to obtain pure component C and pure component B in the front and real of the elution, respectively. This analysis was extended to reactive cases.
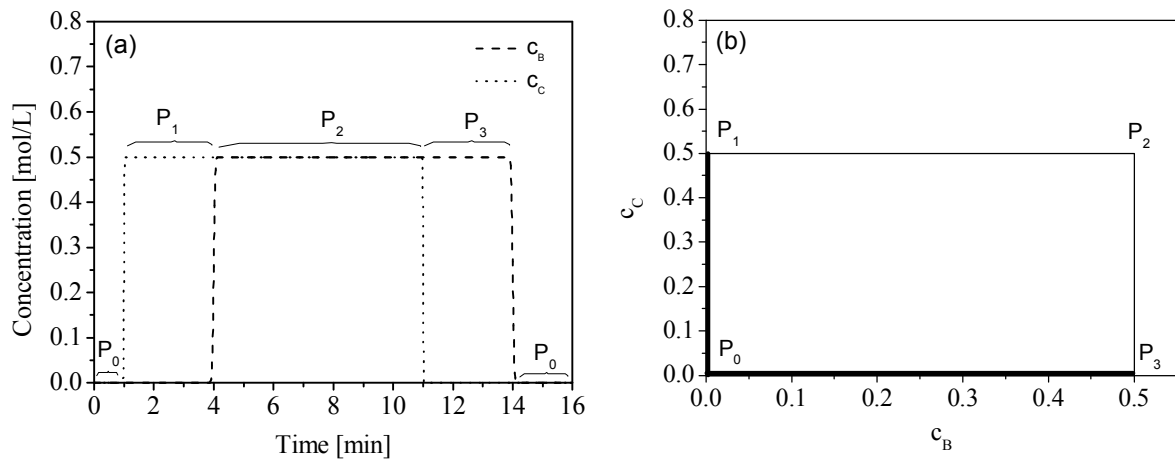
Figure 2-6: Hodograph space and conventional space for chromatographic separation of a non-reactive mixture of B and C. (a) Elution profiles of components ; (b) Hodograph plot (L = 0.25 [m]; N = 10^4; u = 1 [m/min]; c_B^{inj} = 0.5; and c_C^{inj} = 0.5 [mol/L]; t^{inj} = 10 [min], Linear isotherms K_B = 5, and K_C = 1).

In the second case (reaction type $A \rightleftharpoons B + C$), only reactant A is injected into the initially unloaded column. Components B and C are reaction products. Concentration profiles of A, B and C at the column outlet generated with the equilibrium-dispersion model are shown in Figure 2-7a for typical parameter set. Typically in chromatographic processes often small particles are well parked into the column offering large plate number (e.g., in this cases $N = 10^4$). Therefore these elution profiles correspond to the results obtained by the extended equilibrium model. Using the definition in Eq. 2-28, the transformed variables C$_1$ and C$_2$ are expressed as follows:

$$C_1 = c_B + c_A \qquad\qquad C_2 = c_C + c_A$$
$$Q_1 = q_B + q_A \qquad\qquad Q_2 = q_C + q_A \tag{2-95}$$

The corresponding concentration profiles of C_1 and C_2 are shown in Figure 2-7b. To eliminate the time coordinate, the variable C_2 is again expressed as a function of the variable C_1 (see Figure 2-7c). The initial point P$_0$ in Figure 2-7c corresponds to base lines of C_1 and C_2 in Figure 2-7b. The point P$_1$ captures the plateaus at the front of C_2. The point P$_2$ is presented for plateaus of C_1 and C_2 and it is also presented for feed concentration of reactant A. In Figure 2-7c, the vertical fat line is presented for a fraction of pure component C that can be obtained from the front of the elution profile, whereas the horizontal fat line is present for a fraction of pure component B that can be collected from the rear of the elution profile.
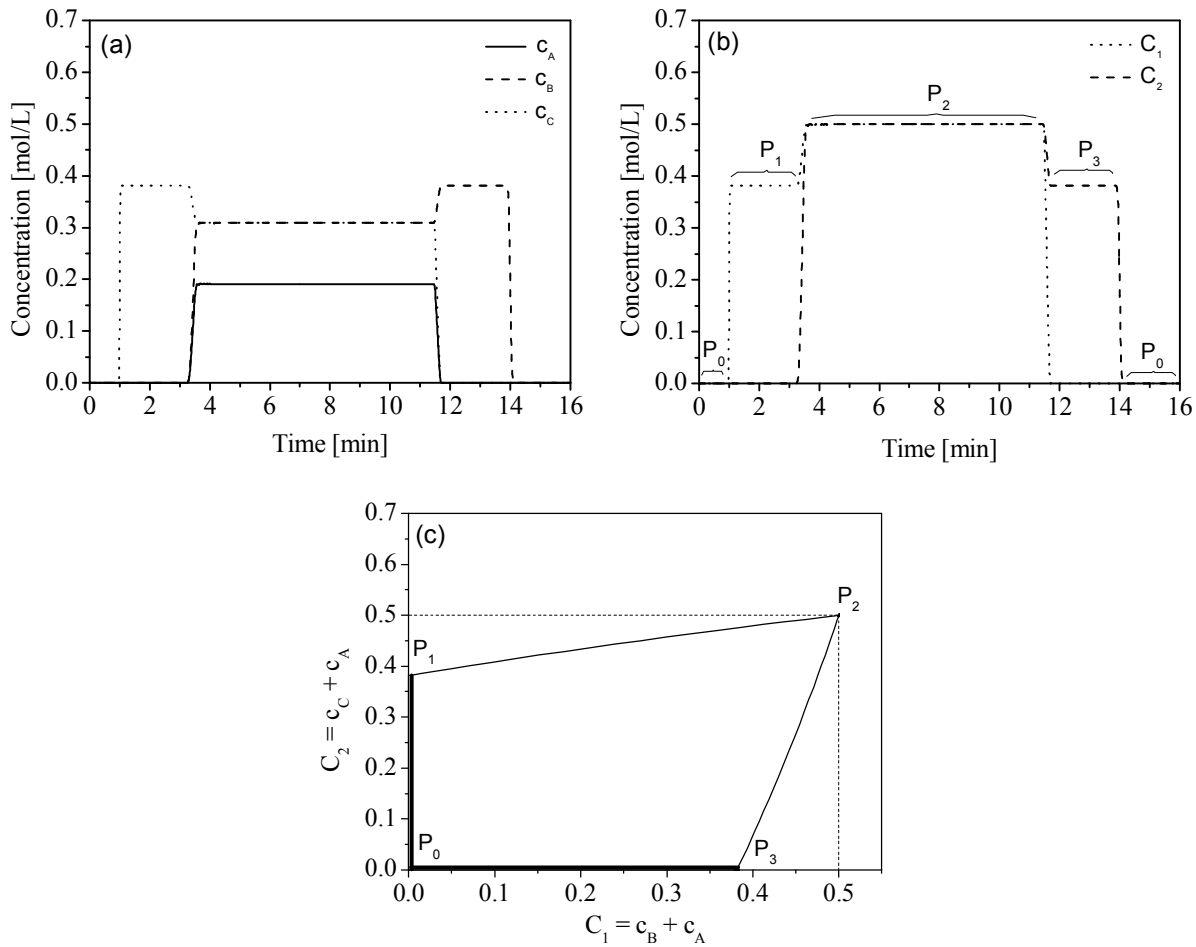
Figure 2-7: Hodograph space and conventional space for the reactive case of $A \rightleftharpoons B + C$ (a) elution profiles of components (b) Transformed concentrations   (c) Hodograph plot ($L = 0.25$ [m]; $N = 10^4$; $u = 1$ [m/min]; $c_A^{inj} = 0.5$ [mol/L]; Linear isotherms $K_A = 3$, $K_B = 5$, and $K_C = 1$; $k^{het} = 5 \times 10^3$ [min^{-1}]; $K_{eq} = 0.5$).

For the two illustrative cases, hodograph plots reflect the dynamics of processes more clearly than the concentration trajectories. Transformation of elution profiles to hodograph representations has been applied for particular cases. However, for general predictions, pathgrids of eigenvectors of Jacobians $\partial Q(C)/\partial C$ need to be generated to scale all possibilities of pulse and wave pattern. From the analysis discussed in more detail [Vu05], the following important geometrical condition for total conversion and total separation can be extracted:

Total conversion and total separation in a fixed-bed chromatographic reactor with pulse injection of the reactant is possible, if the relevant wave solutions through the origin of the corresponding hodograph plot lie on the pure component axes of the products.

2.3.3 Illustration of feasibility analysis for typical reactions

Extended equilibrium theory has been applied more extensively to study feasibility of FBCR [Vu05]. Reactions of the type a) $2A \rightleftharpoons B + C$ with Langmuir adsorption isotherms (Eq. 2-60) and b) $A \rightleftharpoons B + C$ with linear adsorption isotherms (Eq. 2-48) were chosen as illustrative cases. Differences in types of adsorption isotherms, stoichiometry and relative adsorption affinity of the reactant A can lead to different feasibilities of separation processes. If A is chose as the reference component for the dependent transformed variables in both phases follows:

$$
\begin{aligned}
C_1 &= c_B - \frac{c_A}{v_A} & C_2 &= c_C - \frac{c_A}{v_A} \\
Q_1 &= q_B - \frac{q_A}{v_A} & Q_2 &= q_C - \frac{q_A}{v_A}
\end{aligned}
\tag{2-96}
$$

a) Reactions of the type $2A \rightleftharpoons B + C$ *with Langmuir adsorption isotherms*

Figure 2-8 shows three different cases for the relative adsorption affinity of A (the product B always has higher adsorptivity than the product C). The parameters for these cases are given in Table 2-1. They can be considered as realistic values being in the range characteristic for many situations.

Table 2-1: Sets of adsorption isotherm parameters referred to Eq. 2-60 and chemical equilibrium constants for ternary system in Figures 2-8, 2-9 and 2-10

	Reactant A has		
	(a) intermediate adsorptivity	(b) highest adsorptivity	(c) lowest adsorptivity
$K_A = b_A$	3.0	5.0	1.0
$K_B = b_B$	5.0	3.0	5.0
$K_C = b_C$	1.0	1.0	3.0
K_{eq}	1.0	1.0	1.0

In case (a), the wave solutions adjacent to the origin coincide with the axes $C_1 = 0$ and $C_2 = 0$, corresponding to a fraction of pure component C in front during loading and a fraction

of pure component B in the rear during regeneration of the bed (Figure 2.8a). In the cases (b) and (c), a line of reactive azeotropy occurs according to:

$$\frac{Q_1}{C_1} = \frac{Q_2}{C_2} \tag{2-97}$$

Along this line, reaction and separation compensate each other. Hence, this line cannot be crossed in a chromatographic column. In Figures 2-8b and 2-8c, this line is represented by the sloped boundary of the shaded region. Hence, in Figure 2-8b, the axis $C_2 = 0$ is not accessible. On the reverse, in Figure 2-8c, the axis $C_1 = 0$ is not accessible. The treatment for this case was represented in detail in [Grün04].

It is worth noting that the patterns of behavior described above do not depend on the specific parameter values in Table 2-1 but only on the order of the adsorptivities. Further, it was shown in studies not documented here that analogous patterns of behavior will arise if the reaction takes place in the solid phase.
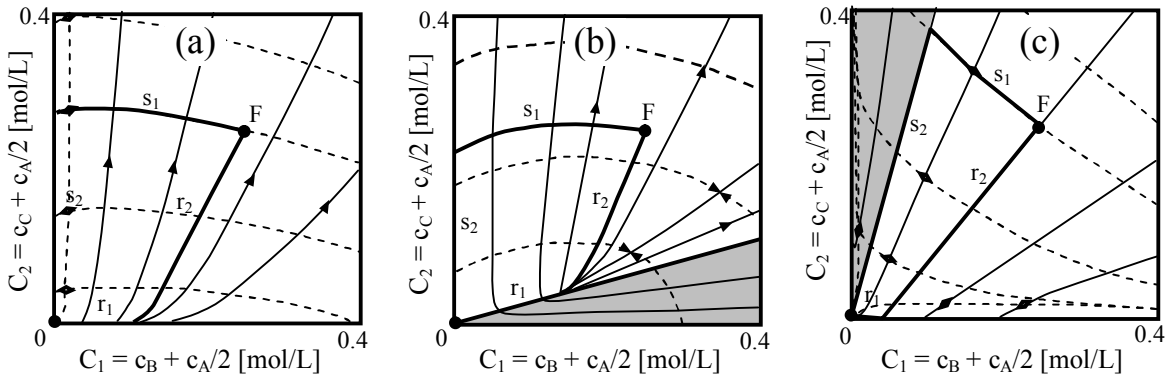
Figure 2-8: Representation of wave solutions in hodograph space of the transformed concentration variables for a reaction of the type $2A \rightleftharpoons B + C$ in the fluid phase and Langmuir isotherms [Grün04, Vu05]. (a) A has intermediate adsorptivity, total separation and total conversion are possible. (b) A has highest adsorptivity, separation is partly for C. (c) A has lowest adsorptivity, separation is only partly for B.

b) Reactions of the type $A \rightleftharpoons B + C$ *with linear adsorption isotherms*

The parameters for the reaction and adsorption equilibrium are taken again from Table 2-1 with $b_i = 0$. Under these conditions, again, reactive azeotropy arises if reactant A has the highest or lowest adsorptivity, corresponding to cases b) and c) in Table 2-1. The line of reactive azeotropy can be calculated from Eq. 2-97 and is illustrated in Fig 2-9 for cases (b) and (c) in Tab 2-1. In contrast to Figure 2-8, the line of reactive azeotropy is now a

parabola. However, it can be shown that only the branch corresponding to the solid line is relevant, since the physical concentrations c_B and c_C are always negative on the branch through the origin.
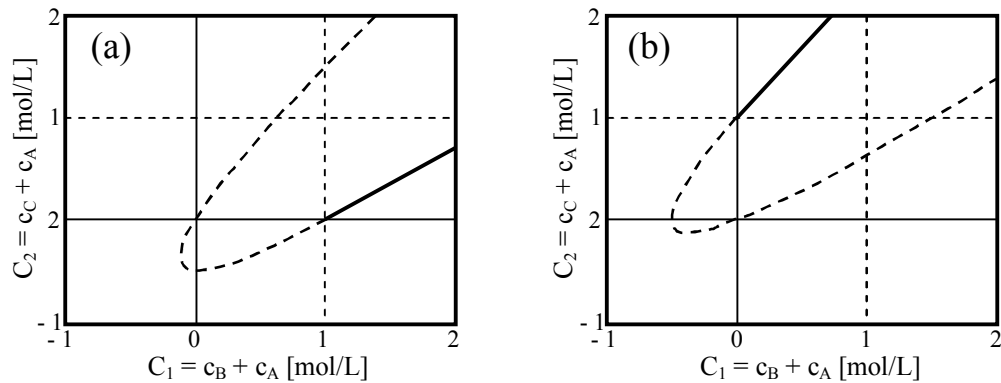
Figure 2-9: Curve of reactive azeotropy in the hodograph space of the transformed concentration variables for a reaction of the type $A \rightleftharpoons B + C$ in the fluid phase and linear isotherms [Vu05]. (a) A has highest adsorptivity, (b) A has lowest adsorptivity.

This has important consequences for the construction of wave solutions in the hodograph space, as illustrated in Figure 2-10 again for three different orders of adsorptivities. For sufficiently small feed concentrations represented by F_1 in Figs 2-10b and 2-10c, the relevant wave solutions through the origin lie completely on the pure component axes of products B and C. This gives rise to a fraction of pure product C in front during loading and a fraction of pure product B in the rear during regeneration in all three cases. So, in contrast to the previous case a) ($2A \rightleftharpoons B + C$), total conversion and total separation for a pulse injection of reactant A is now possible in all three cases, which is in agreement with the geometric condition given above.

The same arguments apply for large feed concentrations, e.g., F_2 in Figure 2-10c, since the wave solutions through the origin contain a fraction of pure product C during loading and a fraction of pure product B during regeneration. Hence, the geometric condition also applies.

Further, separation during loading and regeneration and, hence, total conversion and total separation for a pulse injection of reactant A are also possible in all three cases if the linear isotherms are replaced by the Langmuir isotherms.
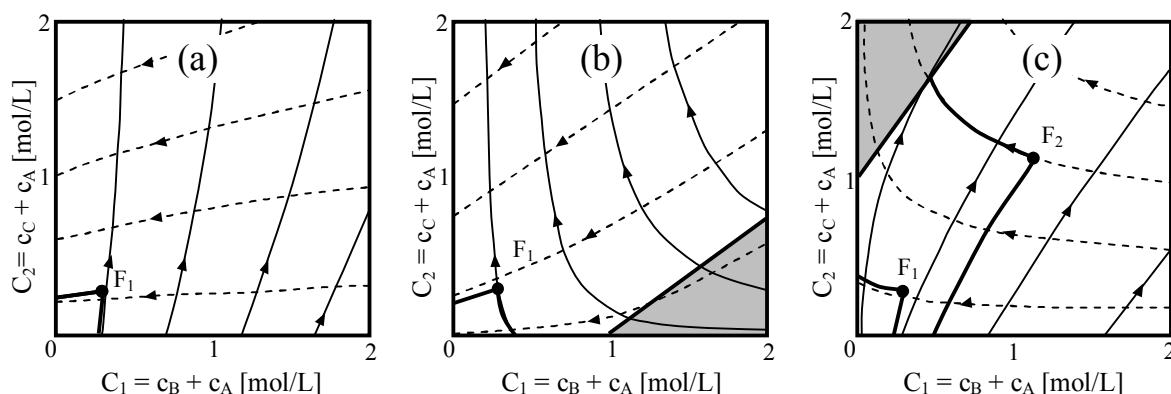
Figure 2-10: Representation of wave solutions in hodograph space of the transformed concentration variables for a reaction of the type $A \rightleftharpoons B + C$ in the fluid phase and linear isotherms [Vu05]. (a) A has intermediate adsorptivity. (b) A has highest adsorptivity. (c) A has lowest adsorptivity.

Consequently, the difference in behavior between the two reaction systems considered in this section can be clearly attributed to the different stoichiometries.

In this section the feasibilities of typical reaction models with arbitrary parameters were studied and discussed. The ester hydrolysis reactions with water in excess which will be introduced in the next chapters and studied in this work can be considered as reaction type of $A \rightleftharpoons B + C$. Based on above results, feasibility of these reactions should be possible for any relative affinities of the involved esters, alcohols and acids to the adsorbent. Thus, further studies (Step 2) on FBCRs can be carried out. Feasibilities of the ester hydrolysis reactions with real parameters determined experimentally will be discussed later in Chapter 6.

Model Reactions
and Stationary Phases

3.1 Hydrolysis of esters

A carboxylate ester can be broken into the corresponding carboxylic acid and alcohol by a hydrolysis reaction. This process starts with pure water very slow. The autocatalyzed effect of its own acid product in the beginning of the processes is not worth considering. Therefore, the spontaneous hydrolysis of esters is never used. For acceleration of the reaction rate, ester hydrolysis is usually catalyzed by acids or bases. The basic hydrolysis catalyzed by alkaline hydroxides is called saponification, because one of its products is the corresponding carboxylate salt - an important ingredient of soap. Acid catalyzed hydrolysis has more applications because it is useful method to produce pure carboxylic acids (see Chapter 8). Mechanisms of ester hydrolysis reactions catalyzed by acids or bases with several steps are well known and represented in textbooks of organic chemistry as [Clayd01]. Besides inorganic acids like sulfuric acid or hydrochloric acid, acidic ion-exchange resins are used as catalyst agents due to many advantages (catalyst immobilization selectivity in adsorption and separation). The hydrolysis reaction is a reversible reaction. Its backward reaction is the esterification reaction. Both of the reactions are often used as typical reversible reactions for kinetic studies of reactive chromatography. Recently, several studies on ester hydrolysis or esterification catalyzed by ion exchange resins were published [Mazz97, Pöpk00, Gelo03, Falk03, Lode03, Sein05, Schl06, etc.].

In this work, hydrolysis reactions of the four esters methyl formate, ethyl formate, methyl acetate and ethyl acetate catalyzed by strong acidic ion-exchange resins are studied. The resins used are functionalized by sulfonic acid groups ($-SO_3H$). Exchangeable H^+ ions play the catalytic role of a strong acid. The four reactions investigated are:

$$HCOOCH_3 + H_2O \overset{H^+}{\rightleftharpoons} CH_3OH + HCOOH \tag{3-1a}$$

$$HCOOC_2H_5 + H_2O \overset{H^+}{\rightleftharpoons} C_2H_5OH + HCOOH \tag{3-1b}$$

$$CH_3COOCH_3 + H_2O \overset{H^+}{\rightleftharpoons} CH_3OH + CH_3COOH \tag{3-1c}$$

$$CH_3COOC_2H_5 + H_2O \overset{H^+}{\rightleftharpoons} C_2H_5OH + CH_3COOH \tag{3-1d}$$
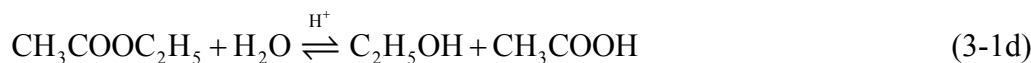
In order to highlight similarities, the investigated compounds are grouped and abbreviated as shown in Table 3-1. Hydrolysis products are abbreviated by first letters of their names. Abbreviations for the esters are composed by the abbreviations of the corresponding alcohol and acid.

Table 3-1: List of compound abbreviations used

	Compound	Abbreviation
	Methyl formate	MF
	Ethyl formate	EF
Es	Methyl acetate	MA
	Ethyl acetate	EA
Al	Methanol	M
	Ethanol	E
Ac	Formic acid	F
	Acetic acid	A
-	Water	W

The four products of the ester hydrolysis reactions are M, E, F, and A. In the literature, M is commonly produced from synthesis gas [Fied05]. E is produced industrially both as a petrochemical process, through the hydration of ethylene, and biological process, by fermenting sugars with yeast [Kosa02]. About 75% A is made by methanol carbonylation, about 10% by bacterial fermentation and the rest by other processes [Cheu05]. About 49% F is produced by hydrolysis of MF, about 26% by acidolysis of alkali formates and about 22% by hydrocarbon oxidation [Reut05]. Although the MF hydrolysis process can be used to produce F, the ester hydrolysis reactions performed in FBCRs seem to be lack of a

technical meaning due to high operating cost of chromatographic techniques. However, they are good illustrative cases to discover performance of FBCRs.

3.1.1. Physical properties

Selected physical properties of the compounds are shown in Table 3-2. Most of them are given at a standard temperature of 20°C. The esters and their hydrolysis products are arranged in order of increasing molecular weight (M_i). Some of them have the same molecular weight but different structural formulas. The acids and alcohols are soluble in water, whereas the solubility of the esters depends on polarity and molecular chain length. For HPLC analysis the refractive indeces $n_D^{20°C}$ and UV cut-off wavelengths are important information. RI detection depends on the difference in refractive index of the solutes and the solvent (i.e., water). In this table, the reflective indeces values refer to a wavelength of 589nm (sodium D line). The UV cutoff wavelengths present the lower limit for the wavelength, at which the compound absorbance is getting problematic.

Table 3-2: Selected physical properties of the compounds [Merc05] [CRC04]

Compound	M_i [g/mol]	$\rho_{i,20°C}$ [g/mL]	$n_D^{20°C}$	UV cutoff [nm]	Dielectric constant	Polarity	Solubility in water (20°C) [g/L]	Solubility in water (20°C) [mol/L]
MF	60.05	0.97	1.342	-	-	-	300	5.00
EF	74.08	092	1.361	-	-	-	105	1.42
MA	74.08	0.93	1.361	-	6.7	29.0	250	3.37
EA	88.11	0.90	1.372	255	6.0	23.0	85.3	0.97
M	32.04	0.79	1.329	210	32.6	76.2	*soluble*	*soluble*
E	46.07	0.79	1.361	210	22.4	65.4	*soluble*	*soluble*
F	46.03	1.22	1.371	-	-	-	*soluble*	*soluble*
A	60.05	1.05	1.372	260	6.2	64.8	*soluble*	*soluble*
W	18.02	1.00	1.333	191	79.7	100.0	-	-

3.1.2. Thermodynamic properties

The standard enthalpies of formation $\Delta H_{f,i}^{298K}$ and standard free Gibbs energies of formation $\Delta G_{f,i}^{298K}$ of reactants and products can be found in the literature (e.g., [CRC04, Bari95, Perr84 and Stull69] etc.). These data are shown in Tables 3-3 and 3-4.

Based on the values of the standard enthalpy of formation in Table 3-3, the standard enthalpies of reactions are calculated by Eq. 2-79. Ester hydrolysis reactions are endothermic and the calculated values of enthalpy of reactions have to be positive. In contrast, some results given by [Stull69] are negative. The results sourced by [CRC06] and [Hine74] seem to be more reliable. These values are given in Table 3-5 and compared with others found in the literature.

Table 3-3: The standard enthalpies of formation of the investigated compounds from [CRC04, Perr84, Perr99 and Stull89]

	$\Delta H_{f,i}^{298K}$ [kJ/mol]					
Compound	Liquid			Gas		
	[CRC06]	[Stull69]	[Hine74]	[CRC06]	[Stull69]	[Perr99]
MF	-386.1	-376.73	-391.0	-357.4	-349.78	-352.40
EF	-	-399.32	-430.5	-	-371.29	-388.30
MA	-445.9	-441.41	-	-413.3	-409.61	-411.90
EA	-479.3	-479.03	-	443.6	-442.92	-444.50
M	-239.2	-238.57	-	-201.0	-201.17	-200.94
E	-277.6	-276.98	-	-234.8	-234.81	-234.95
F	-425.0	-425.04	-	-378.7	-378.61	-378.60
A	-484.3	-484.09	-	-432.2	-434.84	-432.80
W	-285.8	-	-	-241.8	-241.84	-241.81

The standard free Gibbs energy of formation of ethyl format and methyl acetate are not available in the literature. Based on the dependence of Gibbs energy on the pressure [Silb01, p114], these values can be calculated from the standard free Gibbs energy of

formation in gas state [Perr99] and vapor-pressure of the compounds. The vapor pressure can be determined by Antoine equation and the coefficients of this equation can be found in the literature (e.g., [Lang99]). The procedure is represented in Appendix A. The calculated values of the free Gibbs energy of formation of the esters in liquid state are show in Table 3-4. They are used to compute the free Gibbs energy of reactions ΔG_r^{298K}, using the other standard Gibbs energy formation of other compounds sourced by [CRC06] and the Eq. 2-73. The results are given in Table 3-5.

Table 3-4: The standard free Gibbs energies of formation of the investigated compounds from [CRC04, Perr84, Perr99 and Stull89]

Compound	$\Delta G_{f,i}^{298K}$ [kJ/mol]						
	Liquid				Gas		
	[CRC06]	[Perr84]	[Stull69]	Calculated [*]	[CRC06]	[Perr99]	[Stull69]
MF	-	-299.28	-	-299.05	-	-295.00	-297.19
EF	-	-	-	-306.14		-303.10	-
MA	-	-	-	-327.11	-	-324.20	-
EA	-	-318.44	-332.71	-330.02		-328.00	-327.40
M	-166.6	-166.52	-166.23	-	-162.3	-162.32	-162.51
E	-174.8	-174.72	-174.14	-	-167.9	-167.85	-168.28
F	-361.4	-346.02	-361.46	-	-	-351.00	-351.00
A	-389.9	-391.46	-389.36	-	-374.2	-374.60	-376.69
W	-237.1	-237.19	-	-	-228.6	-228.59	-228.61

[*] *see Appendix A (based on [Perr99, Lang99])*

Table 3-5: The standard free Gibbs energies and enthalpies of hydrolysis reactions were calculated by Eqs. 2-73 and 2-79 using the values given in Table 3-3 and 3-4

Reactant	ΔG_r^{298K} [kJ/mol]	ΔH_r^{298K} [kJ/mol]	
	Eq. 2-73 [Perr99, CRC06]	Eq. 2-79 [CRC06, Hin74]	Literature
MF	8.15	7.7	16.3 [Reut05]
EF	7.04	13.7	-
MA	7.71	8.2	6.51 [Song98]
EA	2.42	3.2	5.83 [Yu04]

3.1.3. Dissociation equilibria

The esters are not dissociable, whereas other relevant components can be dissociated to form H^+ ions by following reactions:

$$CH_3OH \rightleftharpoons CH_3O^- + H^+ \tag{3-2}$$

$$C_2H_5OH \rightleftharpoons C_2H_5O^- + H^+ \tag{3-3}$$

$$HCOOH \rightleftharpoons HCOO^- + H^+ \tag{3-4}$$

$$CH_3COOH \rightleftharpoons CH_3COO^- + H^+ \tag{3-5}$$

$$H_2O \rightleftharpoons OH^- + H^+ \tag{3-6}$$

Because the catalytically active species for ester hydrolysis reactions are H^+ ions or OH^- ions, the H^+ ions formed these reactions can be considered as possible autocatalytic agents. These reactions are characterized by the acid dissociation constant pK_a which is defined as the negative of logarithm of the equilibrium constant K_a.

$$pK_a = -\log K_a \tag{3-7}$$

In Table 3-6 are provided acid dissociation constants of the hydrolysis products and water at different temperatures [CRC93]. Because of minus sign in the definition, the lower the acid dissociation constant pK_a, the larger the equilibrium constant K_a, the stronger the acidity. Formic acid has the strongest acidity, about ten times stronger than acetic acid. The acidity of the alcohols is weaker than that of water. In the temperature range, the

dependence of the acid dissociation constants of the acids on temperature has a different trend in comparison with that of water.

Table 3-6: The acid dissociation constants pK_a (Eq. 3-7) of the alcohols, the acids and water at different temperatures (298~328K) [CRC93]

Compound	pK_a [-]			
	298K	308K	318K	328K
M	15.5	-	-	-
E	15.5	-	-	-
F	3.752	3.758	3.773	-
A	4.756	4.762	4.777	-
W	13.995	13.685	13.405	13.152

3.1.4 Chemical equilibria

Theoretical basics of chemical equilibrium have been mentioned in Section 2.2.3. Applying Eq. 2-76 for ideal systems, the general equilibrium expression for homogeneously catalyzed ester hydrolysis reactions K_{eq}^{hom} is:

$$K_{eq}^{\text{hom}} = \frac{c_{Al,eq}\, c_{Ac,eq}}{c_{Es,eq}\, c_{W,eq}} = \frac{1}{K_{eq,esterification}^{\text{hom}}} \tag{3-8}$$

For reactions involving ideal or nearly ideal solutions, the equilibrium constant K_a^{298K} at standard temperature can be calculated by Eq. 2-77 using the standard free Gibbs energy of reactions given in Table 3-5. The equilibrium constants K_a^T at other temperatures are computed by Eq. 2-80 (i.e., Van't Hoff equation). The calculated values of equilibrium constants at different temperatures are shown in Table 3.7.

For real solutions, the equilibrium constant should be determined by experiments. Several experimental studies related to chemical equilibrium of hydrolysis or esterification of the four esters can be found in the literature (e.g., [Schultz39, Trim40, Indu93, Mazz96, Song98, Lode02, Falk02, Mai 06 etc.]). Chemical equilibria of methyl formate and ethyl formate hydrolysis reactions catalyzed by hydrochloric acid were studied by [Schul39]. All

experiments were carried out at 378°K for 48~60 hours. It indicated that the equilibrium constants were strongly depended on initial ratio between esters and water. For the initial ratio of methyl formate and water varied from 1:1 to 0.05 [mol/mol], the equilibrium constant of methyl formate hydrolysis changed from 0.232 to 0.14. The equilibrium constant of ethyl formate hydrolysis changed from 0.203 to 0.307 for the initial ratio varying from 3.13 to 0.25. However, the equilibrium constants strongly depend on the initial ratios if the initial ratios are higher than solubility of the esters in water. The equilibrium constants depend on the concentration of hydrochloric acid also. For water-ester mixtures (1:1), the concentration of homogeneous catalyst increased from 0.0047 to 0.019 M, the equilibrium constants decreased as follows: methyl formate 0.155 to 0.122, ethyl formate 0.239 to 0.193. Contrary to [Schul39], the equilibria of methanol-formic acid esterification using sulfuric acid as catalyst were studied by [Indu93]. With a wide range of sulfuric acid concentration varied from 0 to 5 [mol/L], the inverse equilibrium constant for methyl formate hydrolysis at a temperature of 25°C changed from 0.233 to 0.073. Recently, a value of $K_{eq}^{hom} = 0.12$ for methyl formate hydrolysis at 298K has been determined by [Falk03].

Table 3-7: The equilibrium constants K_a^T at different temperatures (298~328K) were calculated by the values of ΔG_r^{298K} and ΔH_r^{298K} given in Table 3-5 using Eqs. 2-77 and 2-80

Reactant	K_a^T [-]			
	298K	308K	318K	328K
MF	0.037	0.041	0.046	0.050
EF	0.058	0.064	0.070	0.076
MA	0.045	0.049	0.054	0.059
EA	0.377	0.389	0.400	0.412

Temperature effects on the equilibrium constant of methanol-acetic acid esterification using ion-exchange resin were studied by [Song98]. Determined values of the equilibrium constant decreased from 30.2 to 24 when the temperature varied from 313K to 323K. Independently, a value of the equilibrium constant at 298K is 35 determined by [Lode02]. Thus, the inverse equilibrium constants for methyl acetate hydrolysis interpolated from [Song98] are 0.033 to 0.042 in the temperature range.

The chemical equilibria of ethyl acetate esterification with perchloric acid as catalyst were experimentally studied by [Trim40]. The experiments were carried out at 308K with the initial ratio (1:1) between ethanol and acetic acid. Depending on the concentration of perchloric acid varied from 0.006 to 0.0258, the equilibrium constant for the esterification reaction increased from 3.32 to 13.51. Thus, the inverse equilibrium constant at for ethyl acetate hydrolysis decreased from 0.30 to 0.074. The equilibrium constant of ethyl acetate esterification as a function of temperature was given by [Mazz96]. The inverse function for equilibrium constant of ethyl acetate hydrolysis reaction is:

$$K_{eq} = \exp\left(-\frac{854}{T}\right) \tag{3-9}$$

Due to different experimental conditions and contradictions, the available data in the literature are not fully satisfactory for the goal of this work. That is the reason why chemical equilibria of the ester hydrolysis reactions were determined experimentally in this work in a collaboration work with [Mai06] (see Section 4.2.2).

3.2 Stationary phases

3.2.1 Introduction

For many chemical reactions, conventional catalysis can be effectively replaced by ion-exchange resins because of their lack of corrosiveness and their significant advantages to improve separation between catalyst and fluids. Most applications of ion-exchange resins for organic synthesis have been reviewed by [Helf95, Gelb05]. Typical ion-exchange resins are based on the copolymer of styrene and divinylbenzene (PS-DVB) in form of beads. The resins can have a gel or macropore structure, depending on the DVB content varying from 2 to 20% or higher. The percentage of DVB is also defined as the degree of crosslinking of the network and it has significant influences on many physical and chemical properties of the resins. Additional treatment of the copolymer can produce the resins capable of cation and anion exchange. This kind of the resins was first synthesized by [Alel44] and then commercialized by chemical companies under different trade names (e.g., Dow Chemical Company (DOWEX), Rohm and Hass Company (Amberlyst), Sybron Chemicals Inc. - Bayer Group (Lewatit), Degussa (Deloxan), Finex Oy (FINEX) etc.). For the most studies on reactive chromatography that are summarized in Table 1-3 , the strongly acidic cation exchange resins characterized by the sulfonic acid group (-SO$_3$H) were used as the catalysis and adsorbent.

Although polystyrene can be soluble in many solvents, the crosslinked resin is insoluble because of interconnect the various hydrocarbon chains. Matrix of PS-DVB is hydrophobic, whereas the sulonated resin is hydrophilic. Therefore, the ion-exchange resin represents different behaviors when they are placed in polar or nonpolar solvents, aqueous or non-aqueous solutions. Some properties of the resins related to the investigated compounds are withdrawn from [Helf95] and introduced here.

3.2.1.1 *Ion-exchange and exchange capacity*

Initially, the resins are used in hydrogen form, in which H^+ ions are bound to the active sites. There H^+ ions can be removed either by dissociation in solution or by replacement with other positive ions. When an H^+ ion is exchanged in aqueous solution, it combines with a water molecule to form the hydronium ion H_3O^+.

$$R\text{-}SO_3H + H_2O \rightleftharpoons R\text{-}SO_3^- + H_3O^+ \tag{3-10}$$

When pure water is passed though a packed bed of the resin, only a minute fraction of the acidic hydrogen is lost from the active groups. The imbalance of positive and negative charges is insignificant because the system has to remain electrically neutral. Sulfonic acidic groups are close relatives of the more familiar sulfuric acid and they can be considered as insoluble acid. The resin can be converted easily to sodium form by the following exchange process:

$$R\text{-}SO_3H + Na^+ + H_2O \rightleftharpoons R\text{-}SO_3Na + H_3O^+ \tag{3-11}$$
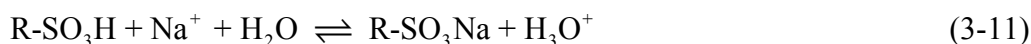
Exchange capacity is characterized by weight capacity or volume capacity. The weight capacity is defined by the number of ionogenic groups contained in the specific amount of the dry resin. Volume capacity is calculated by the number of ionogenic groups per unit of packed bed (in fully swollen state).

3.2.1.2 *Swelling*

Ion-exchange resins are able to adsorb solvents in which they are placed. During taking up solvent, the resins usually expands or "swell". The coil and packed chains of the matrix unfold and make rooms for solven molecules, but the chain cannot separate completely because they are interconnected by crosslinks. As the result, the resin swells but not dissolves. The resins swell to only a limit degree. Functional groups (e.g., sulfonic acid group) tend to surround themselves with polar solvent molecules and thus to stretch the

matrix. The stretch is resisted by an increasing resistance by the elastic forces of matrix. Swelling equilibrium is attained due to a balance of these opposite forces.

The swelling ratio is defined as the volume ratio of the swollen resin at equilibrium (V_{Re}^{eq}) to the dry resin (V_{Re}^{0}) depending on the nature of the liquid:

$$Sw = \frac{V_{Re}^{eq}}{V_{Re}^{0}} \qquad\qquad (3\text{-}12)$$

According to [Helf95, p. 100], the swelling depends on the following main factors:

- A high capacity ion-exchange resin contains ions in higher concentration, and thus it swells better than a low capacity resin.

- Polar solvents are better swelling agents than nonpolar solvents. Referring to polarity of the investigated components, swelling of the resins is strongest in water, followed by alcohols, acids and esters.

- Highly crosslinked resins have a reduced ability to swell. Therefore, macropore resins swell more badly than gel style resins.

- Resins with stronger affinity of ionic groups swell more strongly. Obviously, strong acidic cation-exchange resins swell better than weak acidic cation-exchange resins.

When the dry resin is brought into a aqueous solution, it takes up all components of the solvent. However, more polar component is preferred by resin and is taken up more strongly. Therefore, water followed by the alcohols and the acids are preferred more strongly than nonpolar components such as the esters. Particularly, for Amberlite IR-120 (a sulfonated crosslinked polystyrene), [Boda53] found that swelling ratio in ethanol-water mixture is stronger than in pure water.

3.2.1.3 Sorption

Formic acid and acetic acid are weak electrolytes, while the other investigated components (i.e., water, alcohols and esters) are non-electrolytes. Unlike strong electrolytes, weak and non-electrolytes are adsorbed by the ion-exchange resin in a similar way as by usual nonionic adsorbents. In the case of water in excess, sorption of the investigated components can be explained by sorption mechanisms given by [Helf95, p. 125]:

Ionic solvation and salting out: The fixed ionic groups and counter ions in the resin form solvation shells and thus tie up solvent molecules. Therefore, fraction of free solvent inside matrix of the resin is smaller than in the solution. If internal free solvent is not sufficient to dissolve the solute and there are not any interactions of the solute with matrix of the resin, the solute is "salted out". Sorption of acetic acid by sulfonated styrene-type resins can be explained quantitatively by the salting-out effect in a study of [Reic56]

London and Dipole interactions: Sorption of organic nonelectrolytes with hydrocarbon matrix of the resin is affected by two kinds of interactions. First, London forces are specific interactions between solute and the matrix. These forces are usually weak and depend on structure of solute and the matrix. For styrene-type resins, high affinity and thus strong sorption may be expected for aromatic compounds because of similar chemical configurations of the solute and the matrix. Second, stronger contribution may come from dipole-dipole interactions of polar solvent molecules with one another and with polar groups of the solute.

When only little water is present in polymer, chemistry of the resin is different from that in the swollen resin (hydrated resin). Without excess of water, H^+ ions of the $-SO_3H$ groups are not dissociated and $-SO_3H$ groups are the proton donors. [Kabe62] found an evidence that ethanol vapor is adsorbed by a chemisorption process.

The average mesh width of fully swollen resin is about 6 to 30 Å [Helf95], whereas molecular diameter of water (smallest) is 3.43 Å and of ethyl acetate (biggest) is 5.39 Å [Marc99]. Therefore, sieve action of the matrix is neglected. Like nonionic adsorbents, sorption equilibria depend on solution concentration and temperature. Temperature effects on sorption equilibria are discussed in Section 5.3.2.

For the most studies on reactive chromatography, sorption equilibria between solutes and stationary phases are important to study. The sorption equilibria can be obtained for either single components or non-reactive binary mixture. Multicomponent sorption equilibria of esters, acids, alcohols and water on ion-exchange resins at high concentration ranges using binary mixture method have been studied by [Lode02, Gelo03, Strö05, Sain05 etc.]. In contrast, soprtion equilibria of single methyl formate, formic acid and methanol on Dowex 50W-X8 at low concentration range have been determined by [Falk02, Schl06]. Different concentration ranges lead to different adsorptivity order between esters, acids, alcohols.

3.2.2 Stationary phases employed

In this work, two batches of the strongly acidic cation exchange resin Dowex 50W-X8 (Dow Chemical Company) were used. With 8% of DVB, this resin has gel structure (i.e. micropore). Physical and chemical properties of the two batches are shown in Table 3-7. The difference between the two batches was essentially the range of particle sizes and time in use. The stationary phase with the smaller particle size (Cat-1) was already used extensively in the investigations of [Falk02, Mai06]. The second (Cat-2) was purchased prior to the study discussed here. The resin offers high adsorption capacity due to micropore structure and the advantages of an insoluble strong acid. It satisfies virtually all requirements of a good adsorbent and a good catalyst in single bears.

Table 3-8: Physical and chemical properties of the two batches
of the catalyst used in this work [Dow02]

Catalyst characteristic	Cat-1	Cat-2
Particle size [μm]	32-45	38-75
Type	Dowex 50W-X8	
Active group	sulfonic acid	
Matrix	styrene-divinylbenzene	
Ionic form	H^+	
Volume capacity [meq/mL]	-	1.7[*]
Weight capacity [meq/g]	-	4.8[*]
Bulk density [kg/m^3]	800	
Feature	Used since 1998	Used since 2003

3.3 Summary and goal of experimental works

Above several relevant thermodynamic and kinetic data regarding the ester hydrolysis reactions and the sorption processes on ion-exchange resins have been summarized based on information in the literature. Several these data are inconsistent or missing (e.g.,

---

[*] *Brochure of a supplier (Sigma Aldrich, 2006)*

chemical equilibria). Further, the available data are insufficient for a complete description of the four ester hydrolysis reactions investigated in this work. Selected data have been determined in this work in order to allow predicting feasibility of chromatographic reactor operation, studying reaction kinetics and optimizing performance of FBCRs.

For achieving this goal, equipment and procedures described in Chapter 4 were applied. At first, experiments were carried out systematically to characterize properties of stationary phases and to determine chemical and adsorption equilibria as well as other model parameters. More specific efforts were there devoted to quantify the rates of the heterogeneously catalyzed reactions. Quantification of the influence of temperature on the model parameters and in particular on the reaction kinetics is main objectives of this work.

Experimental Procedures

In order to achieve the goal given in Section 1.3, experiments were performed to determine the model parameters represented in Chapter 2 and to study influences of experimental conditions on these parameters. Experimental equipment used and experimental procedures are introduced in this chapter. Preliminary experiments were carried out to collect data for chemical equilbria, properties of stationary phases, adsorption equilibria and characterizations of reactors. Based on the preliminary experiments, model parameters are determined and discussed later in Chapter 5. Finally, other experiments for the ester hydrolysis reactions performed on FBCRs were used for qualitative discussions in Chapter 6 and quantitative studies on reaction kinetics in Chapter 7.

4.1 Chemicals and equipment

4.1.1 Chemicals

The chemicals used for the experiments are supplied by Merck KGaA. Type and purity of the chemicals are given in Table 4-1. Methanol content in methyl formate and ethanol in ethyl formate are relatively high and they have to be considered in concentration calculations. Tap water was deionized and filtered by an ion exchange unit AQUADEM$^{®}$ and a 2-stage reverse osmosis unit (RO 20 manufactured by Wilhelm Werner GmbH). The conductivity of deionized water was in the range of 1~5μS/cm.

4.1.2 Batch reactor

Conventional batch experiments were carried out to determine chemical equilibrium constants. Glass flasks 100mL with tightened screw cap were used as reactors. Reactant mixtures were prepared and poured into the flasks containing homogeneous catalyst. To keep temperature stable, the flasks were placed in a water shaking bath unit SW-21c (JULABO Labortechnik GmbH). The working temperature was controllable in the range of

20~90 $\pm$ 0.1°C and the shaking frequency was adjustable from 40~200 rpm. When reactions reached equilibrium state, the reaction mixtures were sampled and put into standard 2mL vials, then quickly cooled to 1°C to avoid equilibrium changes. To analyze the compositions of the reaction mixtures, the taken samples were injected into a gas chromatography system Agilent 6890 (Agilent Technologies Inc.), with injection volume 2µL (repeat 5 times). This gas chromatography system was equipped with a thermal conductivity detector and a capillary column (25.0 m length, 320µm ID and 0.25 µm film thickness). The stationary phase of the capillary was polyethylenglycol and the mobile phase was helium. Calibrations were carried out to establish a mathematical correlation between concentration of a component and corresponding peak area. For accuracy guarantee, samples for the calibrations were also kept at 1°C. The gas chromatography system was controlled by a computer and the collected data was analyzed by ChemStation® software also supplied by Agilent Technologies Inc.

Table 4-1: Purity of the chemicals used for investigations

Compounds	Purity [%]	Impurity [%]	Notes
MF	~ 97	M ~3	For synthesis
EF	$\geq$ 98	E $\leq$ 2	For synthesis
MA	$\geq$ 99	-	For synthesis
EA	$\geq$ 99.5	W $\leq$ 0.1	For synthesis
M	$\geq$ 99.9	W $\leq$ 0.1	Gradient grade for liquid chromatography LiChrosolv®
E	$\geq$ 99.9	W $\leq$ 0.1	Gradient grade for liquid chromatography LiChrosolv®
F	$\geq$ 99	-	For synthesis
A	$\geq$ 99	-	For synthesis
W	-	-	Deionized, Filtered < 0.2µm

4.1.3 Fixed-bed chromatographic reactors

In order to analyze reaction kinetics and separation, the ester hydrolysis reactions were performed in FBCRs. In this work, there were two kinds of empty standard stainless steel columns of HPLC used as reactors. The 8 x 250mm columns were usually used for semi-preparative separation and the 4.6 x 250 columns were most commonly used for analytical purpose. The columns were packed with the catalysts described in Section 3-2 by Chromatographie Technik GmbH, using slurry technique. For systematical description,

names of the reactors are encoded as in Table 4-2. The first index refers to the size of reactors (R1 for big columns, R2 for small columns), and the second index refers to batches of the catalyst (C1 or C2). Most results shown in this dissertation were obtained from the reactor R1-C1 and the other ones were only used for comparisons.

Table 4-2: Characterization of the different fixed-bed chromatographic reactors applied in combination with the catalysts

Reactor and Catalyst code	Column size ID x L [mm]	Column volume [mL]	Catalyst
R1-C1	8 x 250	12.566	Cat-1
R2-C1	4.6 x 250	4.155	Cat-1
R1-C2	8 x 250	12.566	Cat-2
R2-C2	4.6 x 250	4.155	Cat-2

In order to collect data and observe processes, the experimental system was established as a standard HPLC system shown in Figure 4-1. In this system, temperature, flow rate, feed concentration, and injection volume could be varied as desired.

The columns were placed into a column oven model L-2300 supplied by Hitachi High-Technology Corp. The oven permits a wide range of temperature control from cooling to heating with high accuracy (from 1 to 65 ± 0.1 °C). A pump model 590 and a manual injector model U6K manufactured by Waters Corporation were used. Water was continuously pumped into the columns and thus acted, in addition to being a reactant, as the mobile phase for elution. The flow rate can be set from 0.001 to 20 mL/min and high pressure limit of the pump can be adjusted from 0~480 bars. The injector can accommodate the full range of analytical and preparative injections, with injection volume from 1μL to 2 mL. A degasser (Jour X-Act^{TM}) was placed at the front of the pump to remove dissolved air/oxygen from the mobile phase. Flow rate was also checked by a flowmeter or a microliter flowmeter. The process was monitored by two detectors connected in series. The model K-2300 refractive index detector (RI) was manufactured by Wissenschaftliche Gerätebau Dr. Ing. Herbert Knauer GmbH and the model L-7420 UV-VIS detector was manufactured by Hitachi High-Technology Corp. The specifications of the two detectors are shown in Table 4-3. The detector signals were transmitted to an interface box made by Knauer, and then recorded by a computer with EuroChrom$^{®}$ software. Calibrations of the two detectors were represented in Appendix B. The operating

flow rate of the system was limited by maximum working pressure of the flow cell of RI detector. Before experiments carried out, dead volume of the system without the reactors (incl. total volume of tubes and connectors from the injector to detector) was determined by a tracer and used in calculations to separate between extra and intro column retention.

The four temperatures chosen to carry out experiments were 298, 308, 318 and 328K. Due to the maximum of the acceptable working pressure of the flow cells, operating flow rate was limited to 3.5 mL/min.
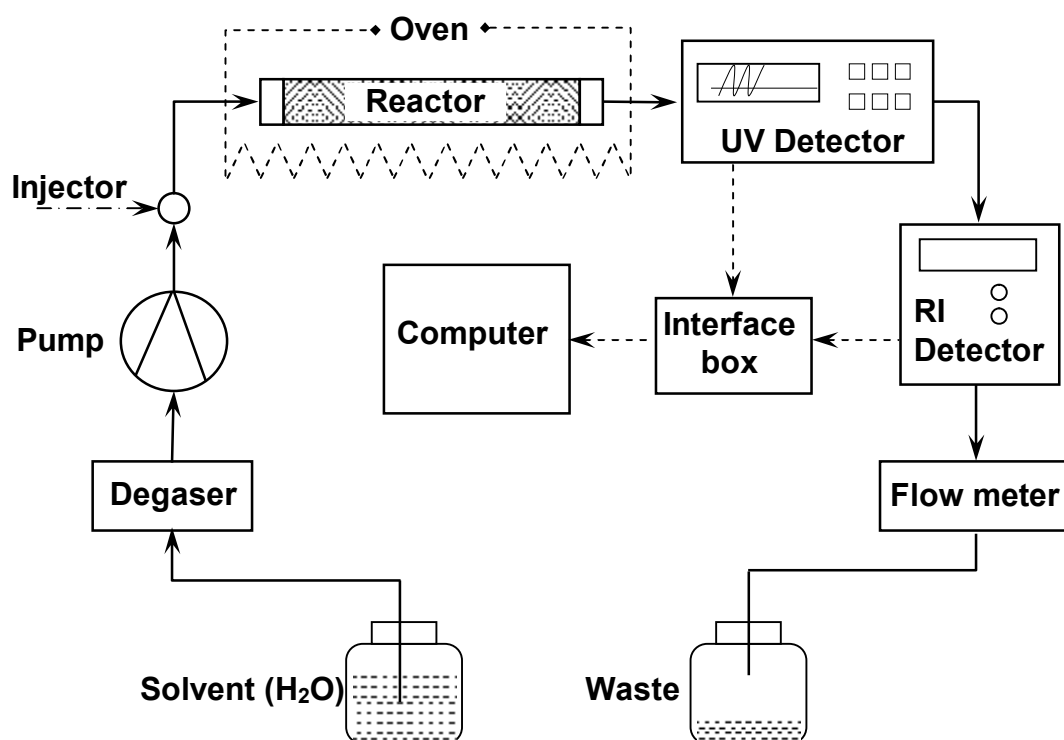
Figure 4-1: Diagram of the experimental system

Table 4-3: Specifications of the detectors used

	RI detector (Knauer, K-2300)	UV-VIS detector (Hitachi L-7420)
Flow cell volume	9 μL	-
Max. pressure	0.2 MPa	1 MPa
Range of measurement	0 ~ 1000 μRIU	0 ~ 3000 mV
Noise	$< \pm 8 \times 10^{-8} \, \Delta n$	$< 0.8 \times 10^{-5} \, AU$

4.2 Preliminary experiments

4.2.1 Characterization of the stationary phases

In addition to initial information provided by manufacturer (Table 3-7), a number of experiments had to be performed to determine other important properties and the swelling behavior of the unpacked resins.

True density: The bulk density of the resins given in Table 3-7 cannot be used in calculations of swelling ratio. Instead, the true density of the resins was determined by a helium pycnometer, model 1305 manufactured by Micromeritics Corp.

Swelling ratio: The dry resins swell when they come into contact with liquids until an equilibrium is reached. The swelling ratio is determined by the definition given in Eq. 3-12. In this work, the swelling ratios of the resins were estimated to be at 298K for all single components (MF, AF, MA, EA, M, E, F, A and W). To this end, the resin was kept in contact with each of the liquid components until no further volume change could be detected. This was usually achieved after only a few minutes. Nevertheless, the final volume of the swollen resin was measured the next day after the resin had been separated from the liquid phase by centrifugation.

Exchange capacity: To compare the exchange capacity of Cat-1 and Cat-2, the amounts of sulfonic acid groups per unit mass of the resins were quantified by titrating approximately 0.15 g of each of the dried resins in 50ml water with sodium hydroxide solution (0.1 N). The number of acid equivalents and thus the capacity of the resins can be calculated from amount of titrant added at the point where a steep rise in pH occured.

4.2.2 Determination of chemical equilibrium constants

Experiments using for determination of chemical equilibria are carried out in collaboration with [Mai06]. In order to determine chemical equilibrium constants of the hydrolysis reactions, experiments were carried out on the batch reactor system described in Section 4.2.2. The initial mixtures of the esters and water were prepared at concentrations near the solubility limits given in Table 3-1. Hydrochloric acid (HCl) was used as homogeneous catalyst at a diluted concentration of 0.05 [mol/L]. The experiments were started at 298K, and then raised to 308, 318 and 328K. At each temperature, when equilibrium was successfully reached, the samples were taken and analyzed by gas chromatography. The running time was varied depending on the operating temperature and fast or slow reactions.

The experimental conditions are summarized in Table 4-4 and the results are given in Table 5-1.

<div align="center">Table 4-4: Summary of experimental conditions
to determine the chemical equilibrium constants K_{eq}^{hom} (Eq. 3-8)</div>

Run	Reactant	Initial ratio of Ester/water [mol/mol]	Temperature
CEQ-1	MF	0.093	298, 308, 318, and 328K
CEQ-2	EF	0.030	298, 308, 318, and 328K
CEQ-3	MA	0.066	298, 308, 318, and 328K
CEQ-4	EA	0.012	298, 308, 318, and 328K

4.2.3 Characterization of fixed-bed chromatographic reactors

In order to estimate the porosity of the reactors ε_t, Blue Dextran, a high molecular weight glucose polymer (the original mol. wt. 2.10^6 g/mol), was used as a tracer. Because of high molecular weight, Blue Dextran does not have any adsorption or ion-exchange with stationary phases. Thus it can be assumed that it is not retained by stationary phases. The experiments were carried out at all investigated temperatures with an aqueous solution 0.5% wt. of Blue Dextran and an injection volume of 20µL. Based on the definition of the porosity ε_t given in Section 2.1.2.1, the total porosities of the columns were estimated from the retention times of the Dextran Blue (t_o) at the corresponding volumetric flow rates ($\dot{V}$), and the volume of the column (V_{col}) according to:

$$\varepsilon_t = \frac{\dot{V} t_o}{V_{col}} \qquad (4\text{-}1)$$

4.2.4 Determination of adsorption equilibrium constants

Comparing to conventional static methods, chromatographic methods are the fastest and often more accurate for the purpose of determining adsorption isotherms [Seid04]. The chromatographic methods and their capability for applications have been reviewed by [Seid04]. The retention time method can be applied to measure adsorption equilibrium constants K_i of single components reliability. Based on Eq. 2-49, these linear adsorption equilibrium constants can be calculated using the following equation:

$$K_i = \left(\frac{\varepsilon_t}{1-\varepsilon_t}\right)\left(\frac{t_{R,i}}{t_o}-1\right) \tag{4-2}$$

where $t_{R,i}$ is the average retention time of component i. It was determined by analyzing a series of pulse injections with different sample concentrations. For these experiments, injection volume was 100µL, the sample concentrations of the investigated components were varied from 0.1 to 0.5 mol/L and each sample was repeatedly injected 3~5 times. Conditions of experiments to determine adsorption equilibrium constants are summarized in Table 4.5.

Table 4-5: Summary of experimental conditions
to determine adsorption equilibrium constants K_i (Eq. 4-2)

Run	Component	Reactor	Flow rate [mL/min]	Temperature [K]	Form of resin	Concentration [mol/L]
AEQ-1	M, E, F, A	R1-C1	0.75	Room temp.	H+	0.1~0.5
AEQ-2	M, E, F, A	R1-C2	0.75	Room temp.	H+	0.1~0.5
AEQ-3	MF, EF, MA, EA	R1-C1	2.5~3.5	Room temp.	H+	Pure esters
AEQ-4	MF, EF, MA, EA	R2-C2	2.5~3.5	Room temp.	H+	Pure esters
AEQ-5	M, E, F, A	R1-C1	0.75	298, 308, 318, 328	H+	0.1~0.5
AEQ-6	MA, EA	R1-C1	3.5	298, 308, 318, 328	H+	Pure esters
AEQ-7	M, E, MF, EF, MA, EA	R2-C1	0.75	298, 308, 318, 328	Na+	0.1~0.5

In order to compare adsorption behaviour of Cat-1 and Cat-2, additional experiments from AEQ-1 to AEQ-4 were carried out at room temperature (before the column oven was purchased). Because the esters were converted catalytically to products in the presence of the resins, it was very difficult to determine their adsorption equilibrium constants. Sufficiently small pulses of the pure esters were injected at a sufficiently high flow rate (to reduce the contact time between the reactants and the stationary phases) and the adsorption equilibrium constants of the esters can determined from the retention time of the peaks of the unconverted esters.

To estimate temperature effects on adsorption equilibrium constants for Cat-1, experiments AEQ-5 and AEQ-6 were carried out. Following the advice of [Sard93, p. 487] for poisoning catalyst to measure reactants isotherms, ion-exchange resins in H^{+} form were

temporarily converted into Na^+ form (i.e, Eq. 3-11), using a solution NaOH 0.1M. Of course, the adsorption equilibrium constants of the ester were determined more easily without reaction even at higher temperatures and dilute concentration of esters. Adsorption equilibrium for esters and alcohols with Cat-1 in Na^+ form were determined by the AEQ-6. After that, the ion-exchange resins could be regenerated by HCl 0.05M solution to convert back to H^+ form.

Based on the dependence of adsorption equilibrium constants on temperature, heat of adsorption and other related information could be estimated.

4.2.5 Determination of number of theoretical plates:

In the equilibrium-dispersion model (Eq. 2-24), the apparent dispersion coefficients $D_{ap,i}$ of the components are very important parameters. They are lumped parameters for all effects causing band broadening. However, these parameters are usually represented through the corresponding numbers N_i of theoretical plates that can be related to $D_{ap,i}$ by Eq. 2-61. In chromatography the numbers of theoretical plates are typically used to characterize column efficiency. They are a function of flow rate and temperature, and can be determined from results of pulse experiments, using Eq. 2-67. Experimental conditions for estimation of the number of theoretical plates are summarized in Table 4-6. Runs NTP-1 and NTP-2 were used to compare efficiency of columns R1-C1 and R2-C2. Run NTP-3 was used to estimate temperature effects on the number of theoretical plates. Both effects of flow rate and temperature were studied by NTP-4.

Table 4-6: Summary of experimental conditions
to estimate the number of theoretical plate N_i (Eq. 2-67)

Run	Component	Concentration [mol/L]	Injection volume [μL]	Reactor	Flow rate [mL/min]	Temperature [K]
NTP-1	M, F	0.5	100	R1-C1	0.5 ~ 4	Room temp.
NTP-2	M, F	0.5	100	R1-C2	0.5 ~ 4	Room temp.
NTP-3	M, E, F, A	0.5	100	R1-C1	0.75	298, 308, 318, 328
NTP-4	M, A	0.5	100	R1-C1	0.3 ~ 3.5	298, 308, 318, 328

4.3 Experiments for hydrolysis reactions in FBCRs

Subsequent to the non-reactive experiments to determine the model parameters, further experiments for ester hydrolysis reactions were carried out to study qualitatively the influence of various performance conditions (e.g., temperature, flow rate, stationary phases, reactor size, sample size etc.) and to estimate quantitatively reaction rate constants.

4.3.1 Influence of stationary phases on hydrolysis of the esters

Differences between two batches of the resin were identified in preliminary experiments. In order to estimate influence of these differences on hydrolysis of the esters, the feed concentrations of the four esters and other experimental conditions were kept the same for the both reactors R1-C1 and R2-C2. A summary of these experiments is given in Table 4.7. The obtained results are discussed qualitatively in Section 6.2.1 and are used also for estimation of reaction rate constants in Section 7.1.

Table 4-7: Summary of experimental conditions
to estimate influence of stationary phases on hydrolysis of the esters (using reactors R1)

Run	Catalyst	Reactant	Feed Concentration [mol/L]	Injection volume [μL]	Flow rate [mL/min]	Temperature [K]
SP-1	Cat-1	MF,EF, MA, EA	0.5	100	0.3	Room temp.
SP-2	Cat-2	MF,EF, MA, EA	0.5	100	0.3	Room temp.

4.3.2 Influence of flow rate on hydrolysis of the esters

Flow rate is an important parameter in operation of fixed-bed chromatographic reactors. It controls the contact time between the reactants with the stationary phases and the retention time of all components. Therefore, it has effects not only on reaction kinetic but also on separation of the hydrolysis products. In this case, the reactor R1-C1 was used and the flow rate was varied from 0.3 to 1.5 mL/min. Although, the experimental system can operate at higher flow rate, it leads to the inability to observe conversion and separation. A summary of these experiments is given in Table 4-8. The obtained results are discussed in Section 6.2.2 and compared with predictions of the optimum flow rate given in Section 5.5.3

Table 4-8: Summary of experimental conditions
to estimate influence of flow rate on hydrolysis of the esters

Run	Flow rate [mL/min]	Reactant	Feed Concentration [mol/L]	Injection volume [µL]	Reactor	Temperature [K]
FL-1	0.30					
FL-2	0.50					
FL-3	0.75	MF, EF, MA, EA	0.5	100	R1-C1	Room temp.
FL-4	1.00					
FL-5	1.50					

4.3.3 Influence of temperature on hydrolysis of the esters

Temperature is also an important parameter in operation of fixed-bed chromatographic reactors. It has effects on most model parameters. Hydrolysis reactions of the esters are carried out at four different temperatures to estimate influence of temperature on reaction kinetic. The obtained chromatograms are discussed in Chapter 6 and are used for determination of reaction rate constants in Chapter 7. Based on the dependence of reaction rate constants on temperature, the activation energy and frequency factor (Eq. 2-83) can be determined.

Table 4-9: Summary of experimental conditions
to estimate influence of temperature on hydrolysis of the esters

Run	Temperature [K]	Reactant	Feed Concentration [mol/L]	Injection volume [µL]	Reactor	Flow rate [mL/min]
TE-1	298					
TE-2	308	MF, EF, MA, EA	0.5	100	R1-C1	0.75
TE-3	318					
TE-4	328					

4.3.4 Influence of feed concentration on hydrolysis of the esters

Feed concentrations were varied in a narrow range to estimate influences of them on hydrolysis of the esters. For illustration, MA and the reactor R1-C1 were chosen to carry out these experiments. The sample size range covered was relatively small. A summary of these experiments is given in Table 4-9.

Table 4-9: Summary of experimental conditions
to estimate influence of feed concentration on hydrolysis of the esters

Run	Feed Concentration [mol/L]	Reactant	Injection volume [μL]	Reactor	Flow rate [mL/min]	Temperature [K]
FC-1	0.5					
FC-2	1.0	MA	100	R1-C1	0.75	Room temp.
FC-3	1.5					

4.3.5 Influence of reactor diameter on hydrolysis of the esters

Two kinds of reactors were used with the same length and different diameters. The cross-section of the semi-preparative reactors (i.e., ID 8 mm) was three times greater than that of the analytical reactor (i.e., ID 4.6 mm). The reactors R1-C1 and R2-C1 were chosen for these experiments. The flow rate was varied so that linear velocity of the two reactors is the same for each experiment. The ratio between feed concentrations for R1-C1 and R2-C2 was the same with the ratio between their cross-sections. Using these experimental conditions, the throughput over a unit of cross-section for the both reactors is the same. A summary of the performed experiments is given in Table 4-10.

Table 4-10: Summary of experimental conditions
to estimate influence of reactor diameter on hydrolysis of the esters

Run	Reactor	Reactant	Feed Concentration [mol/L]	Injection volume [μL]	Flow rate [mL/min]	Linear velocity [m/min]	Temperature [K]
FC-1	R1-C1	MA	0.5	100	0.3	0.024	Room temp.
	R2-C1		1.5		0.1		
FC-2	R1-C1	MA	0.5	100	0.75	0.060	Room temp.
	R2-C1		1.5		0.25		

Parameter Estimation

To model reactive chromatographic reactors precisely, knowledge of adsorption isotherms, chemical equilibria and proper characterizations of fixed-beds are main prerequisites. Based on the theories given in Chapter 2 and the experiments carried out using the procedures described given in Chapter 4, the parameters of the models introduced also in Chapter 2 were determined.

5.1 Characterizations of stationary phases

5.1.1 True density

Using a helium pycnometer, the true density of solid was extrapolated from the pressure change of helium in calibrated volumes of a reservoir chamber and a sample chamber. Based on measured pressures, the calculated true density of Cat-1 and Cat-2 were 1500 and 1450 Kg/m^3, respectively. These values are twice as high as the bulk density given by the manufacturer in Table 3-8.

5.1.2 Swelling ratio

Using Eq. 3-12, the swelling ratios of the catalysts obtained for all single components are listed in Table 5-1. From these data, it can be concluded that water has a higher affinity towards the resin than the other components. This is due to the strong polarity inside the resin created by the sulfonic acid groups, which attract water most strongly. This highest swelling ratios followed by the values of the alcohols, acids, and esters. It can be also seen from the data that the swelling ratios of the two catalysts are similar, although Cat-1 seems to swell slightly more than Cat-2. It should be also noted that the swelling rates of the resins were found to be rather high. It took only seconds to minutes for the resins to reach their equilibrium volumes after being contacted with a certain liquid.

Table 5-1: Swelling ratios of the stationary phases in different solvents

Component	Sw_i [-]	
	Cat-1	Cat-2
MF	1.49	1.42
EF	1.37	1.38
MA	1.79	1.67
EA	1.78	1.67
M	2.42	2.27
E	2.56	2.38
F	2.22	2.06
A	1.78	1.79
W	3.08	2.89

5.1.3 Exchange capacity

The corresponding sulfonic acid group concentrations of Cat-1 and Cat-2 were found by titration to be 3.9 and 4.8 meq/g, respectively. The value for Cat-2 is consistent with the value given in Table 3-8. The exchange capacity of Cat-1 was altered after long time in use. Because of higher exchange capacity, the catalytic activity of Cat-2 was expected to be higher than that of Cat-1.

5.2 Chemical equilibria

Chemical equilibrium constants $K_{eq}^{\mathrm{hom}}(T)$ for the four ester hydrolysis reactions were calculated by Eq. 3-8 based on the equilibrium concentrations of components determined at 298, 308, 318 and 328K (see the experimental procedures in Section 4.2.2). The obtained results are shown in Table 5-2. These experimental results were obtained in a collaboration work with [Mai06]. Obviously, the hydrolysis of MA is least favorable, and the formation of EF is most favorable. Raising temperature increases the chemical equilibrium constants, and thus shifts the equilibria to the hydrolysis direction (i.e. endothermic direction). The results obtained differ from the theoretical equilibrium constants calculated from the standard free Gibbs energy of formations and van't Hoff equation given in Table 3-7.

Table 5-2: Chemical equilibrium constants $K_{eq}^{hom}(T)$ of the four ester hydrolysis reactions at different temperatures determined experimentally using Eq. 3-8.

Run	Reactant	Es / W [mol/mol]	Temp. [K]	Concentrations in equilibrium [mol/L]				$K_{eq}^{hom}(T)$ [Eq. 3-8]
				Es	W	Al	Ac	
CEQ-1	MF	0.093	298	1.056	39.393	3.146	2.916	0.22
			308	0.969	39.750	3.232	3.002	0.25
			318	0.927	39.265	3.274	3.044	0.27
			328	0.880	39.217	3.322	3.092	0.30
CEQ-2	EF	0.030	298	0.116	47.169	1.451	1.451	0.38
			308	0.107	47.160	1.460	1.460	0.42
			318	0.104	47.157	1.463	1.463	0.44
			328	0.102	47.154	1.465	1.465	0.45
CEQ-3	MA	0.066	298	0.737	41.333	2.105	2.105	0.14
			308	0.658	41.255	2.183	2.183	0.17
			318	0.599	41.196	2.242	2.242	0.20
			328	0.573	41.169	2.269	2.269	0.22
CEQ-4	EA	0.012	298	0.026	51.215	0.667	0.667	0.33
			308	0.024	51.213	0.670	0.670	0.37
			318	0.022	51.211	0.672	0.672	0.40
			328	0.020	51.209	0.374	0.674	0.45

The temperature dependence of the chemical equilibrium constants is illustrated in Figure 5-1. Due to Eq. 2-80, the enthalpies of the reactions can be obtained from the slopes of the plots. However, the experimental results cannot be given straight lines and the reaction enthalpies depend on temperature. For this reason, the enthalpies of three temperature intervals were estimated separately. The free Gibbs energies of reactions calculated by Eq. 2-77 at different temperatures are not significantly different and their average values are acceptable. The calculated results for the free Gibbs energies and enthalpies of the reactions are shown in Table 5-3.
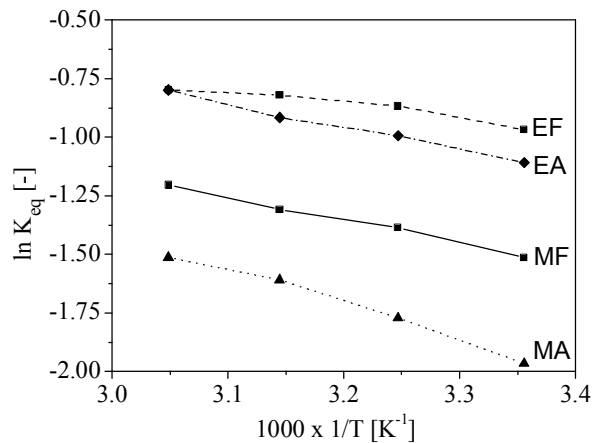
Figure 5-1: Temperature dependence of the chemical equilibrium constants $K_{eq}^{hom}(T)$ based on the data given in Table 5-2 (Runs CEQ-1 ~ CEQ-4).

Table 5-3: The standard free Gibbs energies and enthalpies of hydrolysis reactions calculated by Eqs. 2-77 and 2-80 using the data given in Table 5-2.

Reactant	$\overline{\Delta G_r^T}$ [kJ/mol]	ΔH_r^T [kJ/mol]		
		298~308K	308~318K	318~328K
MF	3.51	9.75	6.27	9.14
EF	2.24	7.64	3.79	1.95
MA	4.45	14.62	13.23	8.27
EA	2.47	8.73	6.35	10.21

(*) average values

5.3 Characterization of fixed-bed reactors

Based on the experiments described in Section 4.2.3, the porosities ε_t of the fixed-bed reactors equilibrated with water were determined from pulse experiments with blue dextran, using Eq. 4-1. The obtained results are shown in Table 5.4. The total porosities of the columns depend on particle size of the catalyst and the packing pressure. Because the ion exchange resins were packed by slurry method and water was used as mobile phase for all experiments, the determined porosities were referred to fully swollen state of the resins in water. The retention time of blue dextran did not change significantly in the investigated temperature range. The porosities of the reactors using the sample batch of catalyst were

similar. Because of using smaller particle size, R1-C1 and R2-C1 were obviously better packed than the other two reactors.

Table 5-4: Porosities ε_t of the fixed-bed chromatographic reactors equilibrated with water [298 ~ 328K]

Reactor	ε_t [-]			
	R1-C1	R2-C1	R1-C2	R2-C2
ε_t [-]	0.240	0.248	0.328	0.331

5.4 Adsorption equilibria

Most chromatographic separation is based mainly on differences between adsorption affinities of components. Therefore, investigation of adsorption equilibria is a very important step of this work. Based on the experiments described in Section 4.2.4, the obtained results are analyzed and discussed here.

5.4.1 Influence of stationary phases on adsorption equilibria

Figure 5-2 shows the elution profiles for various injection concentrations of F, A, M, and E with Cat-1 and Cat-2 (in H^+ form) at room temperature. Because R1-C1 was well packed by smaller particle size, it gives a better resolution than R1-C2. For various concentrations of each component (Runs AEQ-1, AEQ-2), rather symmetrical peaks were observed at the same specific retention times. This indicates that the linear equilibrium model (Eq. 2-48) is adequate. The linear adsorption equilibrium constants K_i can be calculated by Eq. 4-2. Because of the occurrence of the hydrolysis reactions, it was found to be difficult to get a single peak for the esters (especially for MF). For this reason, the pure esters had to be injected into the columns with an appropriate injection volume at a sufficiently high flow rate so that a significant amount was not converted. Table 5-5 summarizes the determined equilibrium constants for Cat-1 and Cat-2 with the stationary phases in H^+ form. Most of the equilibrium constant values (except those values of the alcohols) are slightly smaller for Cat-2 than for Cat-1.
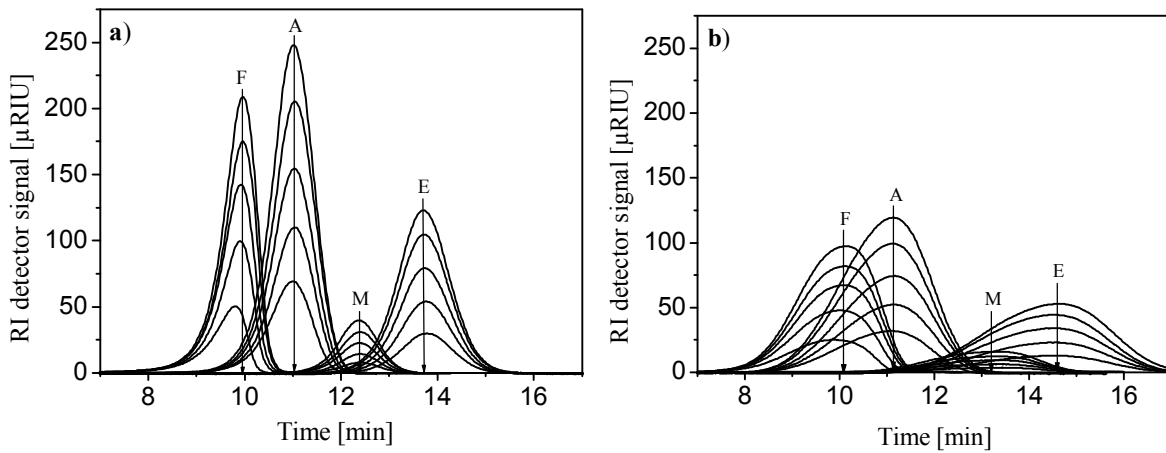
Figure 5-2: Elution profiles for various injection concentrations
(c_i^{inj} = 0.1 ~ 0.5 mol/L; V^{inj} = 100μL, $\dot{V}$ = 0.75 mL/min, room temperature)
a) Cat-1 (Run AEQ-1)   b) Cat-2 (Run AEQ-2)

Table 5-5: Adsorption equilibrium constants K_i of the components
determined for Cat-1 and Cat-2 in H$^+$ form at room temperature

Component	K_i [-]	
	Cat-1	Cat-2
MF	0.850 [a]	0.650 [a,b]
EF	0.995 [a]	0.819 [a]
MA	1.085 [a]	1.009 [a]
EA	1.327 [a]	1.219 [a]
M	0.628	0.673
E	0.736	0.781
F	0.432	0.380
A	0.520	0.476

[a] *using pure esters*
[b] *uncertain value due to difficulties in identifying the corresponding peak*

Because of differences in the surface characteristics between the two catalyst batches, there are differences in the elution orders and in the individual equilibrium constants. The elution order of the components in water is F, A, M, E, MF, EF, MA, and EA. For the alcohols, acids, and esters, the elution orders correspond to the order of molecular weights. In general in the presence of an excess of water, the adsorptivities of the esters and their hydrolysis products are characterized by the following order:

$$K_{Es} > K_{Al} > K_{Ac} \qquad\qquad (5\text{-}1)$$

Thus, in this work, the esters have highest adsorptivity in comparison with their hydrolysis products. In previous studies on methyl acetate synthesis performed by other authors in a broader range of solvent compositions using ion exchange resin Amberlyst 15 [Lode02, Pöpk00, and Sain05] more complex situations and different orders of adsorptivities were observed.

5.4.2 Influence of temperature on adsorption equilibria

5.4.2.1 *The resin in H^+ form*

Obviously, due to the smaller particle size, Cat-1 is more interesting for further study. With support of the column oven, temperature effects on the adsorption isotherm were investigated, using the same procedures carried out at the room temperature. In Figure 5-3 shows elution profiles used to determine the adsorption equilibrium constants of F, A, M, and E at the four different temperatures. The peak widths are reduced significantly at higher temperatures. The retention times of the acids have a tendency to move to the left side with temperature increase, whereas the retention times of the alcohols have the opposite tendency.

Adsorption equilibrium constants of MA and EA can be determined by using pure esters even at the higher temperatures. However, due to fast hydrolysis at high temperatures, these procedures were not successful with MF and EF. Figure 5-4 shows typical elution profiles of pure EA and blue dextran at two different temperatures. At 328K, EA was converted partially. The retention time of EA was shifted to the left side at higher temperatures while the retention time of blue dextran seems to be independent from temperature.
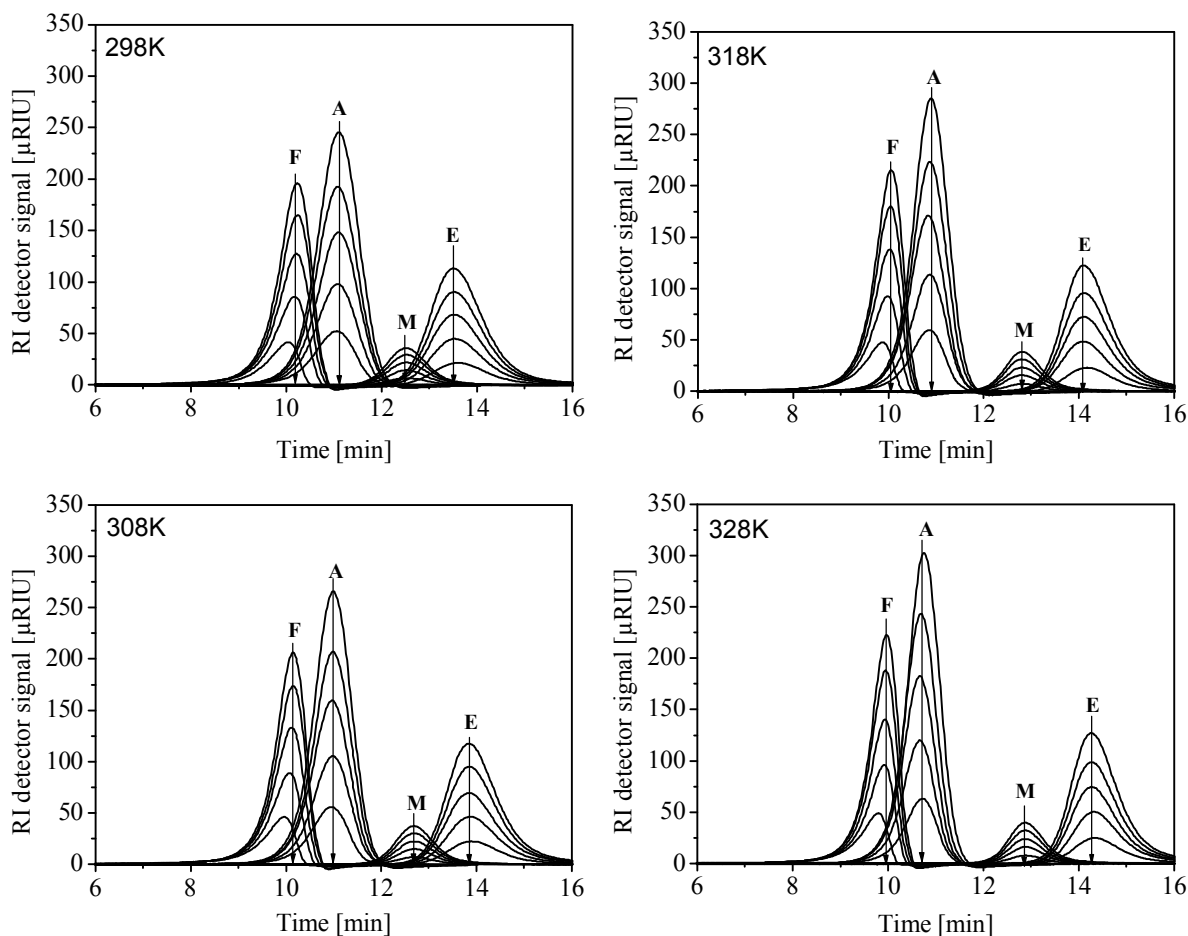
Figure 5-3: Elution profiles for various injection concentrations at different temperatures (Run AEQ-5, R1-C1, $c_i^{inj} = 0.1 \sim 0.5$ mol/L; $V^{inj} = 100\mu L$, $\dot{V} = 0.75$ mL/min)

Adsorption equilibrium constants of M, E, F, A, MA and EA with Cat-1 in H^+ form determined at four different temperatures are summarized in Table 5-6. The elution order of the components is not affected by temperature. In which, the component F is eluted first and followed by A, M, E, MA and EA. As a rule of adsorption, the adsorption equilibrium constants of the acids and the esters decrease when temperature increases. Particularly, the adsorption equilibrium constants of the alcohols are increased by temperature rising. There is an evidence for chemisortion of alcohols on PS/DVB ion-exchange resin but the mechanism is still not known clearly. Due to uncontrollable room temperature, the results in Table 5-5 are more or less close to the results at 298K given in Table 5-6.
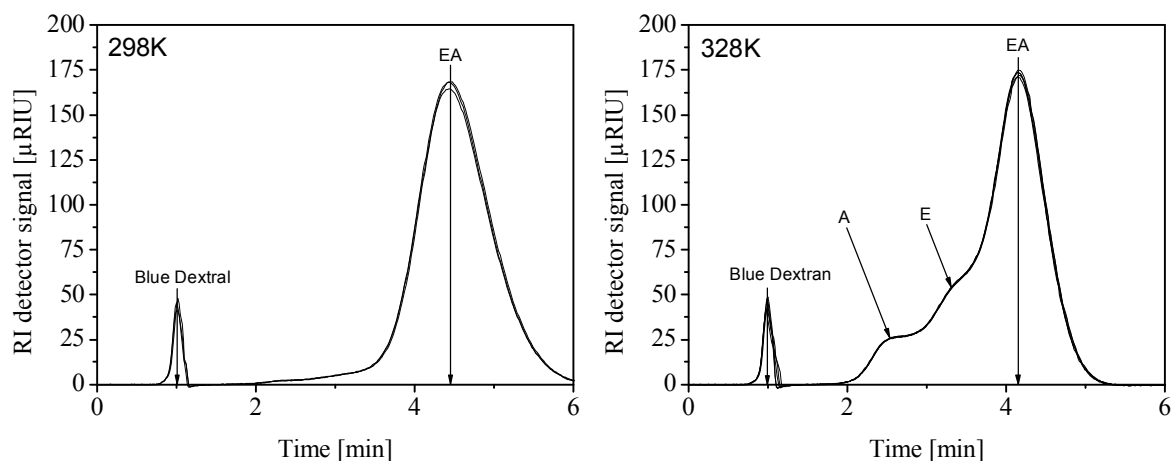
Figure 5-4: Elution profiles for pure EA and blue dextran at 298K and 328K
(Run AEQ-6, column R1-C1, $\dot{V}$ = 3.5 mL/min, $V_{pure\,EA}^{inj}$ = 10μL)

Table 5-6: Adsorption equilibrium constants of the components
determined for Cat-1 in H$^+$ form at different temperatures, using R1-C1

Component	$K_i\ (T)$			
	298K	308K	318K	328K
MF	-	-	-	-
EF	-	-	-	-
MA	1.045[*]	1.021[*]	0.988[*]	0.955[*]
EA	1,287[*]	1.269[*]	1.234[*]	1.184[*]
M	0.643	0.657	0.666	0.672
E	0.724	0.750	0.768	0.782
F	0.458	0.452	0.445	0.439
A	0.531	0.522	0.512	0.500

[*] *using pure esters*

5.4.2.2 *The resin in Na$^+$ form*

In order to determine adsorption equilibrium constants of MF and EF at higher
temperatures, the stationary phase Cat-1 was converted into Na$^+$ form, using the solution of

NaOH 0.1M. Adsorption equilibrium constants of M, E, MA and EA were also determined to compare adsorption affinities between the resin in H^+ form and in Na^+ form. In this case, pure esters were replaced by various dilute concentrations from $0.1 \sim 0.5$ mol/L. Self-catalytic hydrolysis of MF and EF at high temperature are significant. Figure 5-5 shows typical elution profiles for the EF at 298K and 328K. EF was converted partially into F and E. Retention time of EF was constant, whereas retention time of F was unstable due to ion-exchange reaction of H^+ and Na^+. The elution order in Figure 5-5 is the same with the elution order given in Eq. 5-1. The adsorption equilibrium constants of the esters and the alcohols are summarized in Table 5-7.
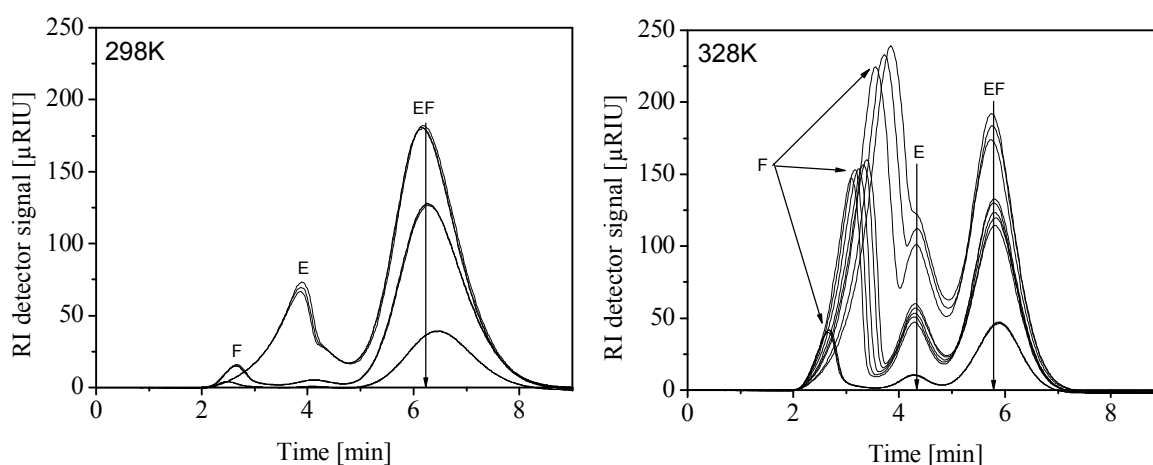
Figure 5-5: Typical elution profiles for EF at 298K and 328K
(Run AEQ-7, R2-C1, $c_{EF}^{inj} = 0.1 \sim 0.5$ mol/L; $V^{inj} = 100\mu L$, $\dot{V} = 0.75$ mL/min)

For the resin in Na^+ form, adsorption equilibrium constants of EF and EA are more or less similar. Adsorption equilibrium constants of EF are higher than of MA and the elution order of the only esters in Table 5-7 is slightly different from that of Table 5-5. Strangely, the adsorption equilibrium constants of alcohols were also increased with temperature increase. This trend was observed for both forms of the resin and chemisorption of the alcohols on the PS/DVB resin could be considered as one possible explanation.

In comparison with Table 5-6, the adsorption equilibrium constants for the resin in Na^+ form are smaller than those values for the resin in H^+ form. This means that the resin in H^+ form has higher affinity than that in Na^+ form. Although counter ions have effects on the adsorption of the components, the elution order given by Eq. 5-1 is right with the both form of the resin. Therefore, the different trend in adsorption of the alcohols can be explained by a particular interaction between molecules of the alcohols with the matrix of the resin.

Table 5-7: Linear adsorption equilibrium constants of the esters
determined for Cat-1 in Na$^+$ form, using R2-C1

Component	K_i (T)			
	298K	308K	318K	328K
MF	0.888	0.862	0.835	0.806
EF	1.110	1.082	1.038	0.993
MA	0.937	0.914	0.885	0.852
EA	1.093	1.074	1.047	1.009
M	0.598	0.625	0.640	0.647
E	0.583	0.600	0.614	0.621
F	-	-	-	-
A	-	-	-	-

5.4.3 Influence of temperature on separation factors

Based on the adsorption equilibrium constants of the alcohols and the acids given in Table 5-5, separation factors of the hydrolysis products for Cat-1 and Cat-2 were estimated by Eq. 2-56 and shown in Table 5-8. Because values of the separation factors are bigger than one, the separation factors are ratio of adsorption equilibrium constant of the alcohols to that of the acids. Due to higher value of separation factors, the products separation of Cat-2 is better than that of Cat-1. The separation of EF hydrolysis products is most favorable, whereas of MA is least favorable.

Based on the Table 5-6, dependence of the separation factors on temperature were determined and shown in Table 5-9. In general, separations of the hydrolysis products at higher temperature are better than that at lower temperature because dependences of the adsorption equilibrium constants on temperature for the alcohols and the acids are characterized by different trends.

Table 5-8: Separation factor $\alpha_{i,j}$ for Cat-1 and Cat-2 at room temperature calculated by Eq. 2-56 using the data in Table 5-5

j & i	$\alpha_{i,j}$ [-]	
	Cat-1	Cat-2
M & F	1.454	1.771
E & F	1.704	2.055
M & A	1.208	1.414
E & A	1.415	1.641

Table 5-9: Temperature dependence of separation factor $\alpha_{i,j}$ for Cat-1 calculated by Eq. 2-56 using the data in Table 5-6

j & i	$\alpha_{i,j}$ [-]			
	298K	308K	318K	328K
M & F	1.404	1.454	1.498	1.531
E & F	1.579	1.659	1.727	1.783
M & A	1.213	1.258	1.301	1.342
E & A	1.364	1.436	1.500	1.563

5.4.4 Thermodynamics of adsorption

Based on dependence of the determined adsorption equilibrium constants on temperature, further thermodynamic properties can be analyzed. In Figure 5-6 is shown the temperature dependence of adsorption equilibrium constants for both form of the resin. Different trends in adsorption of the alcohols are displayed again very clearly on the graphs. Based on van' Hoff equation (Eq. 2-46), the enthalpies of adsorption can be obtained from slope of the plots. The free Gibb energies of adsorption can be calculated by Eq. 2-45. Most of plots seem to be straight lines and average values for the enthalpies and the free Gibb energies of adsorption are acceptable. Calculated values for thermodynamic of both form of Cat-1 are summarized in Table 5-10. In the case of Cat-1 swollen full by water, negative values for isosteric heats of adsorption of the esters and acids indicate that adsorption processes were exothermic. However, adsorption of the alcohols appears as an endothermic process because of positive values for isosteric heats of adsorption. In comparison with the heat of hydrolysis reactions given in Table 5-3, the isosteric heats of adsorption are significantly smaller.
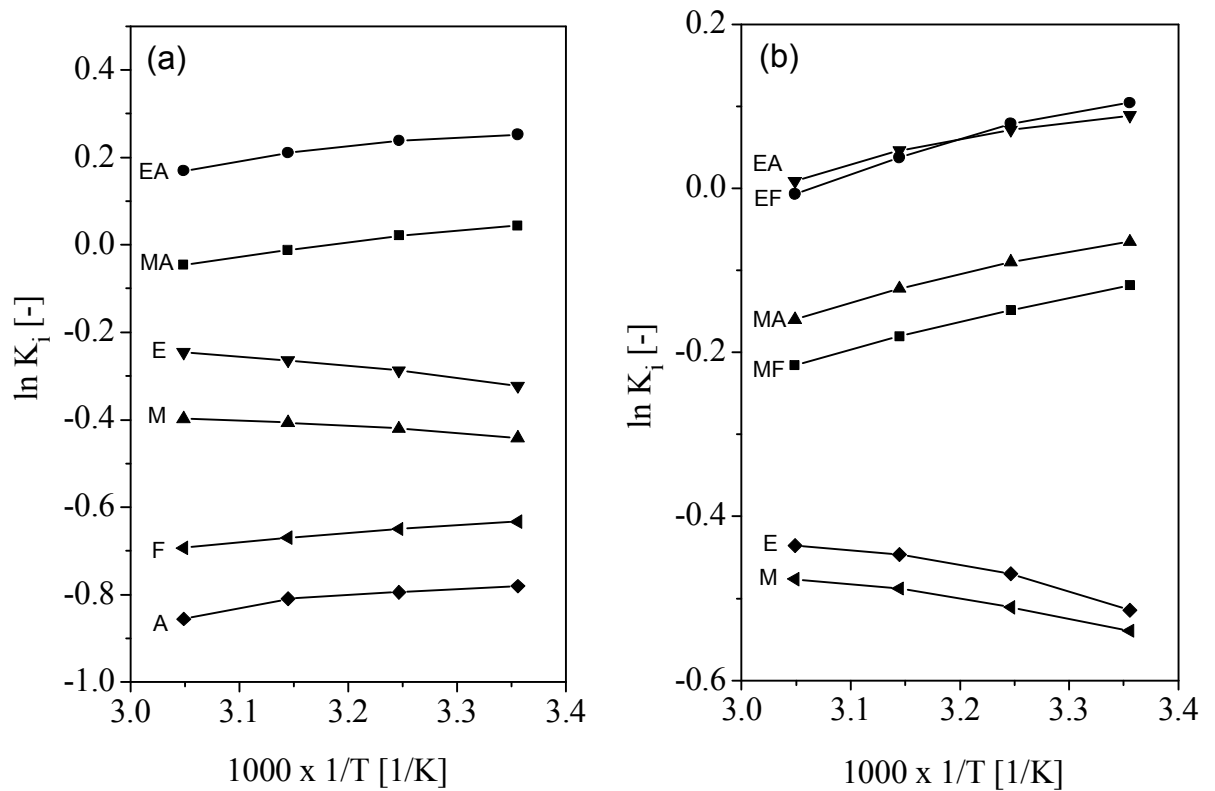
Figure 5-6: Temperature dependence of the adsorption equilibrium constants using values given in Tables 5-6 and 5-7   (a) Cat-1 in H^+ form   (b) Cat-1 in Na^+ form

Table 5-10: The free Gibbs energies and the enthalpies of adsorptions calculated by Eqs. 2-45 and 2-46 using the results given in Tables 5-6 and 5-7

Component	Cat-1 in H^+ form		Cat-1 in Na^+ form	
	$\overline{\Delta G_a}$ [(*)] [kJ/mol]	$\overline{\Delta H_a}$ [(*)] [kJ/mol]	$\overline{\Delta G_a}$ [(*)] [kJ/mol]	$\overline{\Delta H_a}$ [(*)] [kJ/mol]
MF	-	-	0.4349	-2.6416
EF	-	-	0.2878	-2.6059
MA	-0.0012	-2.4649	-0.1350	-3.0580
EA	-0.5629	-2.3132	-0.1373	-2.2059
M	1.0822	1.1765	1.2112	2.0816
E	0.7264	2.0635	1.3085	1.6849
F	2.1106	-2.0884	-	-
A	1.7233	-1.6455	-	-

[(*)] *average values*

5.4.5 Minimum number of theoretical plate necessary for a predefined resolution

For complete separation of the ester hydrolysis products, the resolution should be at least 1.5. Referring to Eq. 2-58, the resolution depends on the separation factor, retention factor and the number of theoretical plates. Conversely, based on the available data and a predefined minimal resolution ($R_{S,min}$ = 1.5), the corresponding minimum number of theoretical plates $N_{i,j}^{min}$ can be calculated by Eq. 2-59. For a bigger value, $N_{i,j}^{min}$ should be calculated by the retention factor of the products that have longer retention time. Therefore, the retention factors of the alcohols were used for the calculations. At room temperature, different $N_{i,j}^{min}$ for the the products of the four hydrolysis reactions and the four reactors were determined and given in Table 5-11. In conformity with the separation factors $\alpha_{i,j}$ given in Table 5-8, the separation of the hydrolysis products of EF needs the smallest $N_{i,j}^{min}$, whereas those of the products of MA need the biggest $N_{i,j}^{min}$. For the same batch of the resins, there is a little difference between $N_{i,j}^{min}$ of the reactors because of difference of the porosities. Because the $N_{i,j}^{min}$ of the reactors packed with Cat-2 are smaller than those packed with Cat-1, separation of Cat-2 is better that that of Cat-1.

Table 5-11: The minimum number of theoretical plates required to achieve $R_{S,min}$ = 1.5 for the ester hydrolysis products for Cat-1 and Cat-2 (using Eq. 2-59 and the adsorption equilibrium constants in Table 5-5)

Reactant	$N_{i,j}^{min}$ [-]			
	R1-C1	R2-C1	R1-C2	R2-C2
MF	835	860	565	572
EF	431	442	361	364
MA	2749	2831	1251	1265
EA	854	876	623	630

Based on the adsorption equilibrium constants in Table 5-6, dependence of $N_{i,j}^{min}$ on temperature is calculated and shown in Table 5-12. The values of $N_{i,j}^{min}$ are reduced by temperature increase.

Table 5-12: The minimum number of theoretical plates corresponding to $R_{S,min} = 1.5$ between ester hydrolysis products for Cat-1 at different temperature (using Eq. 2-59 and the adsorption equilibrium constants in Table 5-6)

Reactant	$N_{i,j}^{min}$ [-]			
	298K	308K	318K	328K
MF	967	810	708	647
EF	553	461	405	368
MA	2600	1874	1460	1199
EA	1044	789	645	547

The parameter $N_{i,j}^{min}$ is independent of flow rate, whereas the number of theoretical plate N_i strongly depends on flow rate. Therefore, comparison of the two parameters leads to identify conditions for complete separation of ester hydrolysis products. Utilization of $N_{i,j}^{min}$ to predict operating flow rate and temperature is represented in Sections 5.3.3 and 5.3.4.

5.5 Number of theoretical plates

For modeling of the fixed-bed reactors, the numbers of theoretical plates N_i of all components in the investigated range of temperature and flow rate were determined. However, within this section a part of the obtained results is shown to illustrate influence of temperature and flow rate on N_i.

5.5.1 Influence of flow rate on the number of theoretical plates

Based on pulse experiments summarized by Table 4-6, the real numbers of theoretical plates have been determined using Eq. 2-67. In Figure 5-6 shows strong dependence of flow rate on the high equivalent a theoretical place HETP and the numbers of theoretical plates of F. In comparison with the typical Van Deemter curve introduced in Figure 2-5, the HETP curve in Figure 5-7a was corresponding to the right branch of the Van Deemter curve. This means that the investigated range of flow rate was higher than the optimum flow rate at which the column has the highest efficiency. Optimization of flow rate for performance of the FBCRs is mentioned again in Chapter 8.
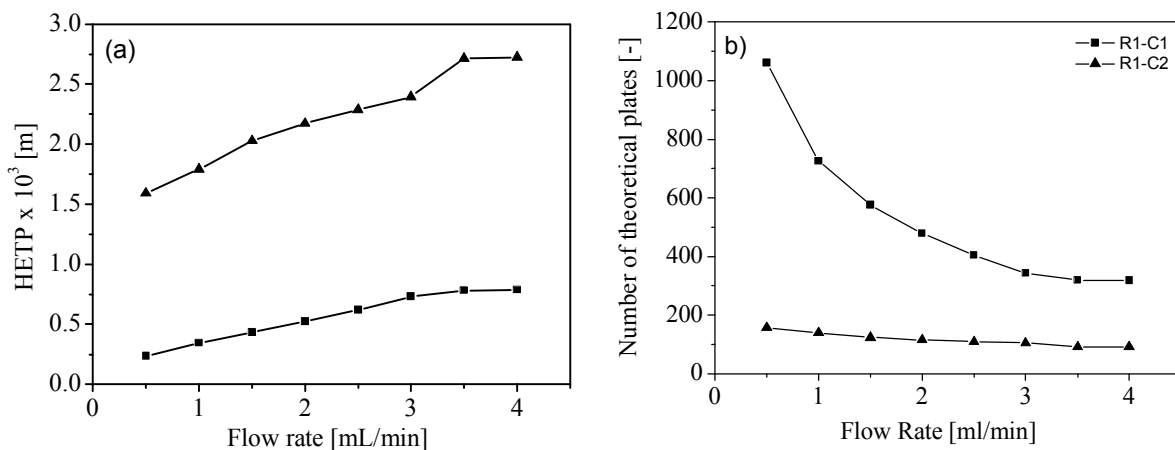
Figure 5-7: Influence of the flow rate on the height equivalent a theoretical plate and the number of theoretical plates of F for the reactors R1-C1 with Cat-1 (□) and R1-C2 with Cat-2 (Δ) (Run NTP-1)
a) The height equivalent to a theoretical plate   b) The number of theoretical plates

The columns have higher efficiency at lower flow rate. At the same flow rate, the number of theoretical plates of R1-C1 is relatively higher than that of R1-C2 due to small particle size of Cat-1. Because the number of theoretical plates is inversely proportional to the high equivalent to a theoretical plate, the curves shown in figures of this section are inverse plots of the Van Deemter curve shown in Figure 2-5. Therefore, the optimum linear velocity determined by the Van Deemter equation corresponds to a certain flow rate smaller than 0.5 mL/min.

5.5.2 Influence of temperature on the number of theoretical plates

In this case, flow rate was kept constantly at 0.75 mL/min and the numbers of theoretical plates of the hydrolysis products were determined at the four different temperatures. Dependence of the numbers of theoretical plates on temperature is summarized in Table 5-13.

The numbers of theoretical plates were increased by temperature rising. This means that the apparent dispersion coefficients decreased at higher temperature. However, the temperature dependence predicts diffusion to increase with increasing temperature (as molecules move more rapidly) and it leads to increase the apparent dispersion coefficients. This paradox can be explained by strong decreasing of mass transfer resistance term in the Van Deemter equation (Eq. 2-62) at higher temperature.

Table 5-13: Temperature dependence of the number of theoretical plates
(R1-C1, Flow rate 0.75 mL/min, concentration 0.5 mol/L, injection volume 100μL)

	N_i (T)			
	298K	308K	318K	328K
M	936	1049	1154	1241
E	624	721	807	916
F	942	1051	1186	1275
A	676	796	922	1031

5.5.3 Identification of useful operating flow rate

If the kinetics of ester hydrolysis reactions is assumed to be very fast, the separation of the hydrolysis products can be considered as the separation of a non-reactive mixture. Based on the dependence of the number of theoretical plates on flow rate $N_i(\dot{V})$ and the minimum number of theoretical plates needed for complete separation of the ester hydrolysis products $N_{i,j}^{min}$ given in Table 5-12, the useful operating flow rate $\dot{V}_j^{opt}$ can be identified. In Figure 5-8 are shown flow rate prediction for complete separation of the hydrolysis products of MF and MA for R1-C1. The dependences of the number of theoretical plates of M (the common alcohol product of MF and MA) on flow rate at four different temperatures are used. The operating flow rates were predicted by intersection points of horizon lines corresponding to $N_{i,j}^{min}$ of MF and MA with the curves $N_i(\dot{V})$ of M.

At 298K, for the original column length, the predicted flow rate for MF was $\dot{V}_{MF(1x)}^{opt} = 0.78$ mL/min, whereas no satisfied flow rate for MA can be found. For a supposed column with double original length, an operating flow rate of 0.37 mL/min was predicted for MA. For the supposed column, the higher operating flow rate for MF ($\dot{V}_{MF(2x)}^{opt} = 2.29$) was predicted. This means that higher throughput of MF can be performed. However, the higher flow rate leads to a higher pressure drop and it is an uneconomic option. The results obtained at all temperatures are provided in Table 5-14.
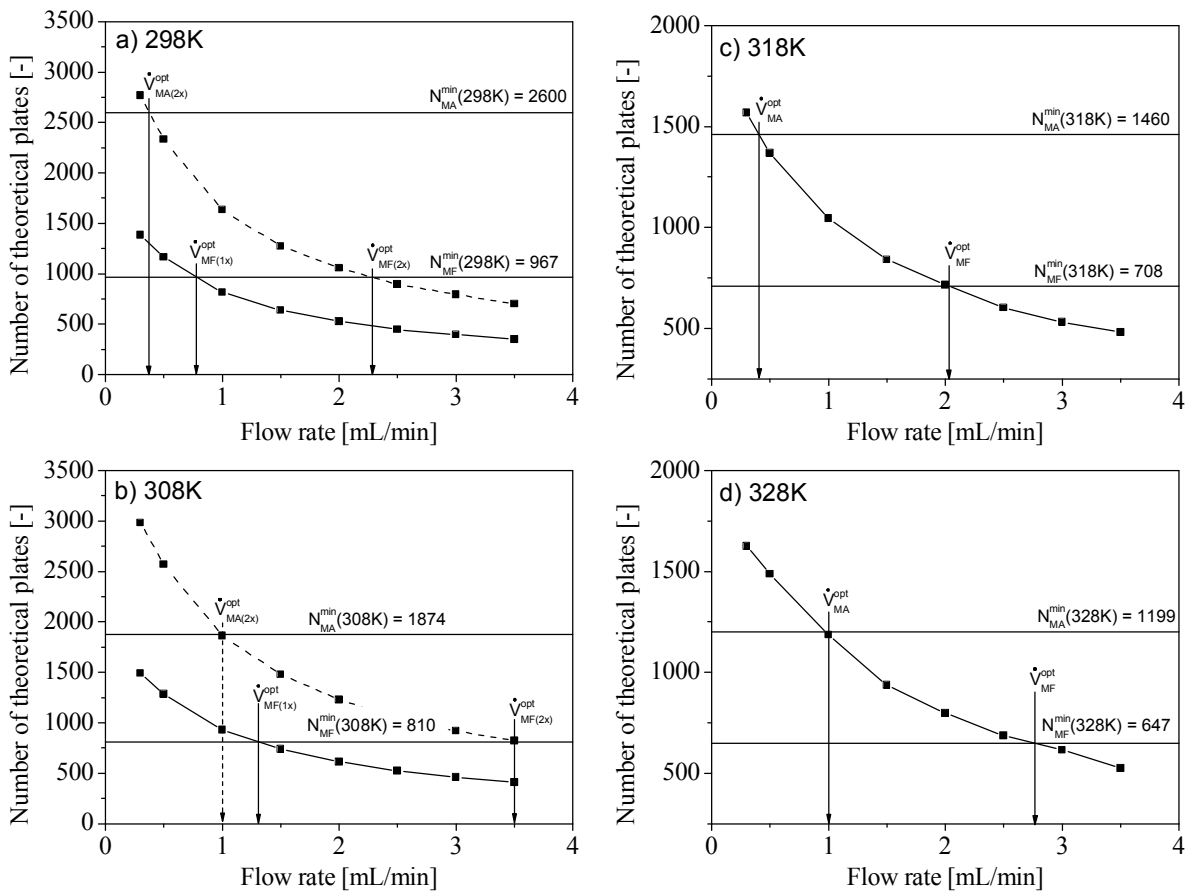
Figure 5-8: Prediction of the operating flow rate for complete separation of the hydrolysis products of MF and MA at four different temperatures (R1-C1, $\dot{V}$ = 0.3~3.5 mL/min) (solid lines - 1x) for origin column length   (dashed lines - 2x) for double column length

Table 5-14: Identified operating flow rate at different temperatures for MF and MA

	Column length [m]	$\dot{V}_j^{opt}$ [mL/min]			
		298K	308K	318K	328K
MF	0.25	0.78	1.31	2.03	2.77
	0.5	2.29[(*)]	3.50[(*)]		
MA	0.25	-	-	0.41	1.00
	0.5	0.37[(*)]	1.00[(*)]		

[(*)] *corresponding to a unreal column length*

5.5.4 Identification of useful operating temperature

At a constant flow rate, the number of theoretical plates in Table 5-13 increases at higher temperature $N_i(T)$, whereas the minimum number of theoretical plates for complete separation of the hydrolysis products of the esters $N_{i,j}^{\min}(T)$ in Table 5-12 decreases at higher temperatures. Therefore, a useful operating temperature T^{opt} can be identified by the intersection points between the curves of $N_i(T)$ and the curves of $N_{i,j}^{\min}(T)$. In Figure 5-9 is shown the determination of T^{opt} for the four esters and the results are summarized in Table 5-15. In comparison with temperatures set in experiments, the predicted T^{opt} for MF and EF are approximate 298K, whereas the predicted T^{opt} close to 328K for MA and 308K for EA.

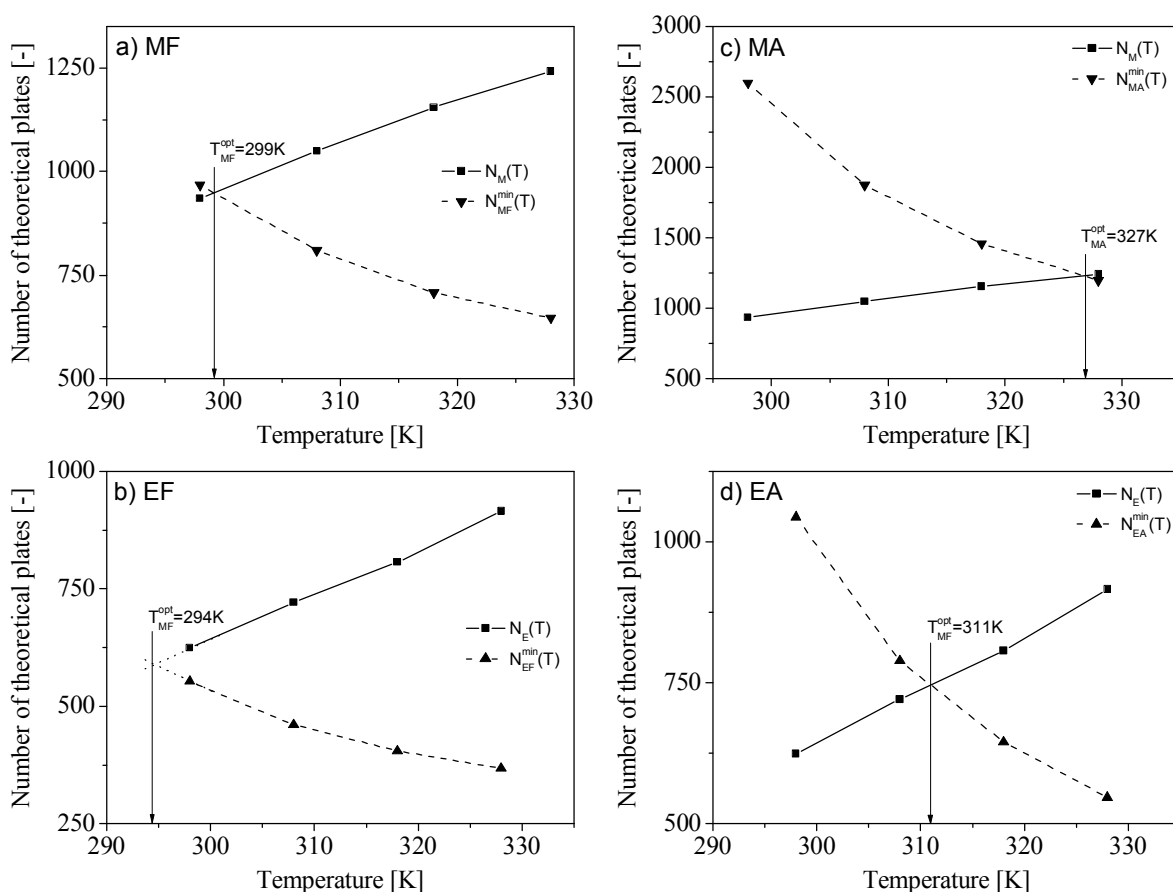**Figure 5-9**: Prediction of the operating temperature for complete separation of the hydrolysis products of the esters for the reactor R1-C1 at a flow rate of 0.75 mL/min (solid lines) the number of theoretical plates of the alcohols; (dashed lines) the minimum number of theoretical plates for complete separation of hydrolysis products of esters)

Table 5-15: The operating temperature predicted for R1-C1 at a flow rate of 0.75 mL/min

Hydrolysis reaction	MF	EF	MA	EA
T^{opt}	299K	294K	327K	311K

The operating flow rate and temperature for complete separation of ester hydrolysis products have been predicted in several specific cases. These results were based an assumption of very fast reaction kinetics. Although, in fact, the kinetics of ester hydrolysis reaction can be different from the assumption, the obtained result can be used to setup conditions for further experiments of the ester hydrolysis reactions performed in FBCRs.

5.6 Parameter validation

The model parameters have been determined by non-reactive pulse experiments. In this section, these parameters are used to calculate backwardly the elution profiles of the single components using the equilibrium-dispersion model (Eq. 2-24) and the calibration factors provided in Appendix B. The simulations are compared with measured detector signals to ensure that the parameters were determined adequately. Figure 5-10 shows the simulations (solid lines) generated for single injections of F, A, M, and E at 298K and 328K. For two different temperatures, these simulations are virtually congruent with the elution profiles obtained experimentally (squares). These validations allow concluding that the determinations of the porosity, adsorption equilibrium constants, the number of theoretical plates, and the calibration factors are reliable. These parameters were applied to study feasibility and kinetics of the ester hydrolysis reactions in Chapters 6 and 7.
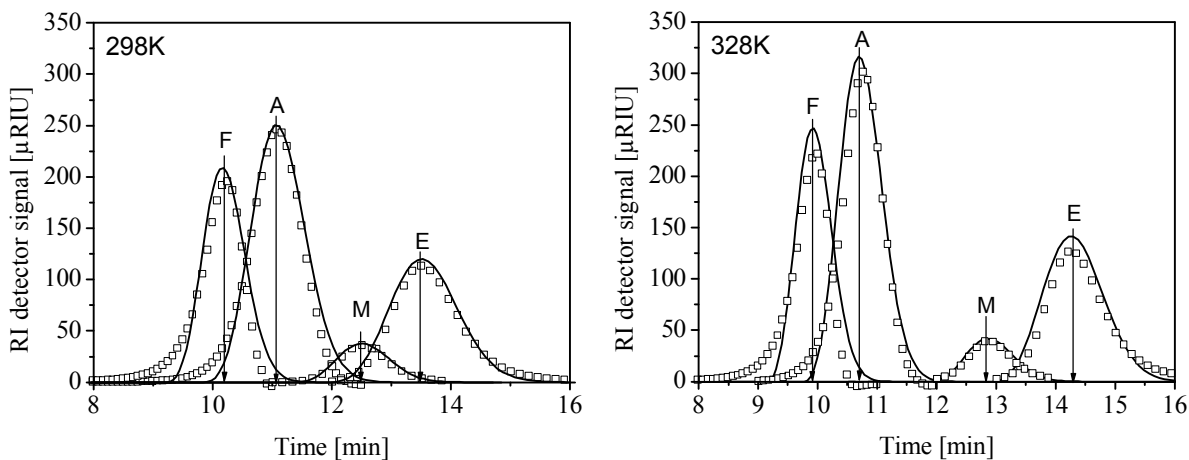

Figure 5-10: Comparison of backwardly computed (solid lines) and measured (squares) detector signals for pulses of the singles components at 298K and 328K ($R1-C1$, $\dot{V} = 0.75$ mL/min, $c_i^{inj} = 0.5$ mol/L, $V^{inj} = 100\mu L$, $N = 676 \sim 1275$)

Feasibility Analysis and Qualitative Discussion of Ester Hydrolysis Reactions

In Section 2.3, the feasibilities of performing typical reactions in a FBCR were analyzed in a generalized manner using the extended equilibrium model. An important result was the fact that complete separation and conversion for the reaction type $A \rightleftharpoons B + C$ are always possible in a FBCR independent of the relative affinity of reactant A. In the case of water in excess, the heterogeneously catalyzed four hydrolysis reactions of the esters can be considered similarly to that typical reaction, and thus their predicted feasibilities are possible.

In this chapter, the model parameters determined in Chapter 5 are applied in the frame of the extended equilibrium model to get more precisely accuracy predictions for the ester hydrolysis reactions. These predictions are compared with qualitative observations of experiments for the hydrolysis reactions.

6.1 Feasibility of the ester hydrolysis reactions

Except reaction rate constants of the hydrolysis reactions, all model parameters were determined experimentally and provided in Chapter 5. The necessary parameters for the extended equilibrium are chemical equilibrium constants, adsorption equilibrium constants and porosity. The adsorption isotherms of all components were linear. Due to the order of adsorptivities given in Eq. 5-1, the esters have the highest adsorptivities in comparison with their hydrolysis products. Therefore, the ester hydrolysis reactions catalyzed by the ion-exchange resins are completely similar to the case shown in Figure 2-10b. Because the adsorptivity of the alcohols are higher than that of the acids, the alcohols play the role of component B and the acids play the role of C in the example of $A \rightleftharpoons B + C$. Regarding to the discussion in Section 2.3.3, complete separation and conversion for this case was

possible. However, the feed concentration of the reactant was limited by reactive azeotropy.

With an assumption of fast hydrolysis of the esters, feasibility analyses for MF and MA at room temperature were given by [Vu06]. A hodograph plot for the hydrolysis of MF is shown in Figure 6-1a. The hydrolysis of MA is shown in Figure 6-1b. In these figures, the grey areas represent for the concentration limitations made by the lines of reactive azeotropy. In comparison with the solubilities provided in Table 3-2, the concentration limitation of MF (10 mol/L) is higher than the solubility of MF (5 mol/L), whereas that of MA (~ 1.8 mol) is lower than the solubility of MA (3.37 mol/L). However, these concentration limitations were predicted in the case of sufficiently large injections. Therefore, this has no effect on the feasibility in the case of pulse injections diluted immediately by a large amount of mobile phase. The obtained results can be attributed to the hydrolysis reactions of EF and EA.
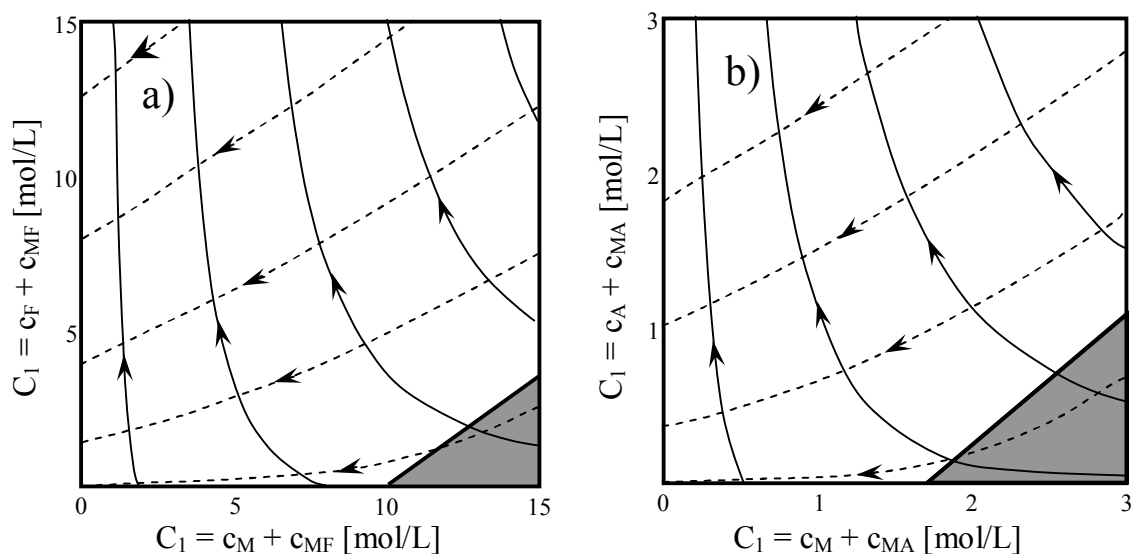
Figure 6-1: Representation of wave solutions in the hodograph space of the transformed concentration variables for the hydrolysis reactions: a) MF   b) MA

From the above geometric conditions, it can be concluded that total conversion and total separation for the ester hydrolysis reactions are possible for the FBCRs with a pulse injection of esters. This conclusion allows carrying out the second step of the strategy provided in Section 2.3.1 to estimate reaction rate constants and to optimize the performance of the FBCRs. The second step is concretized in Chapter 7 and Chapter 8. However, for orientation of further studies, the selected chromatograms of the ester hydrolysis reactions are discussed qualitatively in the following section.

The supports of S. Grüner and Prof. A. Kienle for the feasibility studies of FBCRs in a collaboration work are gratefully acknowledged.

6.2 Qualitative discussion

Base on the procedures provided in Section 4.3, the ester hydrolysis reactions were performed in the FBCRs. The selected chromatograms of these experiments are discussed qualitatively in this section to demonstrate for the prediction in Section 6-1. Influence of the conditions on the ester hydrolysis reactions is analyzed in detail to form a strategy for kinetic studies in Chapter 7.

6.2.1 Influence of stationary phases on hydrolysis of the esters

The experiments were carried out as the procedures given in Section 4.3.1. In Figure 6-2 are shown typical elution profiles for R1-C1 and R1-C2 at 298K and a flow rate of 0.3 mL/min. In all cases, the same amount of esters was injected. Although the corresponding shapes of the elution profiles are similar for the two columns, because of its larger plate numbers, R1-C1 gives sharper peaks than R1-C2. However, due to more or less similar of separation factors given in Table 2-8, separation of the hydrolysis products in R1-C2 is similarly good as that in R1-C1 (e.g., Figures 6-2a and 6-2b). In agreement with the determined adsorption equilibrium constants, there is a difference between the retention times of the same component eluting from R1-C1 and from R2-C2 (e.g., Figure 6-2a). Because both reactant peaks disappeared for MF and EF (Figures 6-2a and 6-2b, respectively), it can be concluded that the corresponding hydrolysis reactions are faster than the hydrolysis reactions of MA and EA, where reactant peaks are still visible (Figures 6-2c and 6-2d, respectively).

Although, the catalytic activity of Cat-2 is higher than Cat-1 due to the discussion on their exchange capacities in Section 5.1.3, the difference of the reaction rates for the two batches of the resin can not observe qualitatively. Influence of the different batches of the resin on reaction rate constants is quantified and discussed in detail in Section 7.1.1.
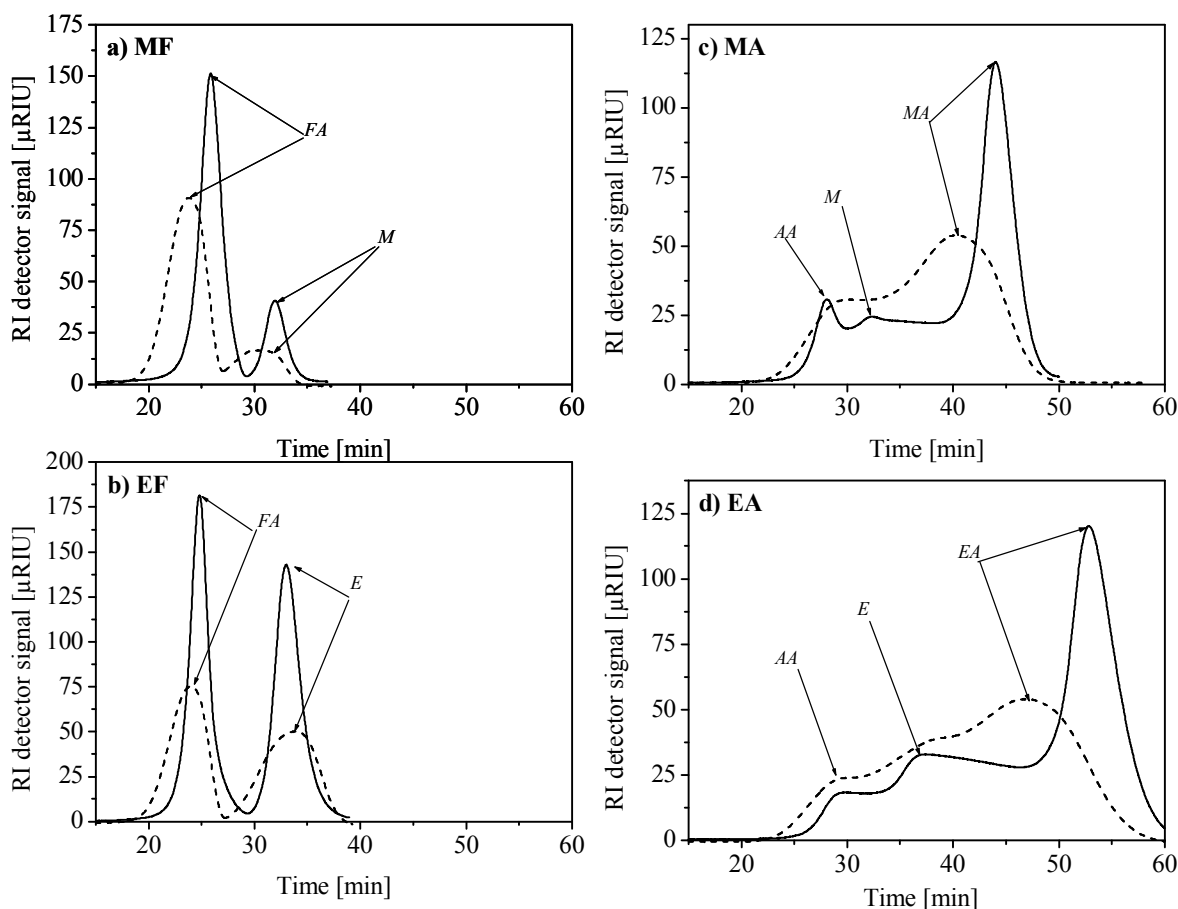
Figure 6-2: Comparison of hydrolysis reactions using R1-C1 (solid) and R1-C2 (dashed)
(a) MF   (b) EF   (c) MA   (d) EA
(flow rate 0.3 mL/min, concentration 0.5 mol/L, injection volume 100μL, 298K)

6.2.2 Influence of flow rate on hydrolysis of the esters

The experiments were performed as the description given in Section 4.3.2. The influence of the flow rate on the course of the hydrolysis reactions is illustrated in Fig 6-3. The conversions of the esters depend strongly on the contact times. Again, the absence of MF and EF in the chromatograms shown in Figures 6-3a and 6-3b indicates that these esters are converted almost completely throughout the range of flow rates studied (0.3-1.5 mL/min), whereas MA and EA still elute from the column even at the lowest flow rate. This figure also indicates that the resolution is significantly improved when the flow rate is decreased (exploiting larger N). Very complex elution profiles are shown in Figures 6-3c and 6-3d (particularly for the lower flow rates). The shapes of these profiles are discussed later in Section 7.2.2 using the model developed.
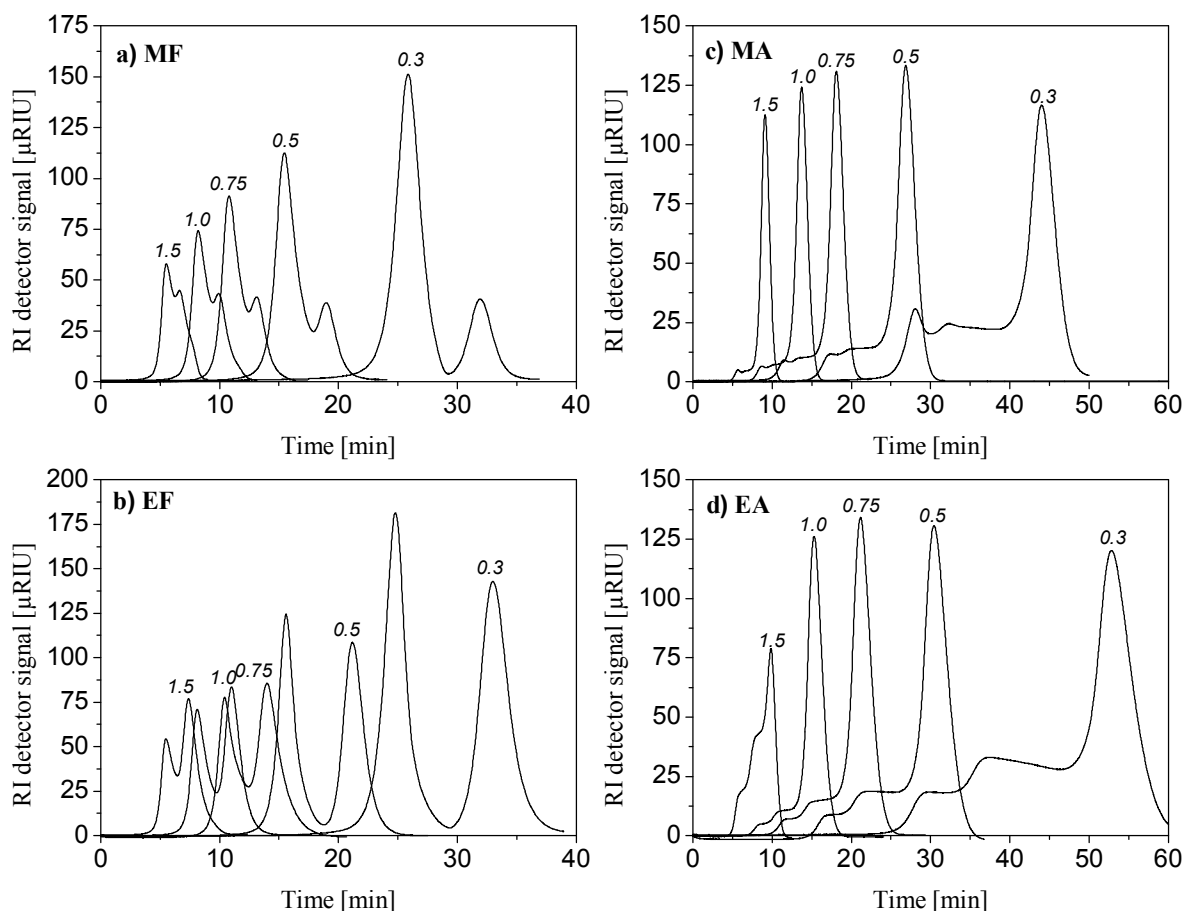
Figure 6-3: Influence of flow rate (0.3 ~ 1.5 mL/min) on the hydrolysis reactions
(a) MF   (b) EF   (c) MA   (d) EA
(R1-C1, feed concentration 0.5 mol/L, injection volume 100μL, room temperature)

In Section 5.5.3, an operating flow rate for complete separation of M and F (MF hydrolysis reactions) predicted at this temperature is 0.78 mL/min. However, at a flow rate of 0.75 mL/min, the real resolution does not match the resolution set at 1.5. This can be explained by insufficiently high reaction rate of MF hydrolysis reaction.

Although, flow rate has no effect on reaction rate constants, it influences the conversion of esters due to control the contact time between esters and the resin. High flow rate leads to difficulty in identification of component. Therefore, the estimation of reaction rate constants should be carried out at a reasonable flow rate. In this case, a flow rate of 0.75 seems to be suitable for the estimation.

6.2.3 Influence of temperature on hydrolysis of the esters

The experiments were carried out as the procedures given in Section 4.3.3. For comparison, the measured elution profiles are presented in two ways. Elution profiles of

the same component at different temperatures are shown in Figure 6-4. Elution profiles of different components at the same temperature are shown in Figure 6-5.

As quantitative of the influence of temperature on column efficiency (N_i) in Table 5-13, an effect can clearly be observed by comparing chromatograms in Figures 6-4a and 6-4b. The peak widths are reduced considerably as the temperature is increased. This means that the number of theoretical plates is augmented and the resolution is improved. Although, MF and EF were converted completely at any temperature in the studied range, the resolutions like the expecting resolution set at a value of 1.5 can be reached only at 308K or higher temperatures. These temperatures are higher than the predictions for the operating temperatures given in Table 5-15. Because MA and EA were converted partially, the operating temperatures of MA and EA do not need to consider here.
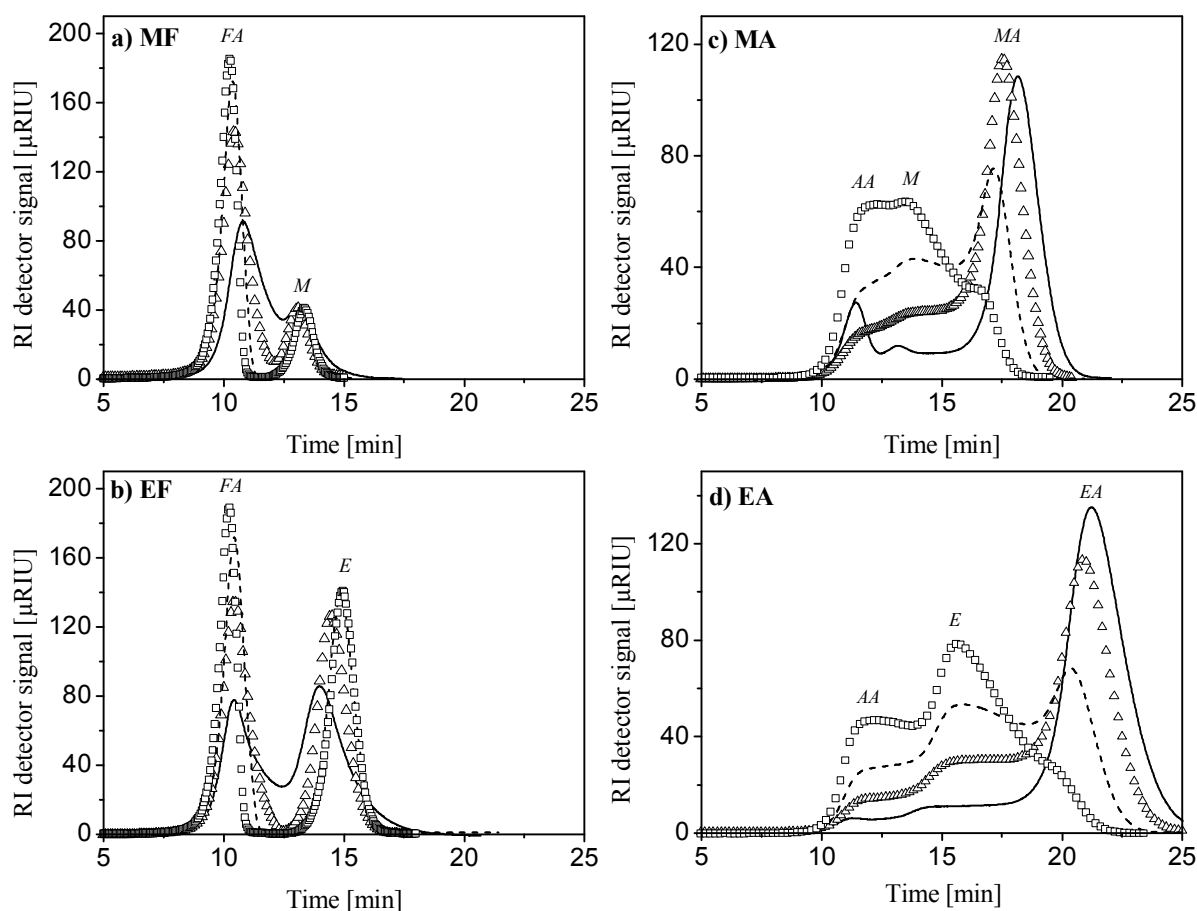
Figure 6-4: Influence of temperature on the hydrolysis reactions
298K (solid), 308K (triangles), 318K (dashed) and 328K (squares)
(a) MF   (b) EF   (c) MA   (d) EA
(R1-C1, flow rate 0.75 mL/min, feed concentration 0.5 mol/L, injection volume 100μL)

In Figs 6-5b to 6-5d, the peaks of FA produced by the hydrolysis of MF and EF at 308K, 318, and 328K, respectively, have the same retention time and area, whereas differences can be seen in Figure 6-5a (298K). This leads to an idea to combine two reactants to improve productivity of the common product. However, this idea can be limited by some difficulties in separation of side products. In Figure 6-5d, the reactants MA and EA still exist and elute from the reactor. This indicates again that the hydrolysis reactions of MA and EA are the slowest among the four reactions studied.
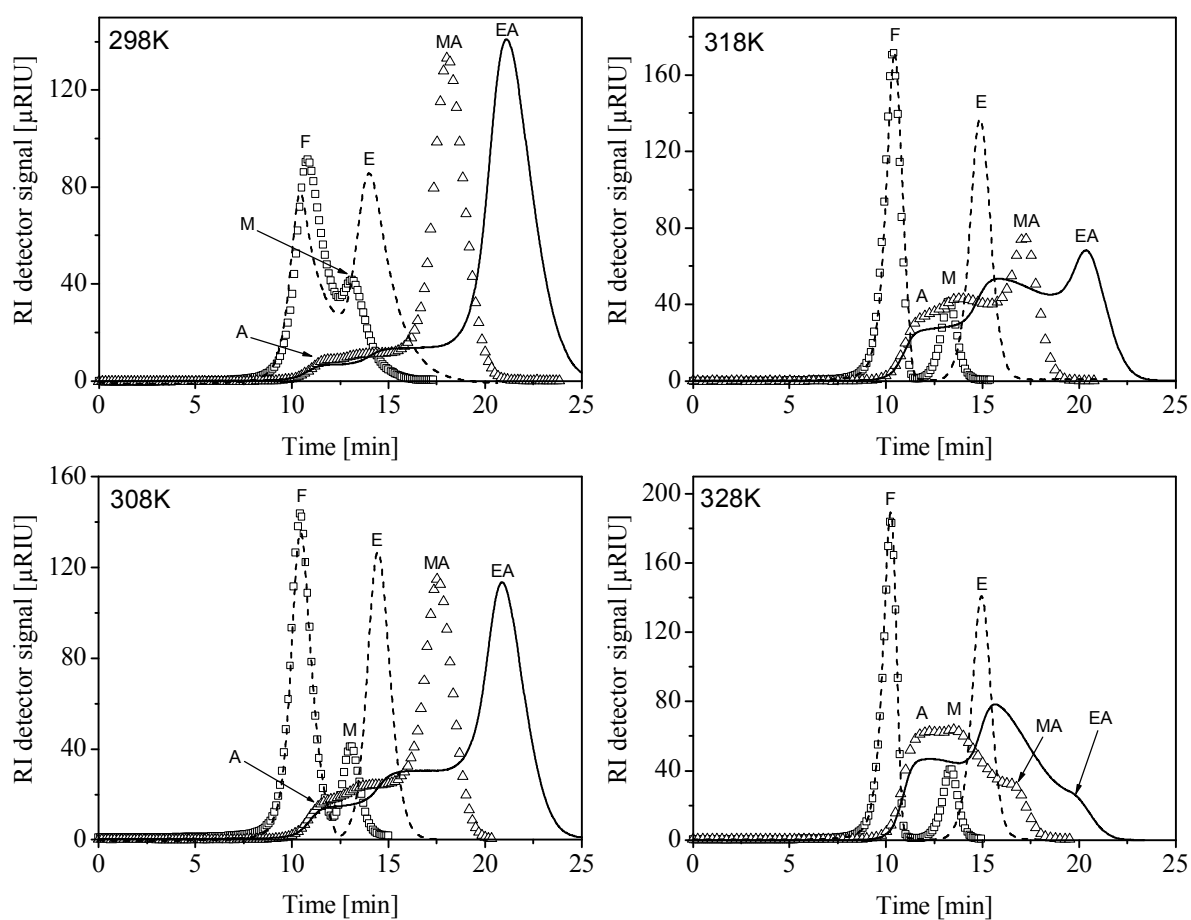
Figure 6-5: Comparison of elution profiles for the hydrolysis reactions of MF (squares), EF (dashed), MA (triangles), and EA (solid)
(R1-C1, flow rate 0.75 mL/min, feed concentration 0.5 mol/L, injection volume 100μL)

In summary, temperature has large effect on the conversion of the esters and the separation of the hydrolysis products. Higher temperature leads to the higher conversion and the better separation. Influence of temperature on reaction rate constants is quantified and discussed in detail in Section 7.1.2.

6.2.4 Influence of feed concentration on hydrolysis of the esters

The experiments were performed as the description given in Section 4.3.4. In Figure 6-6 shows chromatograms of MA with three different feed concentrations 0.5, 1.0 and 1.5 mol/L at a flow rate of 0.3 mL/min and four different temperatures, using the reactor R1-C1. At the same temperature, the chromatograms of the different feed concentrations were congruent. The retention times of A and M were independent from the feed concentrations, whereas the retention time of MA is moved to right side at the higher feed concentrations. The adsorption isotherm of MA seems to be non-linear at the high concentrations. However, in the low concentration range of 0.1 ~ 0.5 mol/L investigated in Section 5.4, the adsorption isotherm of MA was confirmed to be linear.

The different feed concentrations had no effect on conversion and separation was. Therefore, the reaction rate constants estimated at a certain feed concentration can be validated at other feed concentrations. This manner is represented in Section 7.2.3.

Figure 6-6: Influences of feed concentrations and temperature on hydrolysis of MA
(R1-C1, Flow rate 0.3 mL/min, injection volume 100μL)
(dotted) 0.5 mol/L   (dashed) 1.0 mol/L   (solid) 1.5 mol/L

6.2.5 Influence of reactor diameter on hydrolysis of the esters

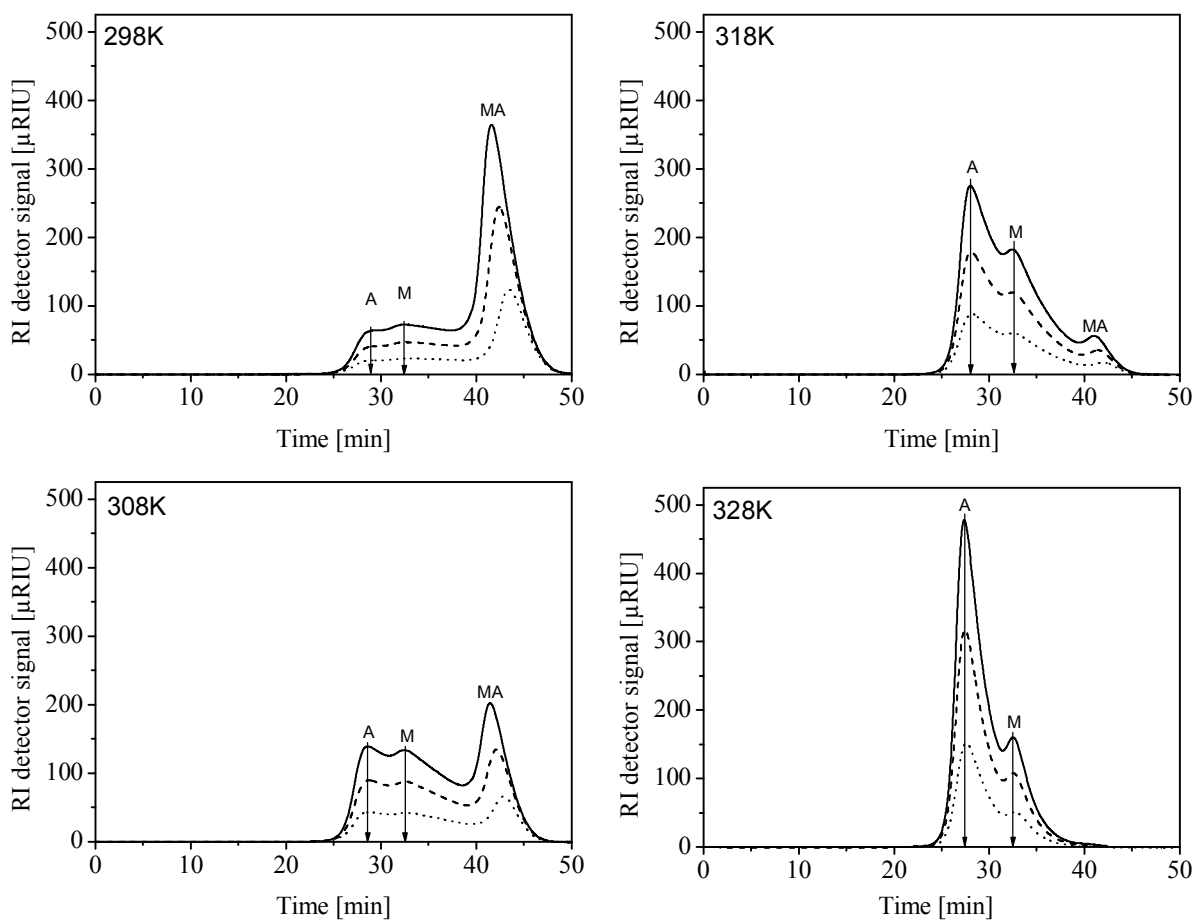In order to estimate influence of reactor diameter on performance of the fixed-bed chromatographic reactors, the experiments were carried out as the procedures given in Section 4.3.5. The obtained results are shown in Figure 6-7. Because the linear velocity for the both reactor is kept the same, retention times of the components are the same for each experiment. Although, the chromatograms got from the two reactors are similar, peak widths of R1-C1 are narrower than that of R2-C1. In this work, an important assumption is no radial gradients for temperature and dispersion. With small diameter and well packing like R1-C1 and R2-C1, this assumption is satisfied. Therefore, these experiments have an engineering meaning in scaling-up fixed-bed chromatographic reactor.
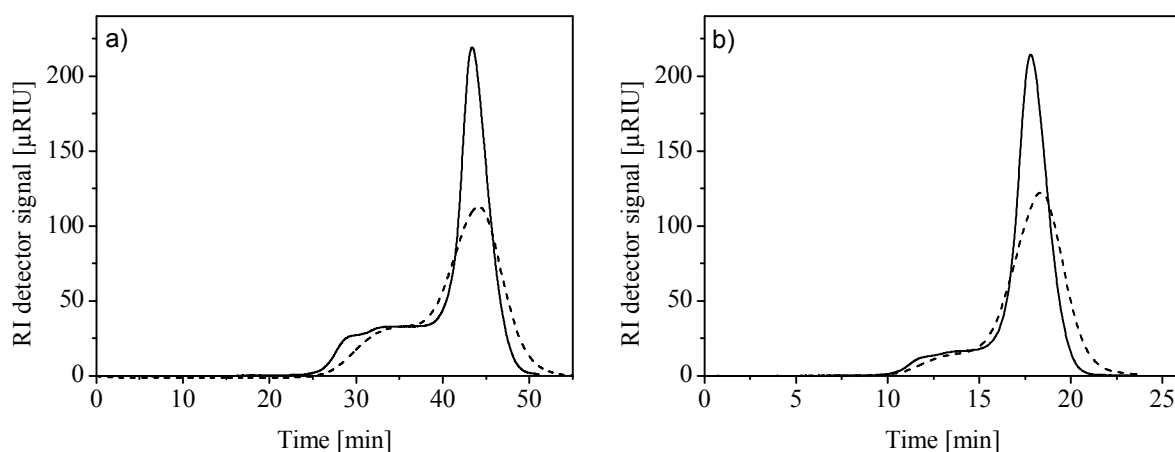
Figure 6-7: Influences of reactor diameter on hydrolysis of MA at room temperature (solid lines: R1-C1 with $c_{MA}^{Feed} = 1.5$ mol/L; dashed lines: R2-C1 with $c_{MA}^{Feed} = 0.5$ mol/L; injection volume 50μL)   a) u = 0.024 m/min   b) u = 0.060 m/min

In this chapter, several remarks can be withdrawn. Based on the parameters determined experimentally, the feasibility of the ester hydrolysis reactions performed in the FCBRs was confirmed again to be possible in Section 6.1. This was illustrated by the several chromatograms in Section 6-2. The chromatograms showed that the complete conversion and separation of MF an EF could be observed at a certain flow rate in the temperature range, where as that of MA and EA could be seen at 328K where the reaction rate of MA and EA seemed to be sufficiently high. Influences of most conditions on the ester hydrolysis reactions were analyzed and they were in conformity with the theories of the reactive chromatography. Particularly, temperature effects on the conversion and separation are interesting for further studies in the next chapters.

Estimation of Reaction Rate Constants and Model Validation

A typical challenge in kinetic studies is to measure accurately concentrations of species at particular times and positions during reaction so that a reaction rate laws can be identified and quantified. Unfortunately, for the reaction system under consideration it is difficult to get instantaneously accurate measurement of the single component concentrations in mixture due to limited possibilities of specific detection. In order to determine reaction rate constants, curve fitting between measured total detector signals and simulated total signals can be performed instead. This technique was applied in this work using an unspecific RI detector at outlet of a column. The kinetic constants obtained can be validated by comparing predicted elution profiles with experiments performed at other conditions.

7.1 Reaction rate expressions

The input parameters of the equilibrium-dispersion model described by Eq. 2-24 were the porosity, the adsorption equilibrium constant, the linear velocity, the apparent dispersion coefficients (corresponding to the number of theoretical plate), and in particular the rate law of the heterogeneous reaction. All parameters were experimentally determined in Chapter 5, except the reaction rate constant k^{het} in the term of reaction rate law. The estimation of k^{het} depends on how to express the term of heterogeneous reaction.

In the literature, there are two approaches to quantify heterogeneous reactions catalyzed by ion-exchange resins. The pseudo-homogeneous model suggested by [Helf95, p. 523] assumed that the counter ions H^+ are mobile and solvated. The reaction mechanism in homogeneous catalysis by an inorganic acid and heterogeneous catalysis by an ion-exchange resin is essentially the same and the differences between the two cases are the diffusion resistances and reactive volume fractions. However, the difference of the

diffusion resistances is not included explicitly in this model. This model is applicable in the presence of strong polar compounds like water. This means that the –SO₃H group are totally dissociated. The H$^+$ ions can move freely in the liquid phase within the pores and act as the active centres whereas the –SO₃$^-$ groups remain fixed on the polymer matrix. The reaction is confined the liquid phase within the catalyst mass. Based on the assumption of permanent equilibrium between concentrations of all components in the liquid and solid phases, reaction rate law for the ester hydrolysis reactions can be the expressed by the following equation:

$$r^{pseudo-hom} = k^{pseudo-hom} \left(c_{Es} c_W - \frac{c_{Al} c_{Ac}}{K_{eq}^{hom}} \right)$$

(7-1)

The reaction rate constant K_{eq}^{hom} was defined by Eq. 3-8 and determined experimentally in Section 5-2.

The second approach is the heterogeneous model, also called surface model. The reaction takes places on the catalyst surface involving adsorption of the reactant. This approach is based on the Langmuir-Hinshelwood or the Eley-Rideal mechanisms introduced in Section 2.2.5. In the case of the ester hydrolysis reaction with excessive presence of water, the Eley-Rideal mechanism appears to be simpler more adequate than the Langmuir-Hinshelwood mechanism. The Eley-Rideal mechanism has been used successfully by [Falk03, Mai06] in the description of experimental data of the same hydrolysis reactions. Applying Eq. 2-91, the expression for reaction rate law is:

$$r^{het} = k^{het} \left(q_{av,Es} c_W - \frac{q_{av,Al} q_{av,Ac}}{K_{eq}^{het}} \right)$$

(7-2)

The heterogeneous equilibrium constant K_{eq}^{het} can not be determined experimentally. However, it is related to the homogeneous equilibrium constants K_{eq}^{hom} and the adsorption equilibrium constants K_i. In this work, the adsorption equilibrium of the components was found to be linear, and thus Eq. 7-2 can be rewritten. For established adsorption equilibria conditions holds:

$$r^{het} = 0 = k^{het} \left(K_{Es} c_{Es} c_W - \frac{K_{Al} c_{Al} K_{Ac} c_{Ac}}{K_{eq}^{het}} \right)$$

(7-3)

Thus, referring to Eq. 3-8, the following relationship can be established:

$$K_{eq}^{het} = \frac{K_{Al}c_{Al}K_{Ac}c_{Ac}}{K_{Es}c_{Es}c_W} = K_{eq}^{hom}\frac{K_{Al}K_{Ac}}{K_{Es}} \tag{7-4}$$

Substituting of Eq. 7-4 into Eq. 7-3 yields:

$$r^{het} = k^{het}K_{Es}\left(c_{Es}c_W - \frac{c_{Al}c_{Ac}}{K_{eq}^{hom}}\right) \tag{7-5}$$

The heterogeneous model expressed by Eq. 7-5 is similar with the pseudo homogeneous model expressed by Eq. 7-1. The difference between the two expressions is the presence of the Henrry constant of the esters in Eq. 7-5. In other word, the reaction rate constant of pseudo homogeneous model includes implicitly effects of adsorption/desorption.

$$k^{pseudo-hom} = k^{het}K_{Es} \tag{7-6}$$

In brief, the both expression of the reaction rate laws do not affect significantly to the curve fitting process because K_{Es} is a constant. For comparison with the previous studies [Falk03, Mai06], the heterogeneous approach is applied in this work.

7.2 Numerical parameter estimation

In this work, the concentration profiles $c_i(t)$ at the end of the column are computed by the equilibrium-dispersion model (Eq. 2-24), using the model parameters determined in Chapter 5. Based on the simulated concentration profiles and the calibration factors $K_{cal,i}$ of the detectors determined for all components in preliminary experiments are given in Appendix B, the detector response for a single component can be calculated as follows:

$$S_i(t) = K_{cal,i}c_i(t) \tag{7-7}$$

For multi components, the sum simulated detector signal $S(t)$ can be computed by:

$$S(t) = \sum_{i=1}^{N_C}S_i(t) = \sum_{i=1}^{N_C}K_{cal,i}c_i(t) \tag{7-8}$$

The simulated total detector signal $S_i(t)$ is fitted with the measured total detector signal $M_i(t)$ using curve fitting. Hereby, the reaction rate constant was the only free parameter. The parameter estimation was carried out by the Presto software. Using this software [CIT00], the parameter estimation is based on minimization of the following objective function:

$$SS_E = \sum_{j=1}^{N_D} \frac{1}{w^2} \left[M_i\left(t_j\right) - S_i\left(t_j\right) \right]^2 \qquad\qquad j = 1, N_D \qquad\qquad (7\text{-}9)$$

where, SS_E is the weighted residual sum of squares; i is the index of data points; N_D is the number of data points; w is the weighting factor and its value is maximum value of the data).

In the case of single free parameter, the standard error of the fit is:

$$s_e = \sqrt{\frac{SS_E}{N_D - 1}} \qquad\qquad (7\text{-}10)$$

However, the standard errors given by Presto seem to be relative small in comparison with the estimated values of the reaction rate constants. Therefore, they were negligible. In fact, the systematic error in the parameter estimation is very complicated to analyze because contributions of possible errors can be originated from the initial assumptions and the measurement errors in determination of each model parameters. Therefore, no detailed error analysis is discussed in this work.

7.3 Estimation of reaction rate constants

The reaction rate constants k^{het} depend strongly on the reaction, the catalyst activity and the temperature. The other conditions were kept constantly during the experiments and the parameter estimation process. Based on the available experimental data, the standard conditions considered were:

- Feed concentration of reactant: $c_{Es}^{inj} = 0.5$ mol/L;
- Injection volume: $V^{inj} = 100$ μL;
- Flow rate: $\dot{V} = 0.75$ mL/min;

The strategy to estimate the reaction rate constants k^{het} was the following:

Step 1: For comparing the two batches of the resin, the reaction rate constants were estimated for different batches of the resin at the same temperature condition. In this step, the reactors R1-C1 and R1-C2 were used.

Step 2: In order to quantify the temperature effects, the reaction rate constants were estimated at the four temperatures of 298, 308, 318 and 328K using only the chromatograms obtained experimentally by the reactor R1-C1.

7.3.1 Influence of stationary phases on reaction rate constants

For comparing the two batches of the resin, the estimation of the reaction rate constants is based on the chromatograms obtained by the reactors R1-C1 and R1-C2 at the same temperature condition. Unfortunately, in the beginning of this work, these experiments were carried out without the support of the column oven. Therefore, no temperature effects are considered in this step. In Figure 7-1 shows the best curve fittings for MF with both reactors R1-C1 and R1-C2 at room temperature and a flow rate of 0.75 mL/min. For explanation, the figures also show the simulated responses for each components and the simulated detector signal is sum of the responses. In the both cases, MF is obviously converted completely to the products.
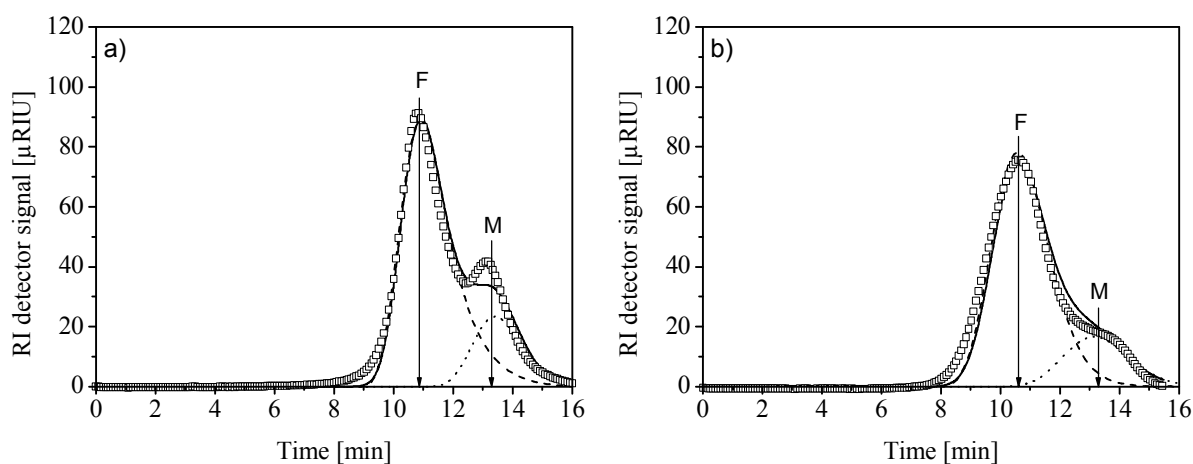
Figure 7-1: The best fittings of simulated and measured signals for MF (Simulations with k^{het} in Table 7-1, $\dot{V}$ = 0.75 mL/min; c_{MF}^{inj} =0.5 mol/L; V^{inj} = 100μL; room temperature).
a) R1-C1; b) R1-C2; (□) measured signal; (solid) sum-simulated signal; simulated response signals for (dashed) simulated response for F; (dotted) simulated response for M.

The best curve fittings for MA with the both reactors R1-C1 and R1-C2 at room temperature and a flow rate of 0.75 mL/min are shown in Figure 7-2. In contrast with the previous cases, MA was converted partially to M and A. The curve fitting for R1-C1 in

Figure 7-2a is better than that for R1-C2 in Figure 7-2b. The good agreement between the measured and simulated detector signals confirms that the applied assumptions and the model are relatively reliable.
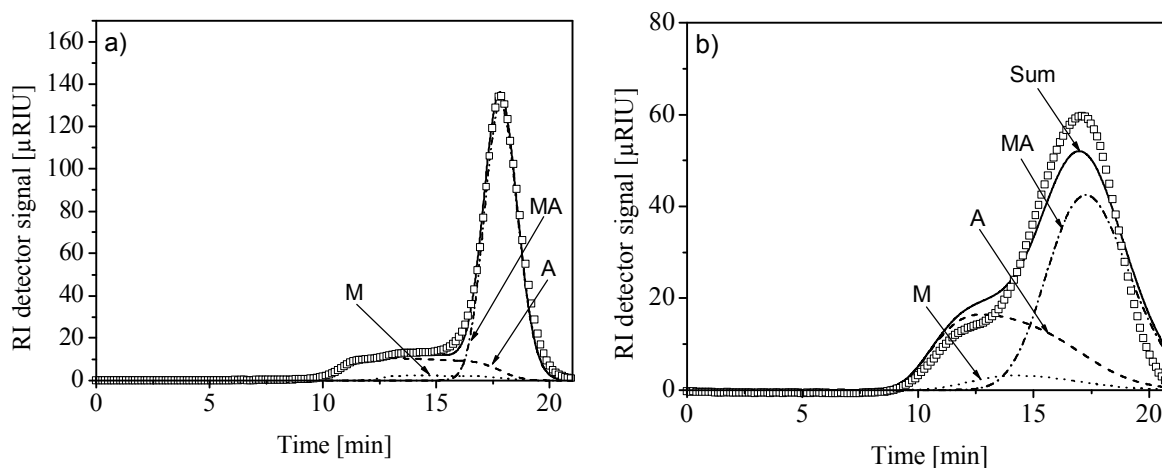
Figure 7-2: The best fitting of simulated and measured signals for MA (Simulations with k^{het} in Table 7-1, $\dot{V}$ = 0.75 mL/min; c_{MA}^{inj}=0.5 mol/L; V^{inj} = 100µL;   room temperature).
a) R1-C1   b) R1-C2
(□) measured signal; (solid) sum-simulated signal; (dashed-dotted) simulated response for MA; (dashed) simulated response for A; (dotted) simulated response for M.

Table 7-1: Reaction rate constants k^{het} (Eq. 7-5) of the of the ester hydrolysis reactions determined for Cat-1 and Cat-2 at room temperature

Component	$10^3\,k^{het}$ [l/(mol min)]	
	Cat-1	Cat-2
MF	14.0	21.4
EF	7.26	13.6
MA	0.38	0.76
EA	0.36	0.65

The reaction rate constants obtained from the elution profiles for the four cases measured at room temperature and a flow rate of 0.75 mL/min are given for both catalysts in Table 7-1. The obtained values of k^{het} indicate that the reactivities of the esters decrease in the order MF, EF, MA, EA and the hydrolysis of all of the esters are faster using Cat-2 than using Cat-1. This is in agreement with the different concentrations of sulfonic acid groups on the two catalysts.

7.3.2 Influence of temperature on reaction rate constants

Due to better separation in performance, R1-C1 is used for further studies of temperature influence on the reaction rate constants of the four ester hydrolysis reaction. Except the porosity, the other model parameters depend strongly on temperature. Based on the temperature dependences of the chemical equilibrium constants, the adsorption equilibrium constants and the number of theoretical plates given in Chapter 5, the rate constants the ester hydrolysis reactions were estimated at four different temperatures using the chromatograms shown in Figure 6-4. In Figure 7-3 shows the best curve fittings of measured and simulated detector signals for EF at four different temperatures. Although EF was converted completely in all cases, the separation of the hydrolysis products is significantly improved at higher temperatures.
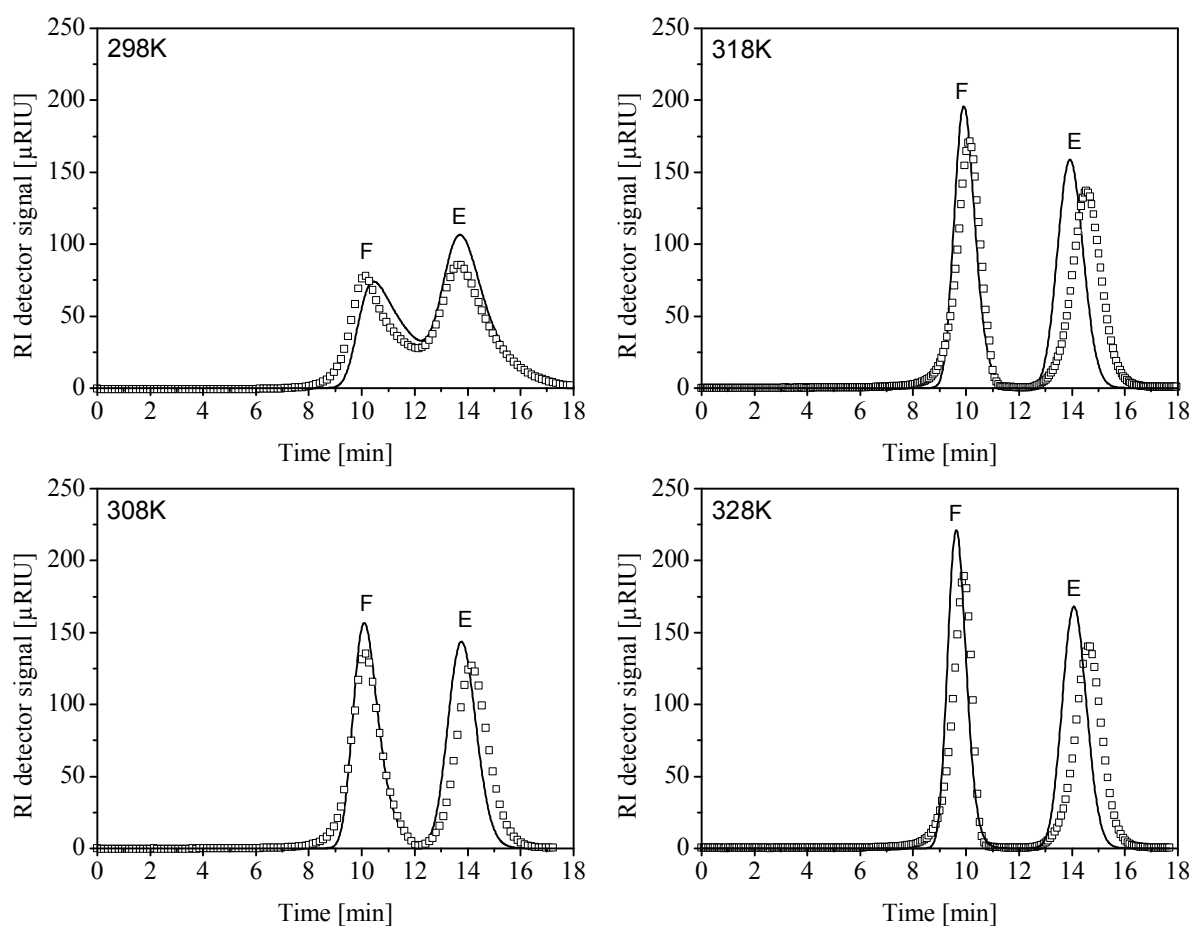
Figure 7-3: The best fitting of the simulated and measured signals for EF at different temperatures (Simulations with k^{het} in Table 7-2; R1-C1; Flow rate 0.75 mL/min; c_{EF}^{inj} =0.5 mol/L; injection volume 100µL)

($\square$) measured RI detector signals;   (solid) sum-simulated RI detector signals;

Figure 7-4 shows the best curve fittings of measured and simulated detector signals for EA at four different temperatures, but EA was not converted completely. In the both figures, the fitting at the front of the chromatograms is better that at the rear of the chromatograms. These simulations are acceptable to obtain the corresponding reaction rate constants.
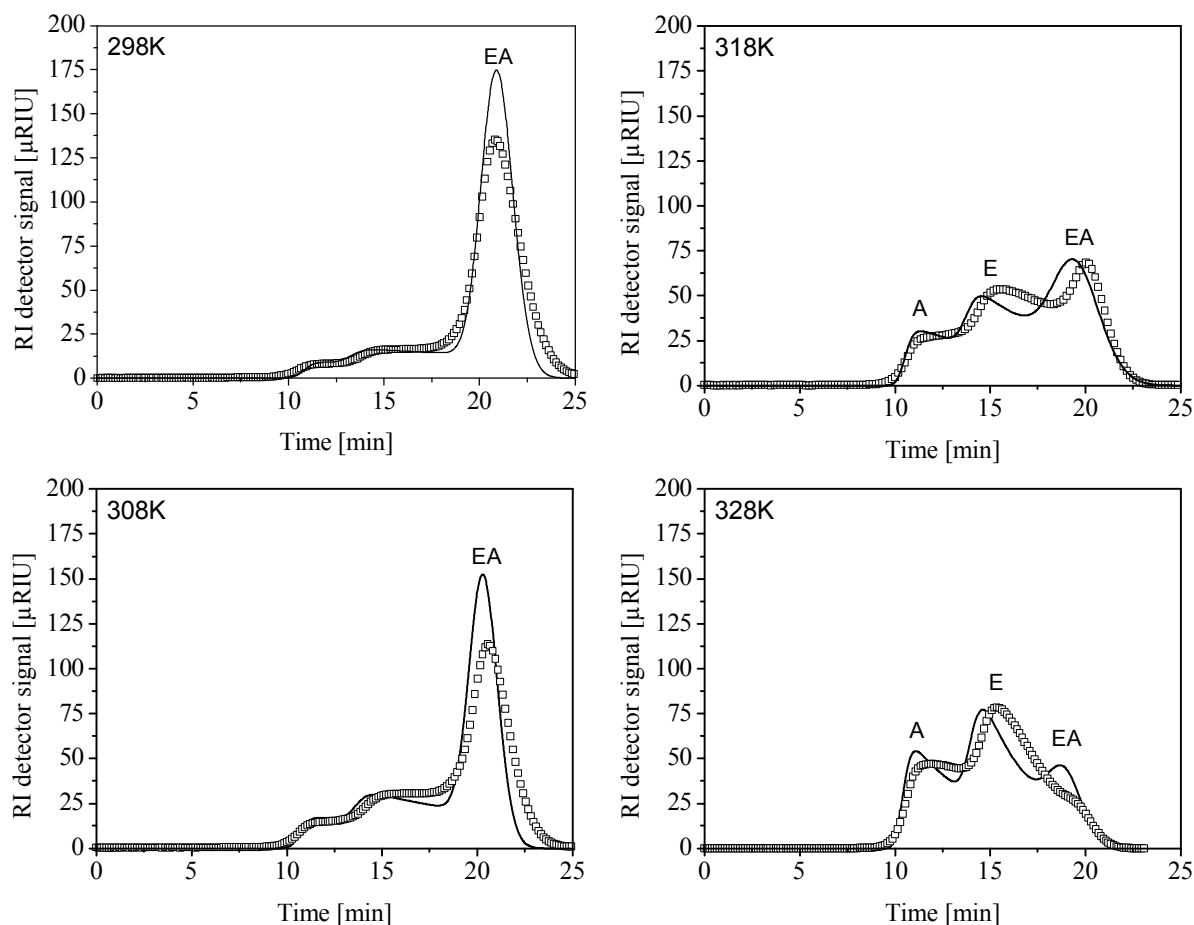
Figure 7-4: The best fitting of the simulated and measured signals for EA at different temperatures (Simulations with k^{het} in Table 7-2; R1-C1; Flow rate 0.75 mL/min; c_{EA}^{inj} =0.5 mol/L; injection volume 100μL)
(□) measured RI detector signals;   (solid) sum-simulated RI detector signals;

The reaction rate constants of the four ester hydrolysis reactions at four different temperatures are summarized in Table 7-2. The rate constants of most reactions increase as the temperature is raised and this is also right with the ester hydrolysis reactions. The hydrolysis of the formate esters is tens times faster than that of the acetate esters. Without support of the column oven, the results in Table 7-1 depend on ambient temperature and they are in the temperature range from 298~308K in comparison with the results in Table 7-2.

Table 7-2: Dependence of the rate constants k^{het} (Eq. 7-5)
of the ester hydrolysis reactions on temperature for Cat-1

	$10^3 \ k^{het}(T)$ [L/mol min]			
	298K	308K	318K	328K
MF	8.38	15.2	46.4	72.2
EF	5.88	23.5	41.6	56.7
MA	0.35	0.80	1.86	4.23
EA	0.45	0.89	1.75	3.32

The temperature dependence of the reaction rate constants obeys Arrhenius equation in Eq. 2-83. The Arrhenius parameters can be obtained using non-linear least squares fitting or using the following linear transformation:

$$\ln k^{het}(T) = \ln k_0 - \frac{E_A}{RT} \tag{7-9}$$

The parameter k_0, which corresponds to the intercept of the lines at *1/T = 0* (at infinite temperature). The activation energies E_A, which is obtained from the slope of the lines $(-E_A/R)$. In Figure 7-5 shows the best linear least squares fits of Arrhenius equation for the four hydrolysis reactions. The fittings for MA and EA are better than that for MF and EF. The quantified values for the Arrhenius parameters are summarized and given in Table 7-3. The MA hydrolysis reaction has the highest activation energy, whereas the EA hydrolysis reaction has the smallest activation energy. The activation energies obtained were more or less around 60 kJ/mol. These values were acceptable in comparison with the other studies [e.g., Sain05, Schl06].
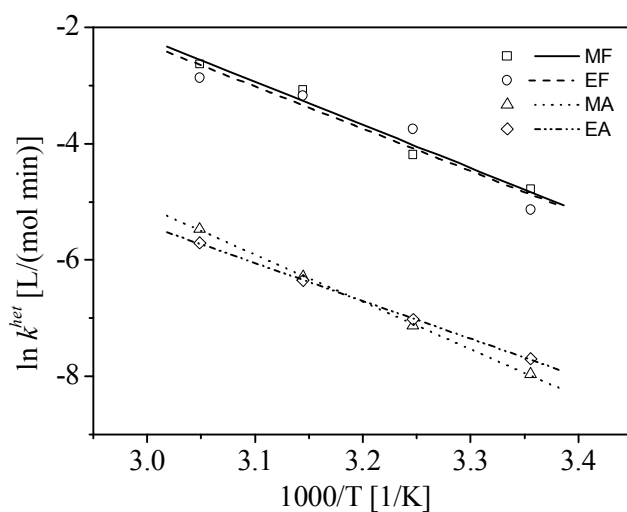
Figure 7-5: Determining Arrhenius parameters for the ester hydrolysis reaction based on the temperature dependence of the reaction rate constants given in Table 7-2.

Table 7-3: The value of activation energies and the frequency factors
of the esters hydrolysis reactions for Cat-1

	E_A [kJ/mol]	$10^3 \, k_0$ [L/mol min]
MF	62	511
EF	60	301
MA	68	250
EA	54	133

7.3.3 Evaluation of the reaction kinetics of the four ester hydrolysis reactions

The kinetics of ester hydrolysis reactions was already investigated by several authors before [e.g., Falk03, Mai06, and Schl06].

The reaction rate constant of MF was determined by [Falk03] at a temperature of 298K, using the chromatographic reactor R2-C1 (i.e., the small reactor size with Cat-1). The total rate of MF hydrolysis was contributed supposedly by rates of auto-catalyst, homogeneously and heterogeneously catalyzed reaction.

The rate of MF with Cat-1 and all the four esters with Cat-2 were determined by [Mai06], using a calorimetric reactor at a temperature of 298K. For reactions with low reaction heat, this method seems to be insensitive to quantify the reaction rate constants.

The rates of MF hydrolysis and esterification reactions have been also investigated by [Schl06] using a perturbation method with R1-C1 (i.e., the big reactor size with Cat-1) and the calorimetric reactor. For the chromatographic reactor, the reaction rate constant of MF hydrolysis reaction was quantified in cases of the constant initial conditions and the variable initial conditions (perturbation method). The temperature effect on the MF hydrolysis was estimate in a temperature range of 288K ~ 298K, using the calorimetric reactor. A model taken homogeneously and heterogeneously catalyzed reactions, and non linear adsorption isotherms was considered.

The comparable results obtained form these works [Falk03, Mai06, Schl06] at 298K are summarized in Table 7-4. Although the investigations were performed by different methods and operating conditions, the results for MF hydrolysis reaction are more or less similar. In the results of [Schl06] and this work, the contribution of homogeneously catalyzed reaction rate was neglected, whereas it was independent determined using homogeneous catalysis by [Falk03, Mai06].

Additionally, the temperature effect on the MF hydrolysis was estimate in a temperature range of 288K ~ 298K by [Schl06], using the calorimetric reactor. The other ester hydrolysis reactions catalyzed by Cat-2 were studied by [Mai06]. However, the systematic experimental study to determine k^{het} of the four different ester hydrolysis reactions at different temperatures as performed in this work has not.

Table 7-4: Comparison of the results of the investigations of the MF hydrolysis reactions at 298K based on [Falk03, Mai06, and Schl06], Table 7-1 and Table 7-2.

Ester	Catalyst	Reaction rate constants x 10^3 [L/(mol min)]							
		[Falk03]		[Mai06]		[Schl06]		[This dissertation]	
		k^{hom}	k^{het}	k^{hom}	k^{het}	k^{hom}	k^{het}	k^{hom}	k^{het}
	HCl	0.33	-	3.19	-	-	-	-	-
MF	Cat-1	0.33	7.83	3.19	12.6	-	5.23	-	8.38
	Cat-2	-	-	3.19	27.1	-	-	-	21.4[(*)]
	HCl	-	-	-	-	-	-	-	-
EF	Cat-1	-	-	-	-	-	-	-	5.88
	Cat-2	-	-	2.98	13.7	-	-	-	13.6[(*)]
	HCl	-	-	-	-	-	-	-	-
MA	Cat-1	-	-	-	-	-	-	-	0.35
	Cat-2	-	-	0.99	0.10	-	-	-	0.76[(*)]
	HCl	-	-	-	-	-	-	-	-
EA	Cat-1	-	-	-	-	-	-	-	0.45
	Cat-2	-	-	0.12	0.75	-	-	-	0.65[(*)]

[(*)] *determined at room temperature (uncontrolled and varied from 298~308K)*

7.4 Validation of reaction rate constants

The reaction rate constants of the four ester hydrolysis reactions have been quantified by the simplified mathematical model given in Eq. 2-24, the initial and boundary conditions in Eqs. 2-21, 2-22 and 2-23 in Chapter 2, using the preliminary model parameters determined experimentally in Chapter 5. To ensure that the obtained results for the reaction rate constants are reliable and can use to simulate precisely the operation of the fixed-bed chromatographic reactors, the results have to be validated with experiments at other conditions. Because the reaction rate constants depend on temperature only, the validation can be carried out at different flow rates and different feed concentrations in reactive conditions.

7.4.1 Validation at different flow rates

The reaction rate constants were quantified by using the elution profiles obtained experimentally at a flow rate of 0.75 mL/min. These results are used to simulate the operation of the fixed-bed chromatographic reactors at other flow rates. These simulations are compared with the measured detector signals to confirm reliabilities of the model and the determined reaction rate constants. For illustration, the simulated elution profiles for MF using the obtained k_{MF}^{het} values given in Table 7-1 are shown in Figure 7-6. The simulations (solid lines) performed for three different flow rates are good agreement with the experimental results (squares).

Figure 7-6: Comparison of simulated (solid lines) and measured (squares) detector signals for single injection of MF at room temperature. (R1-C1, $\dot{V} = 0.5 \sim 1.0$ mL/min, $c_{MA}^{inj} = 0.5$ mol/L, $V^{inj} = 100\mu$L, $N = 817 \sim 1167$, $k_{MA}^{het} = 0.14$ x 10^{-3} mol/(L min))

For other illustration, the simulated elution profiles for MA at a flow rate of 0.3 mL/min using the obtained k_{MA}^{het} values given in Table 7-2 are shown in Figure 7-7. It is to be recognized that the measured and simulated detector signals are virtually congruent at any temperatures. The good agreement between the measured and simulated detector signals confirms that the reaction rate constants were determined precisely. This allows concluding that the initial assumptions and model are reliable.

Figure 7-7 shows also the corresponding simulated responses for the individual components contributed to the sum simulated signals. These are helpful to explain the strange shape of elution profiles for MA. Because the MA hydrolysis reaction takes place

slowly at 298K, the elution profiles of M and F are spread and overlapped. This leads to a complicated sum elution profile shown in Figure 7-7a.
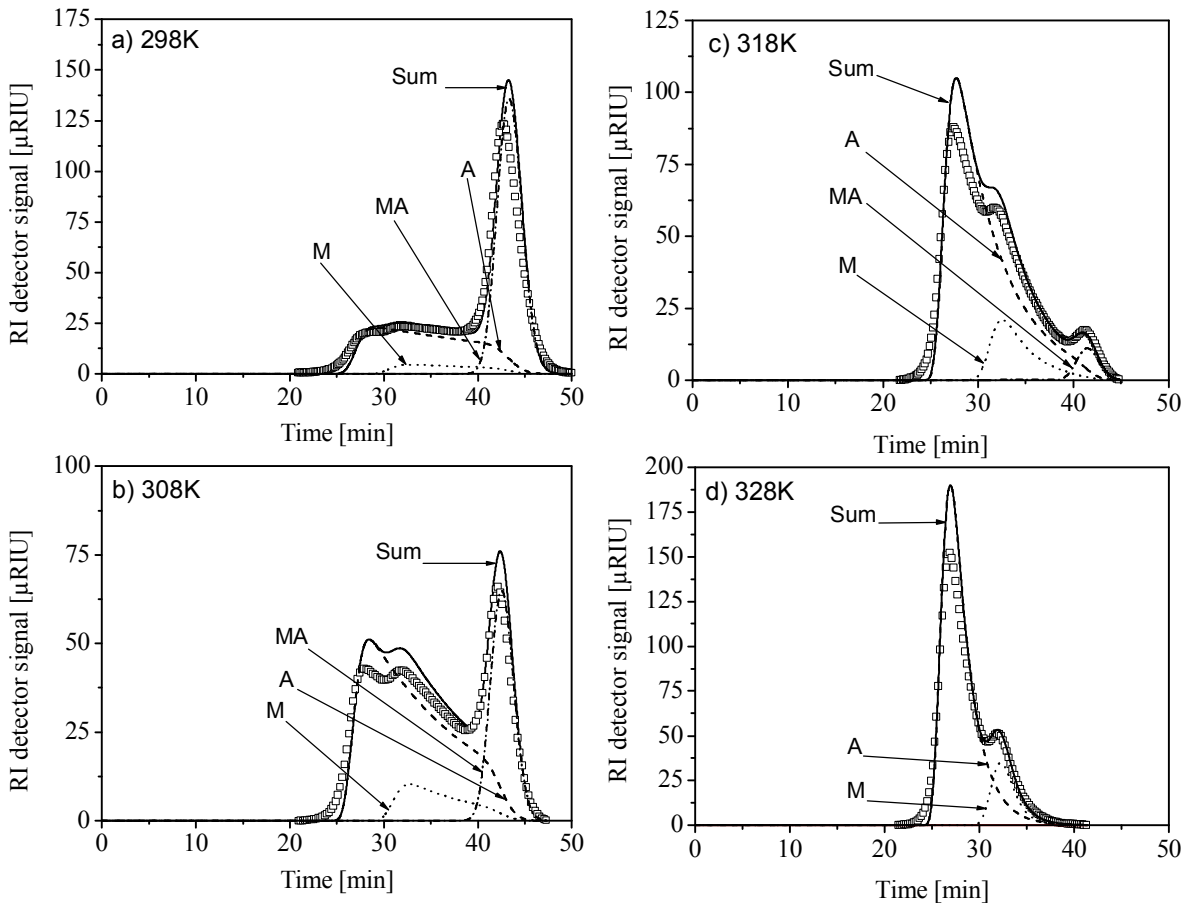
Figure 7-7: Comparison of simulated (solid lines) and measured (squares) detector signals for single injection of MA at a flow rate of 0.3 mL/min. (R1-C1, $c_{MA}^{inj} = 0.5$ mol/L, $V^{inj} = 100\mu L$, $N = 676 \sim 1275$, T $= 298 \sim 328K$, $k_{MA}^{het} = 0.35 \sim 4.23$ x 10^{-3} mol/(L min))

7.4.2 Validation at different feed concentrations

The reaction rate constants were quantified by using the elution profiles obtained experimentally with the identical conditions: $c_i^{inj} = 0.5$ mol/L, $V^{inj} = 100\mu L$, and $\dot{V} = 0.75$ mL/min. In order validate the model, the simulations have to be compared with the experiments with another feed concentration and another injection volume. For illustration, Figure 7-8 shows a simulation for the elution profile of MA with $c_i^{inj} = 1.5$ mol/L and $V^{inj} = 50\mu L$ in comparison with the experimental elution profile at the same conditions. In which, the flow rate and temperature were kept the same with the identical conditions. The good agreement between the simulated and measured detector signal allows to concluding

that the model can be describe precisely the operation of the fixed-bed chromatographic reactor at any feed concentration (in the range of linear adsorption) and any injection volume.
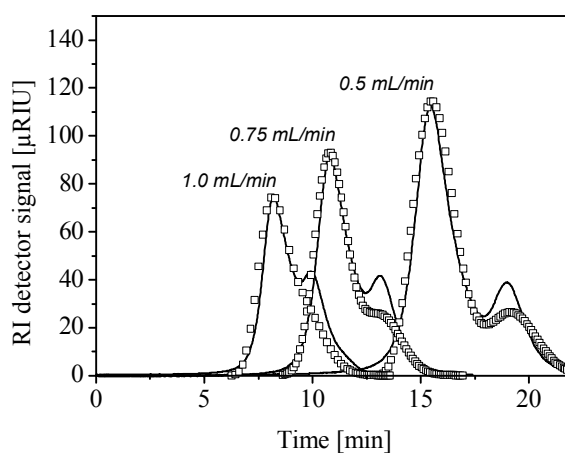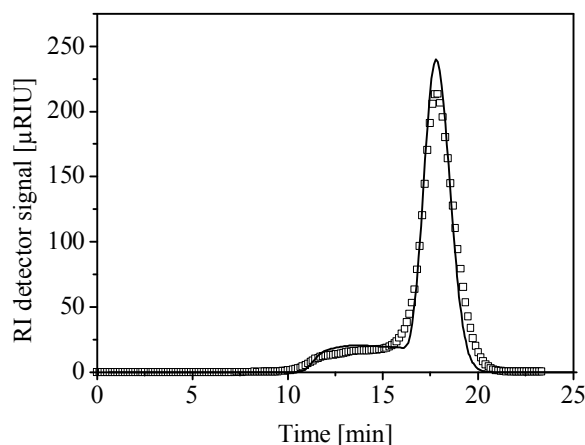

Figure 7-8: Comparison of simulated (solid lines) and measured (squares) detector signals for single injection of MA (R1-C1, c_{MA}^{inj} = 1.5 mol/L, V^{inj} = 50µL, $\dot{V}$ = 0.75 mL/min, N = 936, T = 298K, k_{MA}^{het} = 0.35 x 10^{-3} mol/(L min))

Summary, the reaction rate constants k^{het} determined in this work have been validated successfully at different conditions. These results allow concluding that all the model parameters (including the reaction rate constants) are determined properly and the equilibrium-dispersion model can be used to describe the operation of the fixed-bed chromatographic reactors adequately. In the next chapter, the obtained results are used to evaluate productivity and other objective function of the ester hydrolysis reactions.

Productivity Evaluation

Chromatographic reactors have the potential to improve conversion and selectivity compared to conventional reactors [i.e., Sard93, Falk03]. However, costs for operation of chromatographic could be high. There is a need for evaluation and optimization case by case specific objective functions (e.g. yields, productivity and purity) during the design of chromatographic reactors. In this chapter, based on the model parameters determined in Chapter 5 and the model introduced in Chapter 2 and validated in Chapter 7, the productivity and other objective functions are evaluated and optimized for the ester hydrolysis reactions performed in the FBCRs.

8.1 Methodology

For productivity evaluation of the FBCR, formic acid (F) and acetic acid (A) were chosen for the sake of illustration as target products. Methanol (M) and ethanol (E) were considered as by-products. F can be obtained by hydrolysis reactions of methyl formate MF or ethyl formate EF. A can be obtained by hydrolysis reactions of methyl acetate MA or ethyl acetate EA.

Objective functions of the FBCRs can be evaluated based on experiments or simulations. Using experimental results for productivity evaluation is costly and more difficult due to the related efforts, the overlap of concentration profiles and limited possibilities of detection. Therefore, using simulated concentration profiles is convenient way to quantify and optimize the objective functions. The available model parameters given in Chapters 5 and 7 for catalyst Cat-1 and reactor R1-C1 (i.e., 8 x 250 mm) were chosen for these studies.

Basic expressions related to calculating performance criteria were represented already in Section 2.1.3. The objective functions normally used in preparative chromatography are productivity PR_i (Eq. 2-39) and yield Y_i (Eq. 2-43). However, it is rather difficult to

optimize the two objective functions simultaneously. For example, a high productivity usually leads to a low recovery yield, and vice versa. In order to solve this problem, a product of the productivity and yield $PR_i \times Y_i$ was introduced as another suitable objective function [Feli96]. This objective takes both goals into account. In addition to these functions, of course also conversion of reactants (Eq. 2-42) is an important objective function for reactive chromatography.

The cut times for fraction collection were determined with respect to the predefined purity of target products. The predefined purity of the target products (F and A) was fixed at:

$$Pu_i \geq 99\% \qquad\qquad\qquad (8\text{-}1)$$

Quantifying productivity and yield is related in addition to values of threshold concentrations. The selection of the threshold concentration, $c_{threshold}$ determines the beginning and end times for collection, t^{begin} and t^{end}, and thus the cycle time t^{cycle} (see Eq. 2-37). There are several possibilities to select $c_{threshold}$: as a fixed value or a relative value related to feed or maximum outlet concentrations. Effects of the threshold concentration on the productivity of components were discussed by [Shan04]. Below, $C_{threshold}$ was set as a constant relative value of the feed concentration of the esters injected.

$$c_{threshold} = 0.001 c_{Es}^{inj} \qquad\qquad\qquad (8\text{-}2)$$

Additionally, the concentrations of the target products and the by-products in collected fractions were quantified. These two functions can be taken in the effluent divided by the time $t^{cutpoint}$. The concentration of the target products (the acids) in the first fraction collected is:

$$c_{i,target}^{collect} = \frac{\int_{t^{begin}}^{t^{cutpoint}} c_{i,target}\, dt}{\left(t^{cutpoint} - t^{begin}\right)} \qquad\qquad\qquad (8\text{-}3)$$

It is the goal to maximize the objective functions by changing operating variables. The most relevant operating variables are flow rate, temperature, injection volume and feed concentration. These variables are typically limited by lower and upper boundaries. A global optimization of all the variables is difficult. Therefore, here only a simplified approach was performed changing step by step one or two variables and fixing others constant for each optimization step. The following sequential "optimization" process was carried out:

Step 1: For initialization, the objective functions were evaluated at specific fixed reference conditions ($c_{Es}^{inj} = 0.5$ mol/L; $V^{inj} = 100$ μL, $\dot{V} = 0.3$ or 0.75 mL/min). This was done for several temperatures $T = 298\text{~}328\text{K}$. It was interesting to find out which reactants will offer the highest productivity with respect to the chosen target component at these referent conditions.

Step 2: Since high loadings are more favorable for reaching high productivity, feed concentrations of the esters were increased to values equal to 90% of the solubility (Table 3-2). In this step, the injection volume was still kept relatively small as in the first step (i.e., 100 μL). For these higher feed concentrations the influence of flow rate on the objective functions was analyzed at different temperatures.

Step 3: Based on the best temperatures and flow rates identified in the second step, the injection volume was finally increased to maximize the product of productivity and yield as an objective function.

8.2 Evaluation of objective functions

Following the strategy described above, the objective functions were evaluated at first at the identical feed concentrations and flow rates for comparison and orientation. Based on the qualitative discussion in Chapter 6 and the quantitative discussion in Chapter 7, fast and slow hydrolysis of the esters could be distinguished. For the fast ester hydrolysis reactions of MF and EF, the productivity of F and the other objective functions were evaluated at a flow rate of 0.75 mL/min. For the slower hydrolysis reactions of MA and EA, a lower flow rate of 0.3 mL/min was chosen to evaluate the productivity of A. The conditions used in the calculations are given in Table 8-1.

Table 8-1: Summary of operation conditions using for the evaluation of objective functions for producing F and A

Reactant	Reactor	Feed Concentration [mol/L]	Injection volume [μL]	Flow rate [mL/min]	Temperature [K]
MF, EF	R1-C1	0.5	100	0.75	298, 308, 318 and 328
MA, EA	R1-C1	0.5	100	0.3	298, 308, 318 and 328

In Figure 8-1 are shown the elution profiles simulated for several consecutive injections of MF and EF. The regularly periodic repetition of the concentration profiles indicates that the relative threshold concentrations used were acceptable. For these residence times, no remaining MF and EF could be observed (i.e., complete conversion of the esters).
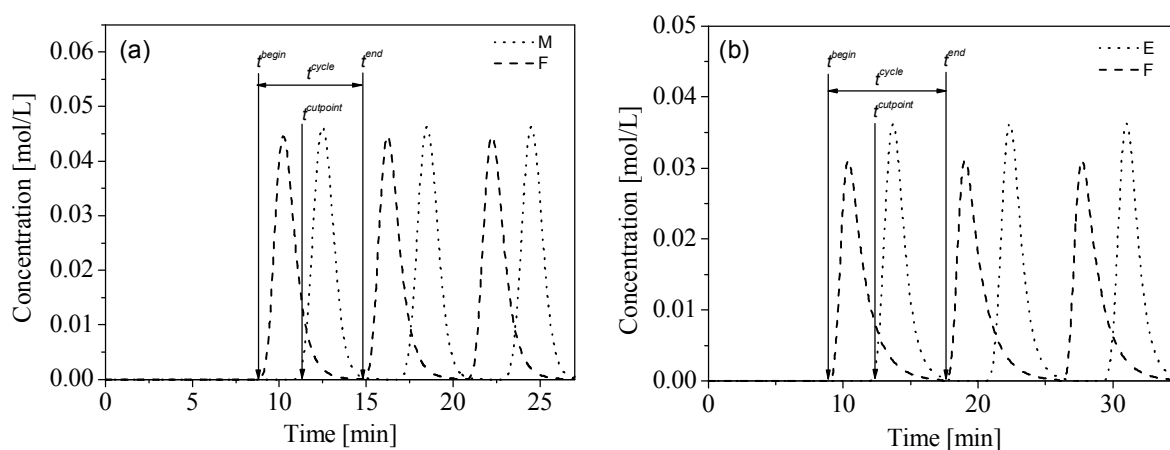
Figure 8-2: Elution profiles for these consecutive injections of MF and EF leading to the complete conversion of reactants and complete separation of the hydrolysis products
($c_{MF}^{inj} = 0.5$; $c_{EF}^{inj} = 0.5$; $V^{inj} = 100$ [µL], $\dot{V} = 0.75$ [mL/min], T = 298K).

Based on the concentration profiles simulated by the conditions given in Table 8-1, the conversion, productivity and yield of ester hydrolysis processes were evaluated. In Table 8-2 are shown the results for MF and EF hydrolysis reactions. The common target product for the two injected esters is formic acid F. The esters were converted almost completely in the whole range of temperatures. For illustration, the temperature dependence of the productivity PR_i and the yield Y_i are shown in Figure 8-2. The influence of temperature on the objective functions was significant. This can be explained by the influence of temperature on separation that was discussed in Chapters 5 and 7. At similar feed conditions, the productivity of producing F from MF was significantly higher than from EF. The maximum productivity of F produced by MF and EF were obtained at 318K (Figure 8-2a). The recovery yields were increased when the temperature was increased (asymptotic to 100%). With the operating parameters in Table 8-1, complete conversions and complete separations can be observed at 318K and higher temperatures for MF and at 308K and higher temperature for EF. Due to complete conversion and separation, the purity of by-products (M or E) was estimated. Concentrations of target products in the collected fraction were quantified by Eq. 8-3. Under the conditions studied the collected concentrations were significantly smaller than the feed concentration 0.5 mol/L.

Table 8-2: Evaluation of the objective functions for MF and EF hydrolysis to produce F ($Pu_F > 99\%$, $c_{ester}^{inj} = 0.5$ mol/L; $V^{inj} = 100$ µL, $\dot{V} = 0.75$ mL/min)

Reactant	T [K]	t^{cycle} [min]	PR_F x 10^6 [mol/min]	Y_F [%]	PR_F x Y_F x 10^4 [mol/min]	X_{Es} [%]	$c_F^{collect}$ [mol/L]
MF	298	6.42	6.09	77.7	4.73	~ 100	0.0219
	308	5.17	9.67	95.0	9.18	~ 100	0.0253
	318	**4.79**	**10.69**	**97.3**	**10.40**	**~ 100**	**0.0322**
	328	5.04	10.25	98.1	10.05	~ 100	0.0333
EF	298	8.26	5.52	88.1	4.86	~ 100	0.0171
	308	6.73	7.53	97.4	7.33	~ 100	0.0191
	318	**6.39**	**7.91**	**97.1**	**7.68**	**~ 100**	**0.0277**
	328	6.64	7.61	97.3	7.41	~ 100	0.0319
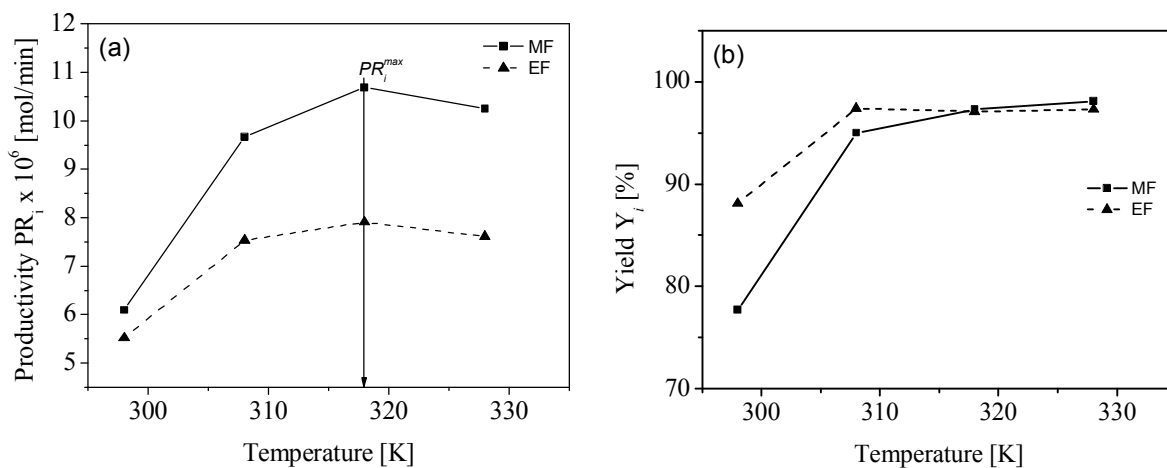
Figure 8-2: Temperature dependence of productivity and yield for MF and EF
(a) Productivity   (b) Yield
($c_{Es}^{inj} = 0.5$; $V^{inj} = 100$ [µL], $\dot{V} = 0.75$ [mL/min], T = 298 ~ 328K).

Table 8-3 shows a similar evaluation of the objective functions Pr_A and Y_A for MA and EA hydrolysis processes. Although, a slower flow rate was assumed in comparison to the MF and EF hydrolysis (Table 8.2), complete conversion could be obtained for the both esters only at 328K or higher temperatures. Influence of temperature on productivity and yield is illustrated in Figure 8-3. Obviously, the productivity of A obtained by MA is higher than

that of EA due to shorter cycle times. The maximum recovery yields are 87.89% for MA and 81.12% for EA. The recovery yields are relative small because no complete separation is obtained in this temperature range.

Table 8-3: Evaluation of the objective functions for MA and EA hydrolysis to produce A
($Pu_A > 99\%$, $c_{Es}^{inj} = 0.5$ mol/L; $V^{inj} = 100$ μL, $\dot{V} = 0.3$ mL/min)

| Reactant	T [K]	t^{cycle} [min]	PR_A x 10^6 [mol/min]	Y_A [%]	PR_A x Y_A x 10^6 [mol/min]	X_{Es} [%]	$c_A^{collect}$ [mol/L]
MA	298	21.87	0.15	6.45	0.95	44.21	0.0025
	308	21.19	0.42	17.62	7.34	75.34	0.0071
	318	18.91	0.91	34.50	31.51	96.36	0.0141
	328	14.00	3.13	87.89	275.41	~100	0.0257
EA	298	30.87	0.25	14.65	3.63	56.64	0.0044
	308	30.05	0.51	29.62	15.24	78.23	0.0072
	318	26.93	1.06	54.69	58.01	98.28	0.0122
	328	23.63	1.79	81.12	145.45	99.13	0.0154
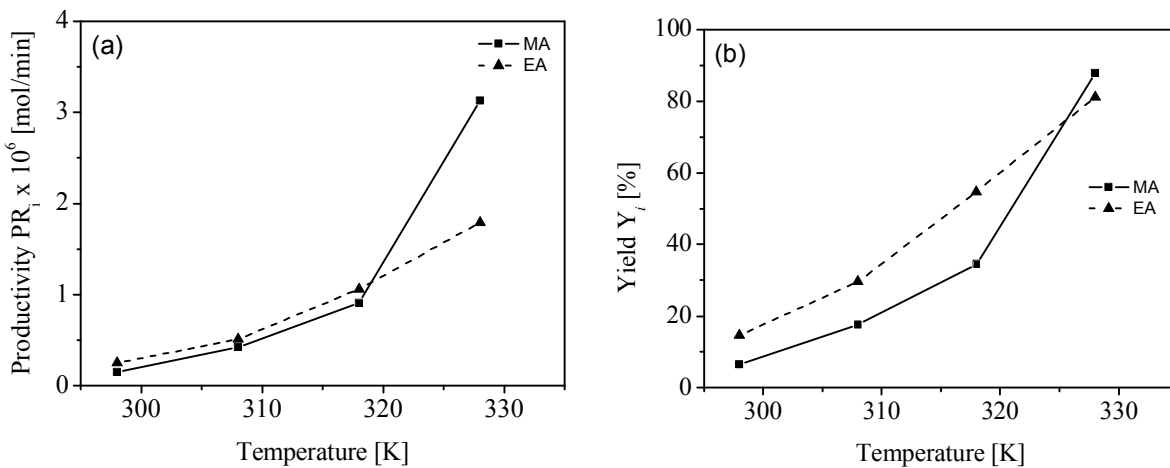
Figure 8-3: Temperature dependence of productivity and yield for MA and EA
(a) Productivity (b) Yield ($c_{Es}^{inj} = 0.5$ mol/L; $V^{inj} = 100$ μL, $\dot{V} = 0.3$ mL/min)

Based on these preliminary evaluations, MF and MA were chosen as the reactors for further optimization steps due to the possibility to achieve higher productivities of F and A. Because of complete conversion of MF in the whole temperature range considered, optimization for MF was carried out at the four different temperatures. For the slower hydrolysis of MA, the optimization was performed only at the highest temperature of 328K.

8.3 Analysis of impact of operating parameters

The goal of the calculation performed is to maximize the PR_i or PR_i x Y_i at maximum possible flow rate and maximum possible efficiency. Following the strategy given above, in this section flow rate, temperature and injection volume are varied to obtain maximum of the objective functions.

8.3.1 Impact of flow rate

It is attractive to use high feed concentration. Thus, in contrast to Section 8.1, the feed concentrations of MF and MA were now selected as 90% of solubility. Although this feed concentration is relative high in comparison with the feed concentrations used in the experiments described above, the corresponding adsorption equilibria of the components were assumed to be still linear. The injection volume was kept similar to the previous step (i.e., 100μL). The operating conditions for the analysis of the impact of flow rate are summarized in Table 8-4.

Table 8-4: Summary of conditions using for analysis impact of flow rate (R1-C1)

Reactant	Flow rate [mL/min]	Feed Concentration [mol/L]	Injection volume [μL]	Temperature [K]
MF	0.3 ~ 3.5	4.5	100	298, 308, 318 and 328
MA	0.3 ~ 3.5	3.0	100	328

a) *Producing formic acid (F)*

The PR_F, Y_F and PR_F x Y_F were quantified for the conditions in Table 8-4. The results are given in Table 8-5a. Normally, at each temperature a best flow rate could be found at maximum of the objective function PR_F x Y_F. However, the best flow rate at 328K could

not be found in the flow rate in the investigated range of flow rate 0.3 ~ 3.5 mL/min. The dispersion coefficients (Eq. 2-61) determined experimentally were available in this range of flow rate. Therefore, a similar value of the dispersion coefficient at 3.5 mL/min was applied for all simulations in the extended range of flow rate 3.5 ~ 7 mL/min. The estimated values of the objective functions in the extended flow rate range are shows in Table 8-5b. Because of using the same values of dispersion coefficients (i.e., no influence of flow rate on dispersion taken into account), the results for the extended range of the flow rate were less reliable.

The influences of flow rate on the objective functions are illustrated in Figure 8-4. The dashed lines represented for the objective functions in the extended range of flow rate. Increasing the flow rate, the PR_F and PR_F x Y_F also increased up to a maximum and then decreased. The recovery yield decreased at higher flow rates due to increasing of inseparable zone of the products and amount of the unconverted reactant. The influence of temperature on the objective functions was significantly. At the same flow rate, a higher temperature offers much greater productivity and recovery yield due to the better separation of the hydrolysis products.

At each temperature, a certain flow rate could be found to maximize PR_F x Y_F. Because of the lack of experimental data for temperatures out of the range of 298 ~ 328K, no further optimization of temperature was done. For the maximum of the PR_F x Y_F, the best flow rates at 298, 308, 318, and 328K were 0.5, 1.5, 3.0 and 6.5 mL/min, respectively. At the best flow rates, the conversions of MF were between 94.5 ~ 100%, whereas the recovery yields were between 73.82 ~ 90%. The concentration of F in the fractions collected was about 20 times smaller than the feed concentration of MF.

Table 8-5a: Impact of flow rate and temperature for producing F from MF
($\dot{V} = 0.3 \sim 3.5$ mL/min, $Pu_A > 99\%$, $c_{MF}^{inj} = 4.5$ mol/L; $V^{inj} = 100$ μL)

T [K]	Flow rate [mL/min]	t^{cycle} [min]	PR_F x 10^6 [mol/min]	Y_F [%]	PR_F x Y_F x 10^3 [mol/min]	X_{Es} [%]	$c_F^{collect}$ [mol/L]
298	0.30	13.26	32.96	97.10	3.20	~100	0.234
	0.50	**9.21**	**43.50**	**88.99**	**3.87**	**~100**	**0.215**
	0.75	6.84	50.18	76.32	3.83	~100	0.187
	1.00	5.58	53.91	66.84	3.60	97.3	0.159
	1.50	4.04	53.35	47.95	2.56	92.5	0.176
308	0.30	11.97	37.59	100	3.76	~100	0.229
	0.50	7.76	57.52	99.21	5.71	~100	0.229
	0.75	4.92	75.46	95.99	7.24	~100	0.219
	1.00	4.64	88.31	91.23	8.06	~100	0.205
	1.50	**3.44**	**103.76**	**79.37**	**8.24**	**99.0**	**0.177**
	2.00	3.59	92.42	73.66	6.81	99.0	0.127
318	0.30	11.99	37.54	100	3.75	~100	0.299
	0.50	7.476	60.19	100	6.02	~100	0.242
	0.75	5.148	87.41	100	8.74	~100	0.235
	1.00	4.004	112.39	100	11.24	~100	0.226
	1.50	2.875	155.31	99.24	15.41	~100	0.215
	2.00	2.274	190.68	96.34	18.37	~100	0.201
	2.50	1.933	214.45	92.12	19.76	~100	0.193
	3.00	**1.703**	**230.98**	**87.39**	**20.19**	**~100**	**0.196**
	3.50	1.472	177.12	57.92	10.26	~100	0.122
328	0.30	12.32	36.51	100	3.65	~100	0.305
	0.50	7.51	59.96	100	6.00	~100	0.257
	0.75	5.16	87.28	100	8.73	~100	0.270
	1.00	3.97	113.22	100	11.32	~100	0.207
	1.50	3.06	147.02	100	14.70	~100	0.203
	2.00	2.25	195.57	97.86	19.14	~100	0.199
	2.50	1.56	226.89	95.02	21.56	~100	0.192
	3.00	1.63	247.95	90.01	22.32	~100	0.180
	3.50	1.45	267.23	86.66	23.16	99.3	0.171

Table 8-5b: Impact of flow rate for producing F from MF (in the extended range of flow rate) ($\dot{V} = 3.5 \sim 7$ mL/min, $Pu_A > 99\%$, $c_{MF}^{inj} = 4.5$ mol/L; $V^{inj} = 100$ μL)

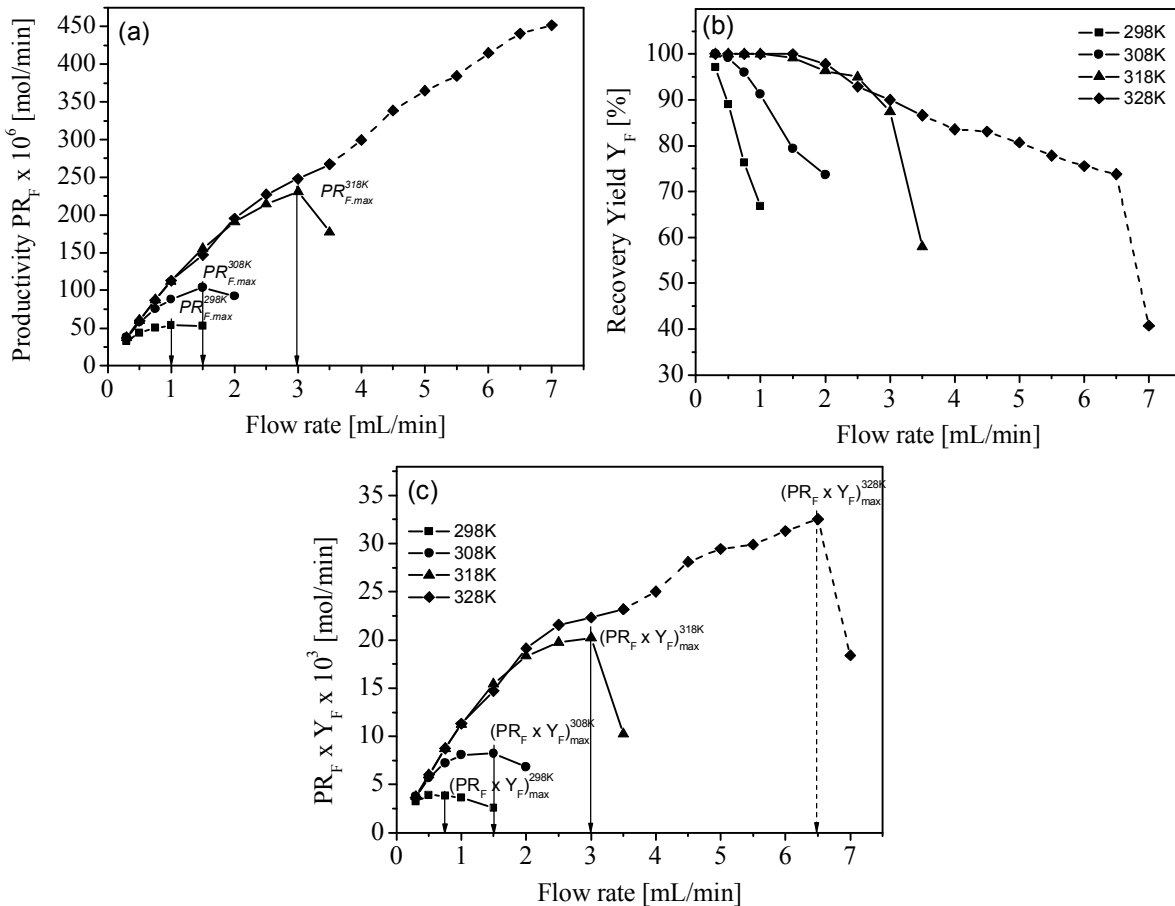| T [K]	Flow rate [mL/min]	t^{cycle} [min]	PR_F x 10^6 [mol/min]	Y_F [%]	PR_F x Y_F x 10^3 [mol/min]	X_{Es} [%]	$c_F^{collect}$ [mol/L]
	4.0	1.256	299.42	83.57	25.02	98.8	0.177
	4.5	1.106	338.12	83.11	28.10	98.2	0.169
	5.0	0.995	364.76	80.68	29.43	97.9	0.162
328	5.5	0.911	384.15	77.82	29.89	96.5	0.157
	6.0	0.820	414.46	75.56	31.32	95.2	0.153
	6.5	**0.754**	**440.64**	**73.82**	**32.53**	**94.1**	**0.147**
	7.0	0.711	451.64	40.77	18.41	95.9	0.146

Figure 8-4: Impact of flow rate for F production from MF (a) Productivity PR_F, b) Yield Y_F,   (c) PR_F x Y_F ($c_{MF}^{inj} = 4.5$ mol/L; $V^{inj} = 100$ μL, T = 298 ~ 328K)

Solid lines for the investigated range of flowrate $\dot{V} = 0.3 \sim 3.5$ mL/min (Table 8-5a)

Dashed lines for the extended flow rate range $\dot{V} = 3.5 \sim 7$ mL/min (Table 8-5b)

Although the highest value of the PR_F x Y_F was obtained at 328 K in the extended range of flow rates, the quantitative results seem to be of limited accuracy due to lack of the influence of flow rate on the dispersion coefficients (i.e., using constant dispersion coefficients). Therefore, it is better to estimate the impact of the injection volume with the real parameters available. The final step of systematic calculations for producing F from MF was carried out at 318 K and a flow rate of 3.0 mL/min.

b) *Producing acetic acid (A)*

Due to slow reaction kinetics, for the MA hydrolysis reaction was difficult to obtain complete conversion at the low temperatures. Therefore, the flow rate was optimized only at the highest possible temperature of 328 K with the running conditions given in Table 8-4. The estimated values for the objective functions are provided in Table 8-6. The influences of flow rate on the objective functions were illustrated in Figure 8-4. The objective functions PR_A and PR_A x Y_A were obtained simultaneously the maximum value at a flow rate of 0.4 mL/min. In this flow rate range, the recovery yield and conversion were relative high. However, in the lower range of flow rate, the productivity of A was much smaller than that of F at the same temperature of 328K. The collected concentration A was also around 20 times smaller than the feed concentration of MA. In the final step, the optimization of the injection volume is carried out at a flow rate of 0.4 mL/min.

Table 8-6: Impact of flow rate for producing A from MA at 328 K
($\dot{V} = 0.1 \sim 0.5$ mL/min, $Pu_A > 99\%$, $c_{MA}^{inj} = 3$ mol/L; $V^{inj} = 100$ [μL])

T [K]	Flow rate [mL/min]	t^{cycle} [min]	PR_A x 10^6 [mol/min]	Y_A [%]	PR_A x Y_A x 10^3 [mol/min]	X_{Es} [%]	$c_A^{collect}$ [mol/L]
	0.1	42.15	6.59	92.61	0.61	~100	0.160
	0.2	20.40	13.65	92.85	1.27	~100	0.164
328	0.3	15.04	17.27	86.64	1.50	~100	0.156
	0.4	**12.25**	**19.94**	**81.45**	**1.62**	**99.8**	**0.140**
	0.5	10.59	20.19	71.27	1.44	99.1	0.125
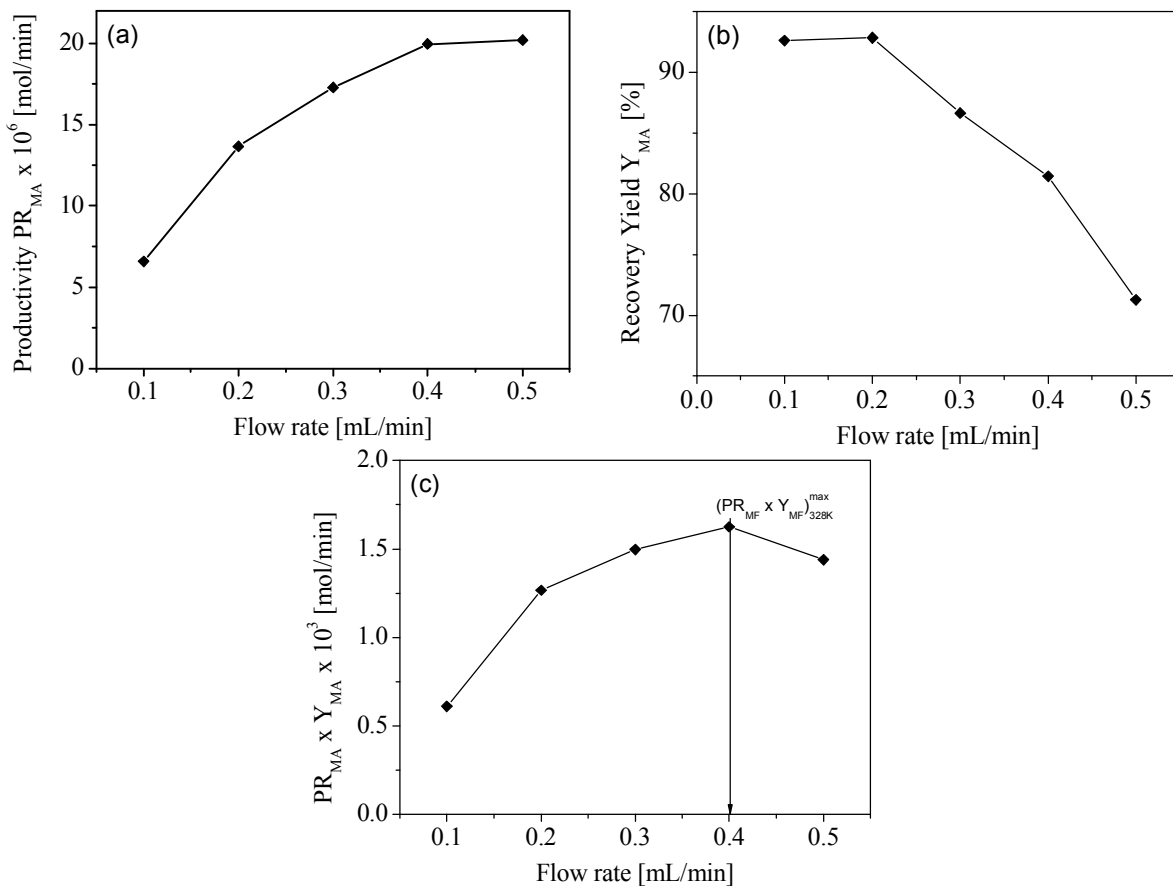
Figure 8-5: Impact of flow rate for producing A from MA
(a) Productivity PR_A (b) Yield Y_A (c) PR_A x Y_A
($c_{MA}^{Feed} = 3.0$ mol/L; $V^{inj} = 100$ µL, $\dot{V} = 0.1 \sim 0.5$ mL/min, $T = 328$K).

8.3.2 Impact of injection volume

In this step the feed concentrations were kept constant. Coming from 100 µL in the previous steps, an increase of injection volume results typically in an increase of the productivity and a decrease of the recovery yield. The different tendencies of the productivity and the recovery yield predict a maximum of the objective function PR_i x Y_i. Based on the best flow rates obtained in the previous section, the impact of injection volume was analyzed with the operating conditions provided in Table 8-7. Then conditions that which were identified before for $V^{inj} = 100$ µL as the best. The feed concentrations of MF and MA were kept again at 90% of the solubility as in the previous step.

Table 8-7: Summary of operating conditions using for analysis
of impact of injection volume

Reactant	Reactor	Injection volume [μL]	Feed Concentration [mol/L]	Flow rate [mL/min]	Temperature [K]
MF	R1-C1	100 ~ 1250	4.5	3	318
MA	R1-C1	100 ~ 1250	3.0	0.4	328

a) Producing formic acid (F)

The influence of injection volume on the objective functions for the production of F is summarized in Table 8-8. Changes in the injection volume alter the cycle times. Conversion did not change considerably in the parameter range studied. The recovery yield decreased significantly for larger injection volumes. The collected concentrations of F were improved for larger injection volumes. The influence of injection volume on the objective functions is shown in Figure 8-6. The objective function PR_F x Y_F was found maximal at an injection volume of 1250 μL. With this injection volume, the recovery yield was 64.52 %.

Table 8-8: Impact of injection volume for producing F from MF at 318 K
and a flow rate of 3 mL/min ($Pu_A > 99\%$, $c_{MA}^{inj} = 4.5$ mol/L; $V^{inj} = 100 \sim 1500$ μL)

T [K]	Injection volume [μL]	t^{cycle} [min]	PR_F x 10^6 [mol/min]	Y_F [%]	PR_F x Y_F x 10^3 [mol/min]	X_{Es} [%]	$c_F^{collect}$ [mol/L]
318	100	1.703	230.98	87.39	20.19	~100	0.196
	250	1.789	533.60	84.83	45.27	~100	0.448
	500	1.873	959.42	79.85	76.61	98.7	0.844
	750	1.986	1291.17	75.99	98.12	97.7	1.132
	1000	2.081	1503.62	69.53	104.55	96.7	1.380
	1250	**2.162**	**1678.74**	**64.52**	**108.31**	**95.8**	**1.590**
	1500	2.263	1669.43	55.97	93.44	94.9	1.665
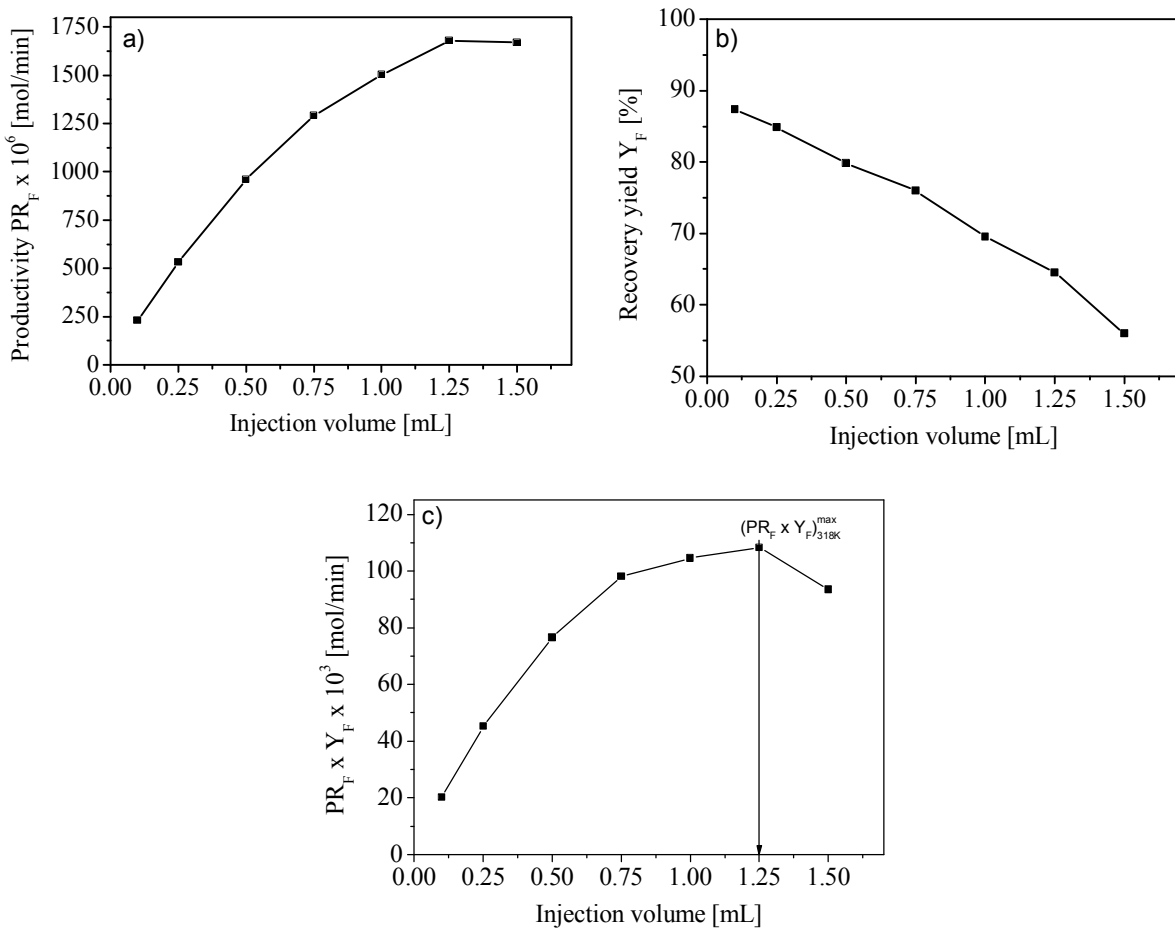
Figure 8-6: Impact of injection volume for A hydrolysis process
(a) Productivity PR_F (b) Yield Y_F (c) $PR_F \times Y_F$
(c_{MF}^{Feed} = 4.5 mol/L; V^{inj} = 100~1500 µL, $\dot{V}$ = 3.0 mL/min, T = 318K).

b) *Producing acetic acid (A)*

The results for the analysis of the impact of injection volume are provided in Table 8-9. The influence of injection volume on the objective functions is shown graphically in Figure 8-7. At the much slower flow rate than in the previous case, the influence of injection volume on the recovery yield was relatively small. The productivity and the collected concentration of A were increased considerably by increasing of the injection volume. The maximum of $PR_F \times Y_F$ was obtained at an injection volume of 1000 µL. In this case, the recovery yield was 96.1 % and thus much higher than previous case (production of F).

Table 8-9: Impact of injection volume for producing A form MA at 328 K
and a flow rate of 0.4 mL/min   ($Pu_A > 99\%$, $c_{MA}^{Feed} = 3$ mol/L; $V^{inj} = 100 \sim 1250$ µL)

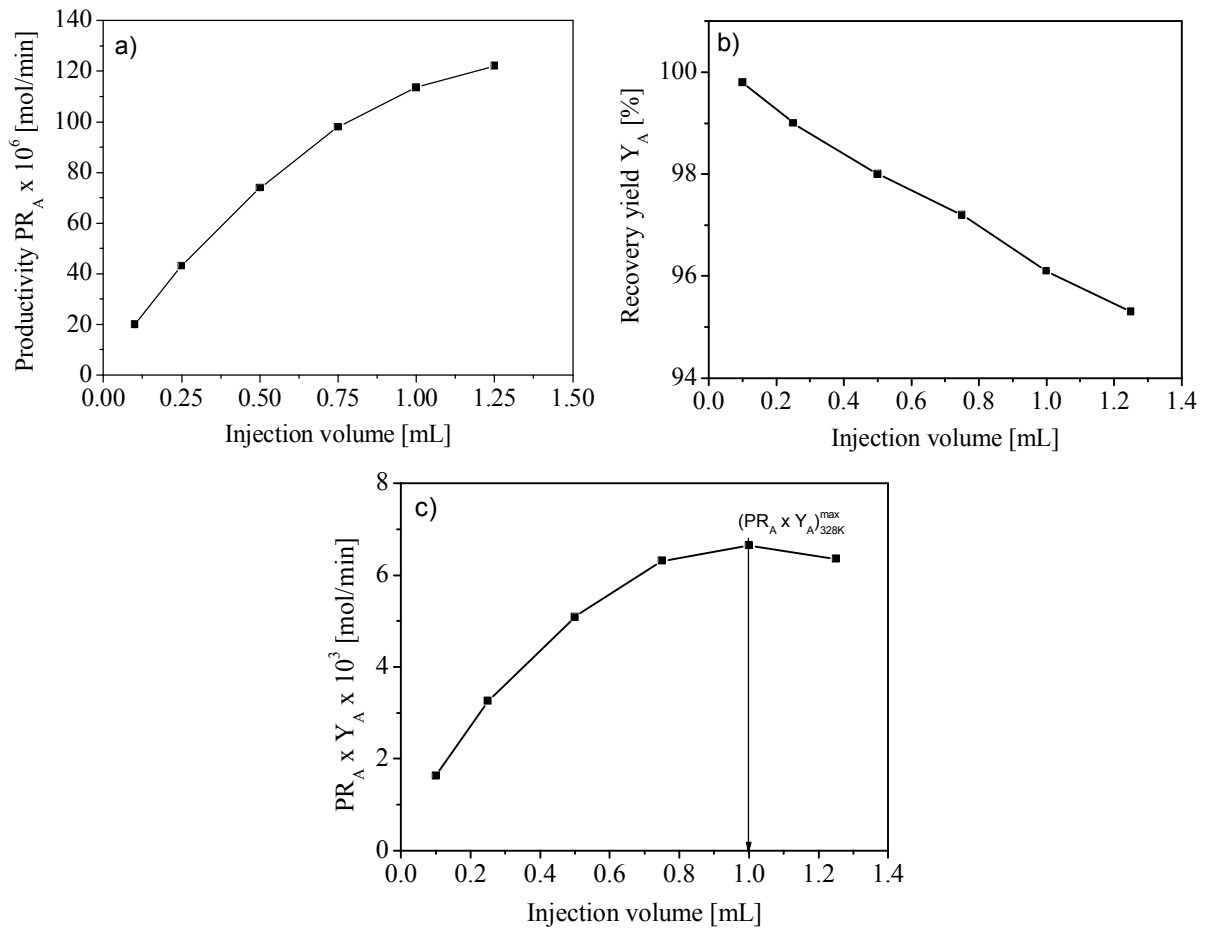| T [K]	Injection volume [µL]	t^{cycle} [min]	PR_F x 10^6 [mol/min]	Y_F [%]	PR_F x Y_F x 10^3 [mol/min]	X_{ester} [%]	$c_F^{collect}$ [mol/L]
	100	12.25	19.943	99.8	1.62	~100	0.140
	250	13.18	43.059	99.0	3.26	~100	0.329
328	500	13.95	73.986	98.0	5.09	98.7	0.601
	750	14.79	98.003	97.2	6.31	97.7	0.783
	1000	**15.47**	**113.558**	**96.1**	**6.65**	**96.7**	**0.938**
	1250	15.95	122.149	95.3	6.35	95.8	1.073

Figure 8-7: Impact of injection volume for A hydrolysis process
(a) Productivity PR_F (b) Yield Y_F (c) PR_F x Y_F
($c_{MA}^{inj} = 3.0$ mol/L; $V^{inj} = 100\sim1250$ µL, $\dot{V} = 0.4$ mL/min, T = 328K).

8.4 Summary with respect to productivity evaluation

Based on the equilibrium-dispersion model, a productivity evaluation for the production of F and A from various ester hydrolysis reactions performed in the chromatographic reactors was made. At the same chosen reference cycle times of MF and MA hydrolysises were shorter than that of EF and EA hydrolysises, respectively. Therefore, production of F and A from MF and MA were found to be more attractive than production from EF and EA. Although the feed concentrations were not optimized, higher feed concentrations typically offer higher productivity and concentrations in the collected fractions. Obviously, the flow rate, the injection volume and the temperature have large effects on the productivity and other relevant objective functions. These parameters were optimized by maximizing a compromise between productivity and recovery yield using the objective function $PR_i \times Y_i$. Temperature was not optimized because of lack of data out of the investigated range of temperature. However, higher temperatures allow for higher reaction rates and higher throughput due to better separation of the hydrolysis products. A clear optimum injection volume exists specific for each reaction system. With respect to flow rate working on the upper possible range appears attractive. In the case of the alcohols considered as target products, similar strategy can be applied to find the best conditions for maximizing the objective function $PR_i \times Y_i$.

Conclusions and Outlook

Chromatographic reactors are already considered a long time as an attractive alternative to conventional fixed-bed reactor operation. However, their industrial applications are still absent because of theoretical and experimental difficulties.

In this work, the difficulties in evaluating the potential of chromatographic reactors and applying them experimentally have been solved by developing a new two-step modeling approach. In the first step, an extended equilibrium model was used to estimate general feasibility of performing complete conversion and complete product separation in such reactors. In the second step, the equilibrium-dispersion model was applied for more detailed kinetic studies, simulations and optimizations. These two steps allow a) an identification of feasible reaction processes and b) precise descriptions of performance of the processes.

Following the proposed modeling approach, the feasibility of several typical reactions with arbitrary parameters were studied and discussed in detail. For the reaction type $2A \rightleftharpoons B + C$, the complete conversion of the reactant and the complete separation of the products B and C could be achieved if the relative adsorptivity of the component A is highest. In contrast, the reactions of the type $A \rightleftharpoons B + C$ could be run to complete conversion leading to pure products B and C independent of the relative adsorptivity of A. The difference in behavior between the considered reaction types can be attributed to their different stoichiometries.

In order to demonstrate the reliability of the predictions, four hydrolysis reactions (methyl formate, ethyl formate, methyl acetate and ethyl acetate) were chosen as case studies. The reactions were performed in fixed-bed chromatographic reactors packed by the ion exchange resin DOWEX 50W-X8. These reactions can be classified according to their rates into relatively fast or slow reactions. Because of water used in all experiments in excess, the ester hydrolysis reactions can be considered to belong to the reaction type

$A \rightleftharpoons B + C$. Therefore, complete conversion and complete separation should be feasible according to the results obtained with the extended equilibrium model.

In order to apply the equilibrium-dispersion model, the model parameters were determined experimentally. The properties of the stationary phases and the reactors were characterized in the temperature range of 298 ~ 328K and the flow rate range of 0 ~ 3.5 mL/min. The swelling ratio of the resin for different components was strongly dependent on the polarity and molecular weight of own component. For full swollen state of the packed resin, the effect of temperature on the porosity of the packing was not significant. The chemical equilibrium constants were found to increase by rising the temperature. In the investigated concentration range of 0.1 ~ 0.5 mol/L the adsorption equilibria of the components were linear for both H^+ and Na^+ forms of the resin. The adsorption equilibrium constants were strongly dependent on the temperature. The adsorptivities of the esters and acids decreased by rising the temperature, whereas those of the alcohols increased. There was an evidence of chemisorption of the alcohols on the resin. The different trends of the adsorptivity between the alcohols and the acids were discussed in detail in Chapter 5. The dispersion of the components inside the reactors strongly depended on both temperature and flow rate. Based on the obtained data of the adsorptivities and the concept of chromatographic resolution, the operating conditions for complete separation of a non reactive mixture of the hydrolysis products were predicted. The determined model parameters were validated by comparing experiment and simulated non-reactive elution profiles of the components involved.

Based on the real parameters of systems investigated, the feasibility of the ester hydrolysis reactions were analyzed again. The complete conversion and complete separation for the ester hydrolysis reactions were possible. This prediction was illustrated by the experimental chromatograms in Chapter 6.

Because of difficulties to quantify the single component concentrations, instead of the direct measurement of the rates of the hydrolysis reactions, the rate constants were estimated by curve fitting between the measured detector signals and simulated signals at the column outlet using the equilibrium-dispersion model. Based on the obtained reaction rate constants at different temperature, the activation energies and the frequency factors were estimated. The obtained results were validated by comparing elution profiles with predictions at different conditions. The good agreement between measured and simulated signals allows to conclude that the parameters were determined precisely and the model was reliable.

Finally, the productions of formic acid and acetic acid from the different ester hydrolysis reactions were evaluated using the concentration profiles simulated by the equilibrium-dispersion model. Although the separation factors of the hydrolysis products of ethyl formate and ethyl acetate are higher than that of methyl formate and methyl acetate, respectively, methyl formate and methyl acetate are the better feedstock and offer higher productivities due to the shorter cycle times. The flow rate, the injection volume and the temperature have large effects on the productivity and other relevant objective functions. Temperature was not optimized because of lack of data out of the investigated range of temperature. However, higher temperatures allow for higher reaction rates and higher throughput due to better separation of the hydrolysis products. The recovery yield was reduced by rising of flow rate and injection volume. The higher flow rate or the higher injection volume helps to enrich the product concentration in the collected fractions. The main objective function considered was the product of the productivity and recovery yield $PR_i \times Y_i$. At each temperature, the best flow rate and the best injection volume to maximize the objective function $PR_i \times Y_i$ could be found.

For the future, the database acquired and the methodology developed in this dissertation can be applied to study other discontinuously and continuously operated reactive chromatography and other integrated processes.

Nomenclature

Latin symbols

A	m	Eddy diffusion term in Van Deemter equation, Eq. 2-13
A_{col}	m^2	Cross-section area of column
a_i	mol/L	Activity
B	m^2/min	Longitudinal diffusion term in Van Deemter equation, Eq. 2-13
b_i	-	Langmuir factor
C	min	Mass transfer resistance term in Van Deemter equation, Eq. 2-13
C_i	mol/L	Transformed concentration variable
c_i	mol/L	Concentration
Da	-	Damköhler number
$D_{ap,i}$	m^2/min	Apparent dispersion coefficient
$D_{ax,i}$	m^2/min	Axial dispersion coefficient
D_S	m^2/min	Surface diffusion coefficient
d_{col}	m	Inside diameter of column
d_p	m	Particle size
E_A	kJ/mol	Activation energy in Arrhenius equation (2-83)
F	-	Phase ratio
G	kJ/mol	Free Gibbs energy
H	kJ/mol	Enthalpy
$HETP$	m	The height equivalent to a theoretical plate
K_{eq}	-	Chemical equilibrium constant
K_i	-	Linear adsorption constant of component i (Herry constant)
k	L/(mol min)	Reaction rate constant
k_i'	-	Retention factor
k_o	-	Frequency factor in Arrhenius equation (2-83)

L	m	Column length
N_C	-	Number of components
N_i	-	Number of theoretical plates
N_R	-	Number of reactions
n_i	mol	Number of moles
P	N/m^2	Pressure
Pe	-	Peclet number
PR_i	mol/(L min)	Productivity
Q_i	mol/L	Transformed concentration variable in solid phase
q_i	mol/L	Concentration in solid phase
R	kJ/(mol K)	Universal gas constant
Re	-	Reynolds number
R_S	-	Resolution
r	mol/(L min)	Reaction rate
S	kJ/(mol K)	Entropy
S_W	-	Swelling ratio
t	min	Time coordinate
$t_{R,i\ (max)}$	min	Retention time of the peak maximum
u	m/min	Linear velocity
$\dot{V}$	m^3/min	Flow rate
$\overline{V}_A$	m^3/mol	Molar volume of solute
$\overline{V}_B$	m^3/mol	Molar volume of solvent
V_{col}	m^3	Column volume
V_{int}	m^3	Interstitial volume
V_{pore}	m^3	Total pore volume
V_{Re}	m^3	Volume of resin
V_s	m^3	Stationary phase volume
V_{solid}	m^3	Solid material volume
x	m	Spatial coordinate
Y	%	Recovery yield
$w_{o.5}$	m	Width of peak at half high

Greek symbols

$\alpha_{i,j}$	-	Separation factor
β	min^{-1}	Mass transfer coefficient
$\beta^{'}$	min^{-1}	Apparent mass transfer coefficient
ε	-	External porosity
ε_p	-	Internal porosity
ε_t	-	Total porosity
γ_1, γ_2	-	Geometric constant of packing
μ	Ns/m^2	Mobile phase viscosity
μ_i	kJ/mol	Chemical potential
μ_t	min	first normalized moment
$v_{i,j}$	-	Stoichiometric coefficient of component i in reaction j
ρ_p	Kg/m3	Particle density
σ_t	min	Second central moment

Superscripts and Subscripts

A	Acid acetic
Ac	Acids
Al	Alcohols
ads	adsorption
ap	apparent
As	Acids
av	average
ax	axial
$back$	backward
col	column
cyc	cycle
des	desorption
$disp$	dispersion
E	Ethanol

EA	Ethyl acetate
EF	Ethyl formate
EL	Eley-Redial mechanism
Es	Esters
eff	effective
eq	equilibrium
F	Formic acid
f	formation
forw	forward
het	heterogeneous
hom	homogeneous
i	component index
init	initial
inj	injection
int	intraparticle
j	reaction index
k	reactant index
LH	Langmuir-Hinshelwood mechanism
M	Methanol
MA	Methyl acetate
MF	Methyl formate
max	maximum
min	minimum
p	particle
pore	pore
r	reaction
reg	Regeneration
W	Water

References

Adac94   Adachi, S., *Simulated moving-bed chromatography for continuous separation of two components and its application to bioreactors,* J. Chromatogr., 658(1994), 271-282.

Agar88a   Agar, D.W., Ruppel, W., *Extended reactor concept for dynamic DeNOx design,* Chem. Eng. Sci., 43(1988), pp. 2073-2078.

Agar88b   Agar D.W., Ruppel, W., *Multifunctional reactors for heterogeneous catalysis*, Chem. Ing. Tech. 60(1988) No. 10, pp. 731-741.

Agar99   Agar, D.W., *Old Preconceptions and New Dimensions*, Chem. Eng. Sci. 54(1999), pp. 1299-1305.

Agar05   Agar D.W., *The Dos and Don'ts of Adsorptive Reactors* in *Integrated Chemical Processes: Synthesis, Operation, Analysis, and Control* edited by Sundmacher, K., Kienle, A., and Seidel-Morgenstern, A., Wiley-VCH, Weinheim, Germany, 2005, pp. 203-231.

Agre84   Agreda, V.H., and L.R. Partin, *U.S. patent 4,435,595* to Eastman Kodak, 1984.

Alel44   D'Alelio, G.F., *U.S. Patent 2,366,007*, 1944.

Atki02   Atkins, P., Physical chemistry, Oxford Press Inc., New York, 2002.

Back23   Backhaus, A., *U.S. Patent 1,400,849*, 1923.

Barb87   Barbosa, D., Doherty, M.F., *A New Set of Composition Variables for the Representation of Reactive-Phase Diagrams*, Proc. Roy. Soc. Lond., A413 (1987), pp. 459-464.

Bari95   Barin, I., *Thermochemical data of pure substances*, 3rd edition, VCH verlagsgesellschaft mbH, Weiheim, 1995.

Bark87a   Barker, P.E., Zafar, I., Alsop R.M., *A novel method for the production of dextran and fructose* in *Bioreactor and Biotransformations*, Elsevier Applied Science Publisher, Amsterdam 1987, pp. 141-157.

Bark87b   Barker, P.E., Zafar, I., Alsop R.M., P*roduction of dextran and fructose in a chromatographic reactor-separator* in *Separation for Biotechnology*, Ellis Horwood Ltd., Chichester 1987, pp. 127-151.

Bark89   Barker, P.E., Ganetsos, G., *Biochemical reaction and separation in chromatographic columns* in *Adsoroption: Science and Technology* edited by A.E., Rodrigues et al., Kluwer Adcademic Publisher, Dordrecht 1989, pp. 491-504.

Bark92   Barker, P.E., Ganetsos, G., Ajongwen, J., Akintoye, A., Chem. Eng. J. 50(1992), pp. 23-28.

Bart96   Bart, H.J., Kaltenbrunner, W., Landschützer, H., *Kinetics of esterification of acetic acid with propyl alcohol by heterogeneous catalysis*, Int. J. Chem. Kin., 28(1996), pp. 649-656.

Bart01   Bart, H.J., *Reactive Extraction*, Springer, Berlin, 2001.

Bass60   Basset, D.N, and Habgood, *A Gas Chromatographic Study of the Catalytic Isomerization of Cyclopropane*, J. Phys. Chem., 64 (1960), pp. 769-773.

Bird60   Bird, R.B., Stewart, W.E., and Lightfoot, E.N., *Transport phenomena*, Wiley-New York, 1960.

Bjor95   Bjorklund, M.C., Carr, R.W., *The simulated countercurrent moving bed chromatographic reactor: a catalytic and separative reactor,* Catal. Today, 25(1995), 159-168.

Bjor02   Bjorklund, M.C., Carr, R.W., *Enhanced Methanol Yields from the Direct Partial Oxidation of Methane in a Simulated Countercurrent Moving Bed Chromatographic Reactor,* Ind. Chem. Eng. Res., 41(2002), pp. 6528-6536.

Boda53   Bodamer, G.W., and Kunin, R., *Behavior of Ion-Exchange Resins in Solvents Other Than Water*, Ind. Eng. Chem., 45 (1953), pp. 2577-2580.

Borr05   Borren, T., Fricke, J., *Chromatographic reactors* in *Preparative Chromatography of Fine Chemicals and Pharmaceutical Agents* edited by Schmidt-Traub, H., Wiley-VCH Verlag, Weinheim, Germany, 2005.

Brou61   Broughton, D.B, Gerhold, C.G., *U.S. Patent 2,985,589,* to Universal Oil Products Company (1961).

Brun02   Brunt, V.V., Kanel, J.S., *Extraction with Reaction* in *Reactive Separation Process* edited by Kulprathipanja, S., Taylor & Francis, New York, USA, 2002.

Carr93   Carr, R.W., *Continuous reaction chromatography* in *Preparative and Production Scale Chromatography* edited by Ganetsos, G., and Barker, P.E., Marcel Dekker, New York, USA, 1993, pp. 421-447.

Cheu05   Cheung, H., Tanke, R.S., Torrence G.P., *Acetic Acid* in *Ullmann's Encyclopedia of Industrial Chemistry*, Wiley-VCH Verlag, Weinheim, 2005[*].

Chey86   Cheyran, M., Mehaia, A., *Membrane Bioreactors*, in: *Membrane Separation in Biotechnology,* edited by McGregor, W.C., Marcel Dekker, New York, 1986, pp. 255-299.

Cho80   Cho, B.K., Carr, R.W., Aris, R., *A Continuous Chromatographic Reactor*, Chem. Eng. Sci., 35(1980), pp. 74-81.

CIT00   CIT GmbH, *Presto – Simulation of kinetic models* (software manual), Rastede, Germany, 2000.

Clayd01   Clayden, J, Greeves, N., Warren, S., and Wothers P., *Organic chemistry*, Oxford University Press, New York, 2001.

Crai44   Craig, L.C., *Identification of small amounts of organic compounds by distribution studies*, J. Biol. Chem., 155(1944), pp. 519-534.

CRC93   *CRC Handbook of Chemistry and Physics 74th*, Editor in Chief - Lide, D.R., CRC Press, Boca Raton, USA, 1993.

CRC06   *CRC Handbook of Chemistry and Physics 87th*, Editor in Chief - Lide, D.R., CRC Press, Boca Raton, USA, 2006.

---

[*] *http://www.mrw.interscience.wiley.com/emrw/9783527306732/ueic/article/a01_045/current/pdf*

Danc53   Danckwerts, P.V., *Continuous flow systems: Distribution of residence times*, Chem. Eng. Sci., 2 (1953), pp. 1-13.

Dinw61   Dinwinddie, J.A., and Morgan, W.A., *U.S. Patent 2,976,132*, to Esso Research and Engineering Company, 1961.

Do98   Do, D.D., *Adsorption analysis: Equilibrium and Kinetics*, Imperial College Press, London, 1998.

Gane90   Ganetsos, G., and Barker, P.E., Akintoye, A., IChemE Symp. Ser., 118(1990), pp. 17-24.

Gane93a   Ganetsos, G., and Barker, P.E., *Preparative and Production Scale Chromatography,* Marcel Dekker, New York, USA, 1993.

Gane93b   Ganetsos, G., Barker, P.E., Ajongwen, J.N., *Batch and continuous chromatographic systems as combined bioreactor-separators* in *Preparative and Production Scale Chromatography* edited by Ganetsos, G., and Barker, P.E., Marcel Dekker, New York, USA, 1993, pp. 375-394.

Gate92   Gates, B.C., *Catalytic chemistry*, John Wiley & Sons, Inc., 1992.

Gazi62   Gaziev, G.A., Roginskii, S.Z., and Yanovskii, M.J., *U.S.S.R. Patent 149,398* (1962).

Gelb05   Gelbard, G., *Organic Synthesis by Catalysis with Ion-Exchange Resins*, Ind. Chem. Eng. Res, 44 (2005), pp. 8468-8498.

Gelo03   Gelosa, D., Ramaioli, and G. Valente, Morbidelli, M., *Chromatographic Reactors: Esterification of Glycerol with Acetic Acid Using Acidic Polymeric Resins,* Ind. Eng. Chem. Res., 42 (2003), pp. 6536-6544.

Grün04   Grüner, S., Kienle, A., *Equilibrium theory and nonlinear waves for reactive distillation columns and chromatographic reactors*, Chem. Eng. Sci., 59 (2004), pp. 901-918.

Grün06   Grüner, S., Mangold, M., Kienle, A., *Dynamics of reaction separation processes in the limit of chemical equilibrium*, AIChE J., 52 (2006), pp. 1010-1026.

Gu95   Gu, T., *Mathematical modeling and scale-up of liquid chromatography*, Springer Velag, Berlin, Germany, 1995.

Guio03   Guiochon, G., Lin, B., *Modeling for preparative chromatography*, Academic Press, California, USA, 2003.

Guio06   Guiochon, G., Felinger, A., Shirazi, S.G., Katti, A.M., *Fundamentals of Preparative and Nonlinear Chromatography 2nd*, Academic Press, Inc., Boston, USA, 2006.

Eigen05   Eigenberger, G.., *Fixed-bed reactors* in *Ullmann's Encyclopedia of Industrial Chemistry*, Wiley-VCH Verlag, Weinheim, 2005[†].

Falk99   Falk, T., Seidel-Morgenstern, A., *Comparison between a fixed-bet reactor and a chromatographic reactor*, Chem. Eng. Sci., 54(1999), pp. 1479-1485.

Falk02   Falk, T., Seidel-Morgenstern, A., *Analysis of a discontinuously operated chromatographic reactor*, Chem. Eng. Sci., 57(2002), pp. 1599-1606.

Falk03   Falk, T., *Untersuchungen zur Kopplung von Reaktion und Stofftrennung in einem diskontinuierlich betriebenen chromatographischen Reaktor*, Dissertation, Logos Verlag, Berlin, 2003.

Fied05   Fiedler, E., Grossmann, G., Kersebohm, D.B., Weiss, G., Witte, C., *Methanol* in *Ullmann's Encyclopedia of Industrial Chemistry*, Wiley-VCH Verlag, Weinheim, 2005[†].

Fish89   Fish, B., Carr, R.W., *An experimental study of the countercurrent moving-bed chromatographic reactor*, Chem. Eng. Sci., 44(1989), pp. 1773-1783.

Fish86   Fish, B., Carr, R.W., Aris, R., *The continuous countercurrent moving bed chromatographic reactor*, Chem. Eng. Sci., 41 (1986), pp. 661-668.

Fiss06   Fissore, D., Barresi, A.A., Botar-Jid, C.C., *NO_x removal in forced unsteady-state chromatographic reactors*, Chem. Eng. Sci., 61(2006), pp. 3409-3414.

Feli96   Felinger, A., Guiochon, G., *Optimizing preparative separations at high recovery yield*, J. Chromatogr. A. 752 (1996), pp. 31-40.

Fric05a   Fricke, J., *Entwicklung einer Auslegungsmethode für chromatographische SMB- Reactoren*, Dissertation, VDI Verlag GmbH, Düsseldorf, 2005.

[†] *http://www.mrw.interscience.wiley.com/emrw/9783527306732/ueic/article/a16_465/current/pdf*

Fric05b   Fricke, J., Schmidt-Traub, H., and Kawase, M., *Chromatographic reactor* in *Ullmann's Encyclopedia of Industrial Chemistry*, Wiley-VCH Verlag, Weinheim, 2005[‡].

Hash83   Hashimoto, K., Adachi, S., Noujima, H., and Ueda, Y., *A new process combining adsorption and enzyme reaction for producing higher-fructose syrup*, Biotech. Bioeng., 25 (1983), Nr. 10, pp. 2371-2393.

Hash93   Hashimoto, K., Adachi, S., Shirai, Y., *Development of New Bioreactors of a Simulated Moving-Bed Type* in *Preparative and Production Scale Chromatography* edited by Ganetsos, G., and Barker, P.E., Marcel Dekker, New York, USA, 1993, pp. 395-419.

Helf67   Helfferich, F.G., *Multicomponent in ion exchange fixed-beds*, Ind. Eng. Chem. Fund., 6 (1967), pp. 362-364.

Helf93   Helfferich, F.G., Carr, P.W., *Non-linear waves in chromatography I. Wave, shocks, and sharps*, J. Chromatogr., 629 (1993), pp. 97-122.

Helf95   Helfferich, F.G., *Ion Exchange*, Dover publications, Inc., New York 1995.

Helf96   Helfferich, F.G., Carr, P.W., *Non-linear waves in chromatography II. Wave interference and coherence in multicomponent systems*, J. Chromatogr. A, 734 (1996), pp. 7-47.

Helf97   Helfferich, F.G., *Non-linear waves in chromatography III. Multicomponent Langmuir and Langmuir-like systems*, J. Chromatogr. A, 768 (1997), pp. 169-205.

Hoff97   Hoffmann, U., Sundmacher, K., *Multifunctional reactors*, Chem. Ing. Techn. 69(1997) No. 5, pp. 613-622.

Holl98   den Hollander J.L., Stribos .B.I, van Buel M.J., Luyben K.C., van der Wielen LA., *Centrifugal partition chromatographic reaction for the production of chiral amino acids*, J. Chromatogr. B, 711 (1998), pp. 223-235.

Indu93   Indu, B., Ernst, W.R., Gelbaumg, L.T., Methanol - Formic Acid Esterification Equilibrium in Sulfuric acid solutions: Influence of Sodium salts, Ind., Chem. Eng. Res. 32 (1993), pp. 981-985.

[‡] *http://www.mrw.interscience.wiley.com/emrw/9783527306732/ueic/article/c07_c01/current/pdf*

Kabe62   Kabel, R.L., Johanson, L.N., Reaction kinetics and adsorption equilibria in the vapor-phase dehydration of ethanol, AIChE, 8 (1962), pp. 621-628.

Kalb89   Kalbe, J., Höcker, H., Brendt, H., *Design of enzyme reactors as chromatographic columns for racemic resolution of amino acid esters,* Chromatographia 28(1989), pp. 1993-1996.

Keni05   Kenig, E.Y., Górak, A., *Reactive absorption,* in: *Integrated Chemical Processes: Synthesis, Operation, Analysis, and Control,* edited by Sundmacher, K., Kienle, A., and Seidel-Morgenstern, A., Wiley-VCH, Weinheim, Germany, 2005. pp. 265-311.

Kosa02   Kosaric, N., Duvnjak, Z., Farkas, A., Sahm, H., Bringe-Meyer, S., Goebel, O., Mayer, D., *Ethanol* in *Ullmann's Encyclopedia of Industrial Chemistry*, Wiley-VCH Verlag, Weinheim, 2005[§].

Krag91   Kragl, U., Gygax, D., Ghisalba, O., Wandrey, C., *Enzymatic Two Step Synsthesis of N-Acetyl-Neuraminic Acid in the Enzyme Membrane Reactor*, Angew. Chem. Int. Ed. Engl., 30 (1991), Nr 7, pp. 827-828.

Krag02   Kragl, U., Dreisbach, C., Membrane Reactors, in: Applied Homogeneous Catalysis with Organometallic Compounds, edited by Cornils, B., Herrmann, W.A., 2nd ed., Wiley-VCH Weinheim, 2002, p. 941-952.

Kris02   Krishna, R., *Reactive separations: more ways to skin a cat*, Chem. Eng. Sci. 57(2002), pp. 1491-1504.

Krug96   Kruglov, A.V., Bjorklund, M.C., Carr, R.W., *Optimization of the simulated countercurrent moving-bed chromatographic reactor for the oxidative coupling of methane*, Chem. Eng. Sci., 51(1996), pp. 2945-2950.

Kulp02   Kulprathipanja, S., Ed., *Reactive Separation Process*, Taylor & Francis, New York, USA, 2002.

Kawa96   Kawase, M., Suzuki, T.B., Inoue, K., K., Yoshimoto, Hashimoto, K., *Increased esterification conversion by application of the simulated moving-bed reactor,* Chem. Eng. Sci., 51(1996), pp. 2971-2976.

[§] *http://www.mrw.interscience.wiley.com/emrw/9783527306732/ueic/article/a09_587/current/html?hd=All*

Kawa99   Kawase, M., Inoue, K., Araki, T., Hashimoto, K., *The simulated moving-bed reactor for production of bisphenol A,* Catal. Today, 48(1999), pp. 199-209.

Lang74   Langer, S.H. and Patton, J.E., *Chemical reactor applications of the gas chromatographic column* in *New developments in gas chromatography* edited by Purnell, H., Wiley-New York N.Y., 1974, pp. 293-373.

Lang99   Langer's Handbook of Chemistry 15th, edited by Dean, J.A., McGraw Hill, inc., New York, 1999.

Laue80   Lauer, K., Starch/Stärke, 32(1980), pp. 11-13

Leve99   Levenspiel, O., Chemical Reaction Engineering, 3rd ed., John Wiley and Sons Inc., New York, 1999,

Li97   Li, J., Carr, W., *Accuracy of Empirical Correlations for Estimating Diffusion Coefficients in Aqueous Organic Mixtures,* Anal. Chem. 69 (1997), pp.2530-2536.

Lode02   Lode, F., *A simulated moving bed reactor (SMBR) for esterifications,* Dissertation ETH Nr. 14350, Shaker Verlag, Aachen 2002.

Mack55   Mackie, J.S., Meares, P., *The diffusion of electrolytes in a cation exchange resin membrane I: Theoretical*, Proc. Roy. Soc., A232 (1955), pp. 498-509.

Mage61   Magee, E.M., *Canadian Patent 631,882* (1961).

Mai06   Mai, T.P., *Experimental Investigation of Heterogeneously Catalyzed Hydrolysis of Esters*, Dissertation 2006, Uni-Magdeburg.

Marc99   Marcus, Y., *The properties of solvents*, John Wiley & Sons, New York, 1999.

Mart41   Martin, A.J.P., Synge, R.L.M., A new form of chromatogram employing two liquid phases, Biochem. J., 35(1941), pp. 1358-1368.

Mart49   Martin, A.J.P., *Summarizing paper*, Discuss. Faraday Soc., 7 (1949), pp. 332.

Mats65   Matsen, J.M., Harding, J.W., Magee, E.M., *Chemical reactions in chromatographic columns*, J. Phys. Chem., 69(1965), pp. 522-527.

Mazz96   Mazzotti, M., Kruglov, A., Neri, B., Gelosa, D., and Morbidelli, M., *A continuous chromatographic reactor: SMB*, Chem. Eng. Sci. 51 (1996), pp. 1827-1836.

Merc05   Merck KGaA, Chemikalien und Reagenzien Katalog 2005, Darmstadt.

Mich05   Michel, M., Epping, A., Jupke, A., *Modeling and Determination of Model Parameters* in *Preparative Chromatography of Fine Chemicals and Pharmaceutical Agents* edited by Schmidt-Traub, H., Wiley-VCH Verlag, Weinheim, Germany, 2005.

Miya00   Miyable, K., Guiochon, G., *A Kinetic Study of Mass Transfer in Reversed Phase Liquid Chromatography on a C18-Silica Gel*, Anal. Chem., 72 (2000), pp. 5162-5171.

Morb96   Morbidelli, M., Kruglov, A., Neri, B, Gelosa, D., Mazotti, M., *A continuous chromatographic reactor: SMBR,* Chem. Eng. Sci., 51(1996), pp. 1827-1836.

Mura68   Murakami, Y., Hattori, T., Hattori, T., *Study on the pulse reaction technique: II. Dealkylation and disproportionation of cumene, J. Catal.,* 10(1968), pp. 123-127.

Myer02   Myerson, A.S., *Handbook of Industrial Crystallization*, Butterworth-Heinemann, Boston, 2002.

Perr84   Perry, R.H., Green, D.W., *Perry's chemical engineering handbook*, 6th edition, McGraw-Hill, New York, USA, 1984.

Perr99   Perry, R.H., Green, D.W., *Perry's chemical engineering handbook*, 7th edition, McGraw-Hill, New York, USA, 1999.

Petr85   Petroulas, T., Aris, R., Carr, R.W., *Analysis and performance of a countercurrent moving-bed chromatographic reactor*, Chem. Eng. Sci.**,** 40 (1985), pp. 2233-2240.

Pool00   Pool, C.F., *Chromatography*, in *Encyclopedia of Separation Science* edited by Pool, C.F., Cooke, M., and Wilson, I.D., Academic Press, California, USA, 2000.

Pöpk00   Pöpken, T., Götze, L., Gmehling, J., *Reaction kinetics and chemical equilibrium of homogeneously and heterogeneously catalyzed acetic acid esterification with methanol and methyl acetate hydrolysis*, Ind. Chem. Eng. Res., 39(2000), pp. 2601-2611.

Ray90   Ray, A., Tonkovich, A.L., Aris, R., and Carr, R.W., The simulated countercurrent moving bed chromatographic reactor, Chem. Eng. Sci., 45 (1990), pp. 2431-2437.

Ray95   Ray, A.K., Carr, R.W., *Experimental study of a laboratory-scale simulated countercurrent moving bed chromatographic reactor*, Chem. Eng. Sci., 50(1995), pp. 2195-2202.

Reut05   Reutemann, W., Kieczka, H, *Formic acid* in *Ullmann's Encyclopedia of Industrial Chemistry*, Wiley-VCH Verlag, Weinheim, 2005[**].

Rhee70   Rhee, H.K., Aris, R., Amundson, N.R., *On the theory of multicomponent chromatography*, Phil. Trans. Roy. Soc., A267(1970), pp. 419-455.

Rhee86a   Rhee, H.K., Aris, R., Amundson, N.R., *First-order partial differential equations: Vol. 1 - Theory and application of single equations*, Prentice-Hall inc., Englewood Cliffs, NJ., USA, 1986.

Rhee86b   Rhee, H.K., Aris, R., Amundson, N.R., *First-order partial differential equations: Vol. 2 - Theory and application of Hyperpolic system of quasilinear equations*, Prentice-Hall inc., Englewood Cliffs, NJ., USA, 1986.

Riem05   Riemenschneider, W., Bolt, M., *Esters, Organic* in *Ullmann's Encyclopedia of Industrial Chemistry*, Wiley-VCH Verlag, Weinheim, 2005[§].

Ruth84   Ruthven, D.M., *Principles of Adsorption and Adsorption Processes,* John Wiley & Sons, Inc., New York, 1984.

Sad96   Sad, M.R., Querini, C.A., Comelli, R.A., Figoli, N.S., and Parera, J.M., *Dehydroisomerization of n-butane to isobutene in a chromatographic reactor*, App. Catal. A: General, 1946(1996), pp. 131-143.

Sard79   Sardin, M., Villermaux, J., Nouveau Journal de Chimie, 3(1979), 255-261.

[**] *http://www.mrw.interscience.wiley.com/emrw/9783527306732/ueic/article/a12_013/current/pdf*

Sard93   Sardin, M., Schweich, D., and Villermaux, J., *Preparative Fixed-Bed Chromatographic Reactor* in *Preparative and Production Scale Chromatography* edited by Ganetsos, G., and Barker, P.E., Marcel Dekker, New York, USA, 1993, pp. 477-522.

Sarm93   Sarmidi, M.R., Barker, P.E., *Saccharification of modified starch to maltose in a continuous rotating annular chromatograph (CRAC)*, J. Chem. Tech. Biotechnol. 57(1993), pp. 229-235.

Sain05   Sainio, T. *Ion-exchange resins as stationary phase in reactive chromatography*, Dissertation, Acta Universitatis Lappeenrantaensis, Nr. 218, Finland, 2005.

Schl06   Schlinkert, A., *Ausarbeitung und Anwendung einer Perturbations-methode zur Ermittlung thermodynamischer und kinetischer Parameter in der heterogenen Katalyse*, Dissertation (*in progress*), Magdeburg University.

Schm05   Schmidt-Traub, H. (Editor), *Preparative Chromatography of Fine Chemicals and Pharmaceutical Agents*, Wiley-VCH Verlag, Weinheim, Germany, 2005.

Schu05   Schulte, A., Epping, A., *Fundamentals and general terminology* in *Preparative Chromatography of Fine Chemicals and Pharmaceutical Agents* edited by Schmidt-Traub, H., Wiley-VCH Verlag, Weinheim, Germany, 2005.

Schu39   Schultz, R.F., *Studies in Ester Hydrolysis Equilibria - Formic Acid Esters*, J. Am. Chem. Soc., 61 (1939), 1443-1447.

Schw78   Schweich, D., Villermaux, J., *The Chromatographic Reactor. A New Theoretical Approach*, Ind. Eng. Chem. Fundam., 17(1978), pp. 1-7.

Schw80   Schweich, D., Villermaux, J., Sardin, M., *An Introduction to Nonlinear Theory of Adsorptive Reactor*, AIChE J., 26(1980), pp. 477-486.

Schw82a   Schweich, D., Villermaux, J., *Model for Catalytic Dehydrogenation of Cyclohexane in a Chromatographic Reactor: Comparisons of Theory and Experience*, Ind. Eng. Chem. Fundam., 21(1982), pp. 47-51.

Schw82b   Schweich, D., Villermaux, J., *Evidence for a Transient Promoting Catalytic Effect in a Chromatographic Reactor*, Ind. Eng. Chem. Fundam., 21(1982), pp. 51-55.

Seid93   Seidel-Morgenstern, A., Guiochon, G., *Thermodynamics of the adsorption of Tröger's base enantiomers from ethanol on cellulose triacetate*, J. Chromatogr., 631 (1993), pp. 37-47.

Seid95   Seidel-Morgenstern, A., *Mathematische Modellierung der präparativen Flüssigchromatographie*, Deutscher Universitäts Verlag, Wiesbaden, 1995.

Seid04   Seidel-Morgenstern, A., *Experimental determination of single solute and competitive adsorption isotherms*, J. Chromatogr. A, 1037 (2004), pp. 255-272.

Seid05   Seidel-Morgenstern, A., *Analysis and Experimental Investigation of Catalytic Membrane Reactors,* in: *Integrated Chemical Processes: Synthesis, Operation, Analysis, and Control,* edited by Sundmacher, K., Kienle, A., and Seidel-Morgenstern, A., Wiley-VCH, Weinheim, Germany, 2005. pp. 359-389.

Shan04   Shan, Y., Seidel-Morgenstern, A., *Analysis of isolation of a target component using multicomponent isocratic preparative elution chromatography*, J. Chromatogr. A, 1041 (2004) 53-62.

Silb01   Silbey, R.J., Alberty, R.A., *Physical chemistry*, John Wiley & Sons, Inc., New York, USA, 2001.

Smit81a   Smith, J.M., *Chemical Engineering Kinetics*, 3rd ed., McGraw-Hill, 1981.

Smit81b   Smith, L.A., *U.S. Patent 4,307,254* to Chemical Research & Licensing Company, 1981.

Song98   Song, W., Venimadhavan, G., Manning, J.M., Malone, Doherty, M.F., *Measurement of Residual Curve Maps and Heterogeneous kinetics of Methyl Acetate Synthesis*, Ind. Eng. Chem. Res. 37 (1998), pp. 1917-1928.

Stan00   Stankiewicz, A., Moulijn, J.A., *Process intensification: Transforming chemical engineering*, Chem. Eng. Progress. 96(2000) No. 1, pp. 22-23.

Stan02   Stankiewicz, A., Moulijn, J.A., *Process intensification*, Ind. Eng. Chem. Res., 41(2002) No. 8, pp. 1920-1924.

Stull69   Stull, D.R., Westrum, E.F., Sinke, G.C., The chemical thermodynamics of organic compounds, John Wiley & Sons, Inc., New York, 1969 (translated in to Russian as Химическая термодинамика органических соединений, printed by МИР, 1971).

Sund05   Sundmacher, K., Kienle, A., and Seidel-Morgenstern, A., Ed., *Integrated Chemical Processes: Synthesis, Operation, Analysis, and Control,* Wiley-VCH, Weinheim, Germany, 2005.

Suzu90   Suzuki, M., *Adsorption Engineering*, Kodansha, Tokyo, Japan, 1990.

Take76   Takeuchi, K., Uraguchi, Y., *Basic design of chromatographic moving bet reactors for product refining*, J. Chem. Eng. Japan, 9 (1976) Nr. 3, pp. 246-248.

Take77   Takeuchi, K., Uraguchi, Y., *Experimental Studies of a Chromatographic moving-Bed Reactor. Catalytic Oxidation of Carbon Monoxide on Activated Alumina as a Model Reaction, J. Chem. Eng. Japan,* 10(1977), pp. 455-460.

Tava95   Tavare, N.S., *Industrial Crystallization: Process Simulation Analysis and Design*, Plenum Press, New York, 1995.

Thom97   Thomas, J.M., Thomas, W.J., *Principles and practice of heterogeneous catalysis*, VCH Publishers Inc., New York, 1997.

Tonk94   Tonkovich, A.L.Y., Carr, R.W., *A simulated countercurrent moving-bed chromatographic reactor for the oxidative coupling of methane: Experimental results,* Chem. Eng. Sci., 49(1994), pp. 4647-4665.

Trap06   Trappe, O., *A Unified Equation for Fast and Precise Access to Rate Constants of First Order Reactions in Dynamic and On-column Reaction Chromatograph, Anal. Chem*., 78(2006), pp. 189198.

Trim40   Trimble, H.M., Richardson, E.L., *Equilibrium in an esterification reaction with perchloric acid as catalyst*, J. Am. Chem. Soc. 62 (1940), pp. 1018-1019.

Ung95   Ung, S., Doherty, M.F., *Calculation of residue curve maps for mixtures with multiple equilibrium chemical reactions*, Ind. Eng. Chem. Res., 34 (1995), pp. 3195-3202.

Unge76   Unger, B.D., Rinker, R.G., *Ammonia-Synthesis Reaction in Chromatographic Regime, Ind. Eng. Chem. Fundam.* 15(1976), pp. 225-227.

Van56   Van Deemter, J.J., Zuiderweg, F.J., Klinkenberg, *Longitudinal diffusion and resistance to mass transfer as causes of nonideality in chromatography,* Chem. Eng. Sci. 5 (1956), pp. 271-289.

Vill81   Villermaux, J., *The chromatographic reactor* in *Precolation Processes: Theory and Application* edited by Rodrigues, A.E., and Tondeur, D., Sijthoff en Noordhoff, Alpena an den Rijn, The Netherlands (1981), pp. 539-588.

Vu05   Vu, T.D., Seidel-Morgenstern, A., Grüner, S., Kienle, A., *Analysis of ester hydrolysis reactions in a chromatographic reactor using equilibrium theory and a rate model*, Ind. Eng. Chem. Res., 43(2005), pp. 9565-9574.

Wei96   Wei, J., *A century of changing paradigms in chemical engineering*, CHEMTECH, 26(1996) No. 5, pp. 16-18.

West84   Westerterp, K.R., van Swaaij, W.P.M., Beenackers, A.A.C.M., *Chemical reactor design and operation*, Wiley, Chichester, US, 1984.

West92   Westerterp, K.R., *Multifunctional reactors*, Chem. Eng. Sci. 47(1992) No. 9-11, pp. 2195-2206.

Wibo05   Wibowo, C., Kelkar, V.V., Samant, K.D., *Development of Reactive Crystallization Processes*, in: *Integrated Chemical Processes: Synthesis, Operation, Analysis, and Control,* edited by Sundmacher, K., Kienle, A., and Seidel-Morgenstern, A., Wiley-VCH, Weinheim, Germany, 2005. pp. 339-358.

Wood68   Wood, B.J., *Dehydrogenation of cyclohexane on a hydrogen-porous membrane*, *J. Catl.*, 11 (1968), pp. 30.

Yu04   Yu, W., Hidrajat, K., Ray, A.K, Determination of adsorption and kinetic parameters for methyl acetate esterification and hydrolysis reaction catalyzed by Amberlyst 15, App. Catal. A, 260 (2004), pp. 191-205.

Zafa88   Zafar, I., Barker, P.E., *An experimental and computational study of a biochemical polymerisation reaction in a chromatographic reactor separator,* Chem. Eng. Sci., 43(1988), pp. 2369-2375.

Calculation of the Standard Free Gibbs Energies of Formation in Liquid State

The standard free Gibbs energy of formation in liquid state $\left(\Delta G_{f,i}^{298K,L}\right)$ of ethyl formate and methyl acetate can not be found in the literature. However, it can be calculated from available data of the standard free Gibbs energy of formation in gas state $\left(\Delta G_{f,i}^{298K,G}\right)$ and vapor-pressure (P^G), using the following equation [Silb01, p.114]

$$\Delta G_{f,i}^{298K,L} = \Delta G_{f,i}^{298K,G} + RT^0 \log\left(\frac{P^L}{P^G}\right) \tag{A-1}$$

where, R is the universal gas constant R = 8.31439e-3 kJ (K mol)$^{-1}$; T^0 = 298K, P^L is the pressure of liquid at standard state P^L = 1 bar (~14.5038 Psi). The vapor-pressure can be computed by Antoine equation [Lang99, p. 5.30]:

$$\log P_i^G = A_i - \frac{B_i}{(T-298)+C_i} \tag{A-2}$$

in which, P_i^G is in pounds per square inch [psi]; A_i, B_i and C_i are the Antoine equation' coefficients. These values of A_i, B_i and C_i for the investigated components are taken from [Lang99, table 5.9] given in Table A-1.

Table A-1: The coefficients of Antoine equation [Lang99, table 5.9]

Compound	Temp. range, [K]	Antoine equation's coefficients		
		A	B	C
MF	294-306	3.0270	3.02	-11.90
EF	277-327	7.0091	1123.94	218.20
MA	274-329	7.0652	1157.63	219.73
EA	288-349	7.1018	1244.95	217.88

A P P E N D I X   B

Calibration of RI and UV detectors

Chromatograms recorded by the detectors do not directly measure concentrations of analyte components. Instead they measure responses such as changes in refractive index (RI) or ultraviolet (UV) absorption of the analytes which are related to the concentrations. Therefore, a calibration curve is often needed to derive from the chromatogram the actual concentration profiles of the components. Calibrations of the detectors using frontal analysis method consist of preparing a series solutions of the investigated compounds at stepwise different concentrations, flushing them successively through flow cells of the detectors, and recording the high of the plateau responses obtained. The high of the plateau obtained is a function of the feed concentrations. For linear response given by the detector, the calibration factors can be determined from the slope of the calibration curves.

As description in Section 4.1.3, the two detectors used are the RI detector (Knauer, K-2300) and the UV-VIS detector (Hitachi L-7420). The operating wavelength of the RI detector was fixed at 950 nm by the manufacturer, whereas this one of UV-VIS detector was adjustable from 190 to 900 nm. For transparency of the mobile phase (water) and capability for detection of the other components, the operating wavelength of the UV-VIS detector was set at 195 nm based on UV cutoff wavelengths of the investigated components given in Table 3.2. The calibration curves for both of the detectors are shown in Figures B-1 and B-2. The calibration factors are summarized in Table B-1. For all investigated components, the RI detector is sensitive to all components, whereas the UV detector is insensitive to the alcohols. The RI detector has bester linear responses than the UV detector.

Table B-1: Calibration factors for the RI and UV detectors

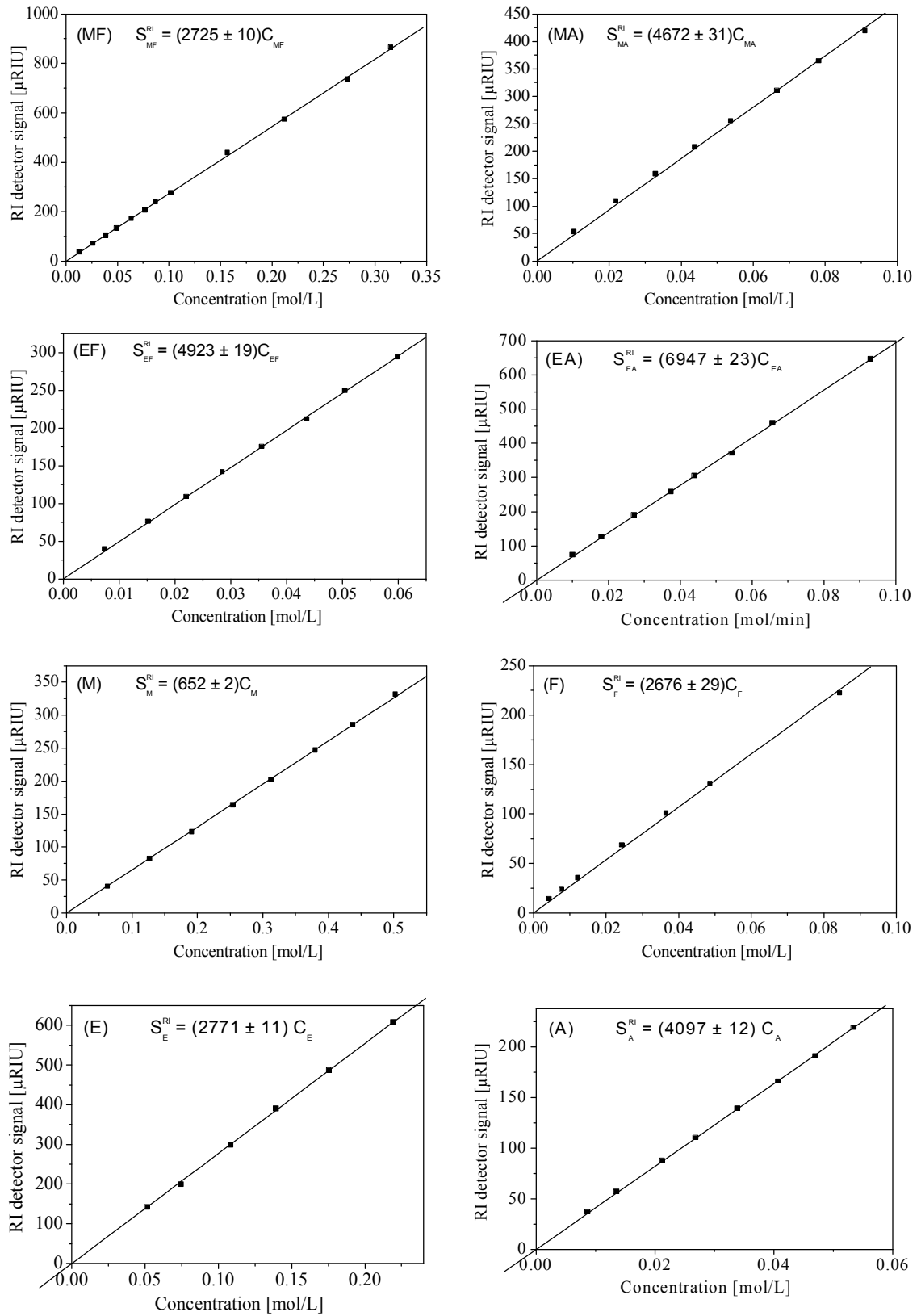| Compounds	RI detector $K^{RI}_{Cal,i}$ [μRIU (mol/L)$^{-1}$]	UV detector $K^{UV}_{Cal,i}$ [mV (mol/L)$^{-1}$]
MF	2,725 ± 10	46,922 ± 635
EF	4,923 ± 19	64,994 ± 1225
MA	4,672 ± 31	46,922 ± 635
EA	6,947 ± 23	52,452 ± 546
M	652 ± 2	200 ± 10
E	2,771 ± 11	371 ± 12
F	2,676 ± 29	40,296 ± 131
A	4,097 ± 12	38,179 ± 565

Figure B-1: Calibration curves of investigated components for the RI detector
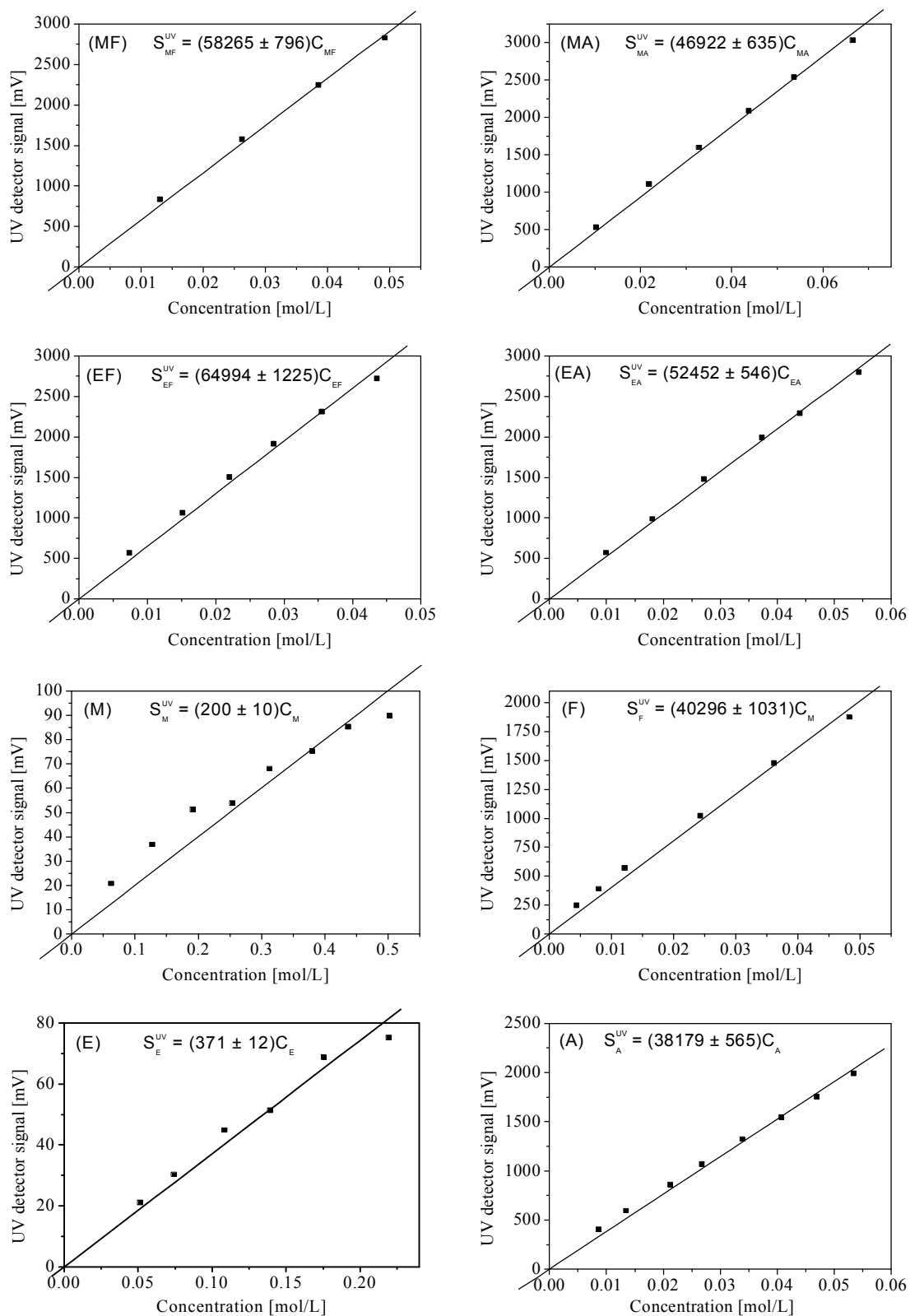
Figure B-2: Calibration curves of investigated components for the UV detector

Curriculum Vitae

Name:	**Vu-Dinh, Tien**
Date of birth:	30.06.1974
Place of birth:	Hanoi, Vietnam
Nationality:	Vietnam
Gender:	Male

Education profile

01/2003 - Present   Ph.D. student at Institute of Process Engineering
at Otto-von-Guericke-University, Magdeburg, Germany
Research subject: *Analysis of heterogeneously catalyzed ester hydrolysis reactions in a fixed-bed chromatographic reactor.*

09/1996 - 02/1999   Master of Engineering in Chemical Process Equipment
at Hanoi University of Technology, Vietnam
Thesis title: *Theoretical and experimental investigation of Steam-Charcoal heterogeneous reactions.*

09/1991 – 06/1996   Bachelor of Chemical Process Equipment
at Hanoi University of Technology, Vietnam
Thesis title: *Investigation of rice husk gasification*

Occupation:

09/1999 - Present   Lecturer at Faculty of Chemical Technology
Hanoi University of Technology
Building C_{3-4}, Room 310
No. 01, Dai Co Viet Road, Hanoi, Vietnam
Tel: (+84) 4 8692510   Fax: (+84) 4 8680070